

PHASE TRANSITIONS AND MICROSTRUCTURES OF ADS BLACK HOLES

Thesis

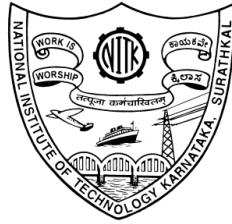
Submitted in partial fulfilment of the requirements for the degree of

**DOCTOR OF PHILOSOPHY
IN
PHYSICS**

by

NAVEENA KUMARA A

Reg.No.135045PH13F07



**Department of Physics
NATIONAL INSTITUTE OF TECHNOLOGY KARNATAKA (NITK)
SURATHKAL, MANGALORE - 575 025
August 2021**

DECLARATION

By the Ph.D. Research Scholar

I hereby *declare* that the Research Thesis entitled “**Phase Transitions and Microstructures of AdS Black Holes**”, which is being submitted to the *National Institute of Technology Karnataka, Surathkal* in partial fulfilment of the requirements for the award of the Degree of *Doctor of Philosophy in Physics* is a *bonafide report of the research work carried out by me*. The material contained in this thesis has not been submitted to any University or Institution for the award of any degree.



Naveena Kumara A
Register No.: 135045 PH13F07
Department of Physics
National Institute of Technology Karnataka,
Surathkal

Place: NITK - Surathkal

Date: August, 2021

CERTIFICATE

This is to *certify* that the Research Thesis entitled “**Phase Transitions and Microstructures of AdS Black Holes**”, submitted by **Naveena Kumara A** (Register Number: 135045 PH13F07) as the record of the research work carried out by him, is *accepted* as the *Research Thesis submission* in partial fulfilment of the requirements for the award of degree of **Doctor of Philosophy**.



Dr Ajith K.M.
Research Guide
Associate Professor
Department of Physics
NITK Surathkal - 575025



Chairperson - DRPC
(Signature with Date and Seal)

Dedication

To my mother, who knew the importance of school.

Acknowledgements

First and foremost, I have to thank my PhD supervisor, Dr Ajith K M. Without his guidance and dedicated involvement in every step throughout the process, this thesis would have never been accomplished. I am deeply indebted to his support and understanding over these past few years. He nurtured me beyond completing this thesis during my PhD life, which made a strong impression on me, and I have always carried great memories of his interactions with me.

I would like to express my deepest appreciation to my research progress assessment committee, including Dr H S Nagaraja and Dr P Parthiban. I was also privileged to work with Dr Deepak Vaid and Dr T K Shajahan, which enabled me to think in various research dimensions. I am profoundly indebted to those great opportunities. Although I have not had the opportunity to work with Dr V Sreenath previously, I am grateful to him for the discussion with him on my research.

In 2015, I went to the Centre for Theoretical Physics (CTP), Jamia Millia Islamia University, Delhi, for several weeks to study with Prof. M. Sami and Prof. Sushant G. Ghosh. My time at CTP has been highly productive, and working with Prof Sami and Prof Ghosh was an extraordinary experience. I am thankful to them for providing a great opportunity. I am also grateful to Prof. Abhishek Dhar, who gave the first research experience to me during the internship at the International Centre for Theoretical Sciences (ICTS), Bangalore. I would like to acknowledge the Science Academies' Summer Research Fellowship Programme's assistance for the above two visits.

I cannot begin to express my gratitude to my collaborators Ahmed Rizwan C.L., Kartheek Hegde and Shreyas Punacha, without whom the materialisation of this thesis would not have been possible. The discussions in the General Physics Lab (GPL) always elated me to realise my understandings and misunderstandings of physics. I also had the great pleasure of working with Dr Md Sabir Ali since my visit to IIT Ropar in 2019.

Getting through my PhD required more than academic support, and I have numerous people to thank for listening to and, every so often, having to tolerate me over the past few years. I cannot leave NITK Surathkal without mentioning Safir T K, Rajani K V, Ananthram K S, Dr Siby Thomas, Dr Manoj Kumar, Dr Sreejesh M, Dr Nimith KM, Manju M S, Ahamed Khasim, Sibesh P P, Anupama Sebastian, Amrutha S V, whose help cannot be overestimated.

I very much appreciate Sterin N S for many memorable evenings out and in and great cooking experiments, which I will be missing in the future. I thank all the research scholars and M.Sc. students of the Department of Physics for their kindness. I would like to recognise the assistance that I received outside NITK from Dr Praveen Prakash DSouza, Sharath Gore, Dr Nilakantan V, Dr Raghavendra S and Shubha C Pranav.

I am grateful to all the faculty members and students of the postgraduate physics departments of St Aloysius College (Autonomous) Mangalore and Alva's College Moodbidri during my service as a faculty there. The teaching experience in these institutes in the initial stage of my research is the most memorable one, which immensely helped me in shaping my perspectives. There is a large number of academic friends I got during my tenure in these institutes, which definitely had an impact on my research. I am thankful to all of them.

A PhD does not take birth in a day. I have come across several steps, which were not trivial if I did not meet some extraordinary personalities at the different locus of my student life. I would like to acknowledge the help of Madhavan Nambiar K, Prasad V and Jagadeesh Master. My teachers played a decisive role in moulding me to develop the scientific temper, humanism, and the spirit of inquiry and reform. Special thanks to the teachers of AUP School Kuntar, GVHSS. Mulleria, BARHSS. Bovikan, Govt. College Kasaragod and SDM College (Autonomous) Ujire.

I would like to thank the UGC Govt. of India for financial assistance under the UGC-NET-SRF scheme.

When I started writing this thesis, I met my soulmate, Dr Kavya K V. Since then, she acted as a catalyst for change in this process. I cannot thank her enough for all her love and support.

Last but not least, none of this could have happened without my family. My mother always offered her encouragement despite my limited devotion to communications. With her own brand of love, she has been kind and supportive to me over the last several years. To my brothers and sisters – it would be an understatement to say that, as a family, we have encountered some ups and downs in these many years. Every time I was ready to leave, you did not let me and I am forever beholden. This thesis stands as a testament to your eternal love and encouragement.

Statements of Contribution

1. This thesis is based on the following published articles.
 - **A. Naveena Kumara**, C. L. Ahmed Rizwan, Kartheek Hegde, Md Sabir Ali, Ajith K. M, “Ruppeiner Geometry, Reentrant Phase transition and Microstructure of Born-Infeld AdS Black Hole”, *Physical Review D* 103, 044025 (2021) [arXiv:2007.07861]
 - **A. Naveena Kumara**, C. L. Ahmed Rizwan, Shreyas Punacha, Ajith K. M., Md Sabir Ali, “Photon Orbits and Thermodynamic Phase Transition of Regular AdS Black Holes”, *Physical Review D* 102, 084059 (2020), [arXiv:1912.11909]
 - **A. Naveena Kumara**, C. L. Ahmed Rizwan, Kartheek Hegde, Ajith K. M, “Repulsive Interactions in the Microstructure of Regular Hayward Black Hole in Anti-de Sitter Spacetime”, *Physics Letters B*, 807, 135556 (2020), [arXiv:2003.10175]
 - **A. Naveena Kumara**, C. L. Ahmed Rizwan, Kartheek Hegde, Ajith K. M., Md Sabir Ali, “Microstructure and continuous phase transition of a regular Hayward black hole in anti-de Sitter spacetime”, *Progress of Theoretical and Experimental Physics*, 7 (2021) 073 [arXiv:2003.00889]
2. The publications which are not included in the thesis and the conference proceedings are given at the end of the thesis under list of publications.

ABSTRACT

The thesis is aimed to understand the aspects of the black hole phase transitions and the underlying microstructures in anti-de Sitter spacetime. In contrast to the conventional black hole thermodynamics, there exist the thermodynamic variables pressure and volume in the extended thermodynamics approach, which arise from the dynamic cosmological constant. With this utility, we have researched the following things: (i) We used Landau continuous phase transition theory to discuss the van der Waals like critical phenomena of the black hole. The well-known interpretation of the phase transition of an AdS black hole as being a large and small black hole transition is re-interpreted as being a transition between a high potential phase and a low potential phase. (ii) We probed the phase structure of the regular AdS black holes using the null geodesics. The radius of photon orbit and minimum impact parameter shows a non-monotonous behaviour below the critical values of the temperature and the pressure, corresponding to the phase transition in extended phase space. The respective differences of the radius of unstable circular orbit and the minimum impact parameter can be seen as the order parameter for the small-large black hole phase transition, with a critical exponent $1/2$. Our study shows that there exists a close relationship between gravity and thermodynamics for the regular AdS black holes. (iii) We studied the interaction between the microstructures of the Hayward-AdS black hole using Ruppeiner geometry. Our investigation shows that the dominant interaction between the black hole molecules is attractive in most part of the parametric space of temperature and volume, as in the van der Waals system. However, in contrast to the van der Waals fluid, there exists a weak dominant repulsive interaction for the small black hole phase in some parameter range. This result clearly distinguishes the interactions in a magnetically charged black hole from that of van der Waals fluid. (iv) By employing a novel Ruppeiner geometry method in the parameter space of temperature and volume, we investigated the microstructure of Born-Infeld AdS black hole via the phase transition study, which includes standard and reentrant phase transition. We found that the microstructures of the black hole that lead to standard and reentrant phase transitions are distinct in nature. The critical phenomenon is observed from the curvature scalar, including the signature of the reentrant phase transition.

Keywords: Black Hole Chemistry; Black Hole Phase Transitions; Landau Theory of Phase Transitions; Photon Orbits; Ruppeiner geometry; Black Hole Microstructures.

Contents

List of figures	vi
List of tables	vii
1 Introduction	1
1.1 Objectives of the Thesis	4
1.2 Organisation of the Thesis	5
2 Ingredients of Black Hole Chemistry	7
2.1 Standard Black Hole Thermodynamics	8
2.2 Smarr Relations for Black Holes	9
2.2.1 Smarr Formula for Asymptotically Flat Black Holes	10
2.2.2 Smarr Formula for AdS Black Holes	13
2.3 Black Hole Thermodynamics in AdS Spacetime	17
2.4 Black Hole Chemistry	19
3 Ruppeiner Geometry and Black Hole Microstructures	23
3.1 First Laws and Ruppeiner Geometry	26
3.2 Scalar Curvature and Phase Transition	31
4 Photon Orbits and Thermodynamic Phase Transition of AdS Black Holes	35
4.1 Introduction	35
4.2 Regular Hayward Black Hole	37
4.2.1 Thermodynamics of Regular Hayward Black Hole	37
4.2.2 Geodesic equations of motion	40
4.2.3 Critical behaviour from unstable photon orbits	43
4.3 Regular Bardeen Black Hole	45

4.4	Discussions	49
5	Microstructure and Continuous Phase Transition of AdS Black Holes	53
5.1	Introduction	53
5.2	Phase Transition of Regular Hayward Black Hole	54
5.2.1	Thermodynamics of the Black Hole	54
5.2.2	Phase Transition of the Black Hole	56
5.3	Ruppeiner Geometry and Microstructure	60
5.4	Discussions	62
6	Repulsive Interactions in the Microstructure of AdS Black Holes	65
6.1	Introduction	65
6.2	Phase structure of the Hayward-AdS Black Hole	66
6.3	Microstructure of the Hayward-AdS Black Hole	70
6.4	Discussions	74
7	Reentrant Phase Transition and Microstructure of AdS Black Holes	77
7.1	Introduction	77
7.2	Thermodynamics and Phase Structure of the Black Hole	79
7.2.1	Standard Phase Transition Case	82
7.2.2	Reentrant Phase Transition Case	85
7.3	Ruppeiner Geometry and Microstructure of the Black Hole	89
7.3.1	Standard Phase Transition Case	89
7.3.2	Reentrant Phase Transition Case	93
7.4	Discussions	96
8	Final Remarks	99
8.1	Conclusions	99
8.2	Future Directions	100
	Appendix	103
	References	107
	List of publications	119

List of Figures

2.1	Gibbs free energy plot and coexistence diagram for Hawking Page transition	20
2.2	Gibbs free energy plot and coexistence diagram for the phase transition of charged AdS black hole	21
4.1	The effective potential for the regular Hayward black hole.	41
4.2	The behaviour of photon sphere parameters with temperature for Hayward black hole.	42
4.3	The behaviour of photon sphere parameters with pressure for Hayward black hole.	42
4.4	The behaviour of photon sphere parameters along the coexistence curve for Hayward black hole	44
4.5	Change in photon sphere parameters along the coexistence curve for Hayward black hole.	44
4.6	Near critical point behaviours of the change of the photon orbit parameters during the black hole phase transition for Hayward black hole.	45
4.7	The behaviour of photon sphere parameters with temperature for Bardeen black hole.	48
4.8	The behaviour of photon sphere parameters with pressure for Bardeen black hole.	48
4.9	The behaviour of photon sphere parameters along the coexistence curve for Bardeen black hole.	49
4.10	Change in photon sphere parameters along the coexistence curve for Bardeen black hole.	49
4.11	Near critical point behaviours of the change of the photon orbit parameters during the black hole phase transition for Bardeen black hole.	50

5.1	The order parameter vs reduced temperature ($\varphi - \chi$) plot of Hayward AdS black hole	57
5.2	The Ruppeiner scalar curvature vs reduced temperature ($R - \chi$) plot for Hayward AdS black hole	61
6.1	Phase structure of Hayward-AdS black hole.	69
6.2	The behaviour of volume change $\Delta V_r = V_{rl} - V_{rs}$ during phase transition of the Hayward black hole.	69
6.3	The behaviour of the normalised curvature scalar R_N against the reduced volume V_r at constant temperature.	71
6.4	6.4(a): The sign changing curve, the coexistence curve and spinodal curves. 6.4(b): The behaviour of normalised curvature scalar R_N along the coexistence line.	72
6.5	The numerical fit of $\ln R_N $ vs. $\ln(1 - T_r)$	73
7.1	The behaviour of the Gibbs free energy G for the standard phase transition (SPT) case.	83
7.2	The coexistence curve and the spinodal curve for the SPT of the Born-Infeld black hole.	83
7.3	The behaviour of the Gibbs free energy G for the reentrant phase transition case.	86
7.4	Phase diagrams for reentrant phase transition case.	87
7.5	The behaviour of the normalised Ruppeiner curvature scalar R_N with the reduced volume V_r at a constant temperature for SPT.	90
7.6	7.6(a): The sign changing curve, spinodal curve and the coexistence curve for SPT. 7.6(b): The behaviour of normalised Ruppeiner curvature scalar R_N along the coexistence curve.	91
7.7	The fitting curves of $\ln R_N$ vs $\ln(1 - T_r)$ near the critical point.	92
7.8	The behaviour of the normalised curvature scalar R_N against the volume V_r at constant temperature T_r for the RPT case.	94
7.9	7.9(a): The sign changing curve, spinodal curve and the coexistence curve for the RPT case. 7.9(b): The behaviour of normalised curvature scalar R_N along the transition line of first-order and zeroth-order phase transition.	95

List of Tables

7.1	The critical values P_c and T_c for different values of b corresponding to the SPT of the black hole.	84
7.2	The values of (P_{c0}, T_{c0}) , (P_{c1}, T_{c1}) , (P_t, T_t) and (P_z, T_z) for different b values, corresponding to the RPT of the black hole.	88
7.3	The values of α and β obtained by numerical fit for the SPT case.	93
7.4	The values of α and β obtained by numerical fit for the RPT case.	96

Chapter 1

Introduction

Physics is like sex: sure, it may give some practical results, but that is not why we do it.

Richard P. Feynman

At the time of writing this thesis, the Nobel prize in physics 2020 was awarded to Roger Penrose, “for the discovery that black hole formation is a robust prediction of the general theory of relativity”, and to Reinhard Genzel and Andrea Ghez, “for the discovery of a supermassive compact object at the centre of our galaxy.” Along with this and other recent developments like detection of gravitational waves and black hole shadow, ushered new astrophysical interests on black hole physics ([Abbott et al., 2016a,b,c](#); [Akiyama et al., 2019b,a,c](#)). However, the theoretical developments are far ahead of astrophysical observations due to the importance of black hole physics in several areas like quantum mechanics, quantum gravity and string theory. Black hole thermodynamics began with a quest for incorporating quantum mechanical nature to a black hole, which had purely classical origin in general relativity. Since the pioneering work in this regard by Hawking and Bekenstein, black hole thermodynamics remains an exciting topic in contemporary research.

The first step taken in establishing such a domain by Hawking and Bekenstein was by introducing temperature and entropy for a black hole, which are related to surface gravity κ and area of the black hole, respectively ([Hawking, 1975](#); [Bekenstein, 1972](#)). The four laws of black hole mechanics parallel to classical thermodynamics were soon proposed by taking the mass of the black hole as the internal energy ([Bekenstein, 1973, 1974](#); [Bardeen et al., 1973](#)). The importance of AdS black holes in black hole thermodynamics was realised in the early stages of these developments from the result that thermodynamically stable black

holes exist only in AdS space. This contrasts with the Minkowskian case, where the black hole has a negative specific heat and disappears by emitting Hawking radiation. This happens because the boundary of AdS space acts like walls of a thermal cavity. Inside this closed box-like space, below a certain temperature, only radiation can exist. Nevertheless, above that temperature, the radiation becomes unstable and hence collapses, resulting in the formation of black holes. The black holes thus formed, exists in two forms, larger ones with positive specific heat, which are locally stable, and smaller ones with negative specific heat, which are unstable. The phase transition between these black holes and radiation at the transition temperature is termed as Hawking-Page transition ([Hawking and Page, 1983](#); [Page, 2005](#)). In high energy physics, the topic AdS space got the attention of a larger audience after the proposal of AdS-CFT correspondence by [Maldacena \(1999\)](#). This gauge-gravity duality relates gravity theory in an AdS space to the conformal field theories at the boundary of that space. When Hawking Page transition is seen in the light of AdS-CFT language, it appears as the confinement/deconfinement phase transition in QCD ([Witten, 1998](#)).

It is interesting to note that the familiar PdV term is missing in the first law of black hole thermodynamics in the elementary approach. The hint for solving this riddle comes from the role of the cosmological constant in Einstein equations, where it gives the pressure term. The introduction of pressure term to black hole thermodynamics is done through *dynamical* cosmological constant Λ , which also has other fundamental implications like the consistency of Smarr relation with first law ([Kastor et al., 2009](#)). In this approach, the conjugate quantity of Λ is taken as the thermodynamic volume. The modified first law of thermodynamics with a PdV term gives a new interpretation to the mass of the black hole as enthalpy ([Dolan, 2011a](#)). The new perspective on mass and cosmological constant in black hole thermodynamics resulted in phenomenal consequences, enabling one to establish newer analogies with the well-known phenomena in classical thermodynamics. Understanding AdS black hole as a replica of van der Waals system by [Kubiznak and Mann \(2012a\)](#) was a milestone in this regard ¹. It is found that the critical exponents corresponding to the critical behaviour of van der Waals fluid and charged AdS black holes belongs to a universality class. i.e. the mean field exponents of the phase transitions are identical in these systems. Since then, many studies were conducted on various AdS black holes in different contexts but with universal

¹In fact, the first progress beyond Hawking Page phase transition happened after the identification of a rich phase structure isomorphic to van der Waals liquid-gas system in RN-AdS black hole ([Chamblin et al., 1999a,b](#)) and Kerr RN-AdS black hole ([Caldarelli et al., 2000](#)).

features. As a result of these new developments, a new research domain was established, known as the *black hole chemistry* (Kubizňák et al., 2017).

In black hole physics, one of the most intriguing questions is whether it has a microscopic structure. As Boltzmann said, “If you can heat it, it has microscopic structure,” which is one of the simplest and elegant answers to this question. As the black hole absorbs or emits matter, its Hawking temperature changes, which suggests that the black hole must have a microstructure. By studying these phase transitions, the microstructure of the black hole can be investigated through thermodynamic geometry methods. Ruppeiner geometry has proven to be quite useful and interesting to probe the interactions of a black hole from its macroscopic thermodynamic properties (Ruppeiner, 2008). In this technique, a line element which is the measure of the distance between two neighbouring fluctuation states, is defined in an appropriate parametric space (Ruppeiner, 1995). The curvature scalar constructed using this line element is an indicator of the nature of the microstructure of the system, a positive sign for repulsive and a negative sign for attractive interactions. The interpretation of this correspondence in black hole physics is adopted from the results obtained by the applications of Ruppeiner geometry to ordinary thermodynamic systems.

Combining the idea of the dynamic cosmological constant in black hole chemistry with the thermodynamic geometry, a new method of investigating the black hole microstructure was proposed by Wei et al. (Wei and Liu, 2015). In this method, mass and pressure were taken as the coordinates of the parameter space, and a new concept of the number density of black hole molecules was introduced. The most spectacular outcome of this construction was the existence of a repulsive interaction in the microstructure of a charged AdS black hole. Despite the substantial generalisations and applications of this method, the scalar curvature thus constructed was lacking the characteristic divergence behaviour near the critical point. This imperfection compared to the earlier geometrical methods called for a re-analysis of the basic setting of the methodology. Recently, a new revised method to rectify the above shortcoming was proposed by Wei et al. within the framework of Ruppeiner geometry (Wei et al., 2019a,b). The vital issue lurking in previous attempts were the non-independence of the thermodynamic variables entropy and volume for a spherically symmetric AdS black hole. This leads to a vanishing specific heat, and hence a singularity in line element and a divergent curvature scalar. In the new approach, treating the specific heat as a tiny constant close to zero and employing the temperature and volume as fluctuation coordinates, a

normalised curvature scalar was defined to probe the black hole microstructure. The new curvature scalar aptly features the critical phenomena and microstructure interactions of the black hole with universal properties.

It is worth noting that the investigation of the microstructure of the black hole system has been one of the major challenges in black hole physics for the past few decades. Even though string theory and loop quantum gravity provide tools to understand quantum gravity, there is no complete theoretical description for it. Therefore the microscopic physics of black holes is confined to some phenomenological approaches. However, when we seek the nature of microstructure, we do not have a clear picture of the black hole constituents; we take an abstract concept that black holes are constituted of black hole molecules.

1.1 Objectives of the Thesis

The primary objective of this thesis is to study the phase transitions and to probe the underlying microstructure of black holes in the anti-de Sitter spacetime. Our research mainly focuses on:

- Investigating the critical phenomena of the charged AdS black holes using the Landau theory of phase transition. Perceiving black hole phase transition in different pictures.
- Understanding the phase structure of the black hole. Obtaining mean-field exponents and order parameters that characterise the black hole phase transition.
- Studying the connection between gravity and thermodynamics of AdS black holes via null geodesics, both analytically and numerically.
- Addressing the challenges in applying thermodynamic geometry to a spherically symmetric AdS black hole using novel methods.
- Probing the nature of microstructure interaction in AdS black holes using the Ruppeiner geometric method.
- Studying the reentrant phase transition in an AdS black hole system and probing the underlying microstructure via a geometric method.
- Devising numerical techniques to implement the above objectives to the black hole systems without analytical solutions.

1.2 Organisation of the Thesis

The thesis is organised as follows:

Chapter 1: This chapter gives a brief introduction to the thesis. The chapter also includes the scope and objectives of the research and organisation details of the thesis.

Chapter 2: Here, we present a comprehensive view of black hole thermodynamics spanning over the pioneer works to contemporary researches. The elements of black hole thermodynamics are followed by their extension to anti-de Sitter spacetime. The extended phase space thermodynamics and critical phenomena of black holes are briefly discussed.

Chapter 3: In this chapter, the thermodynamic geometry is discussed to investigate the microstructure of a thermodynamic system. The novel Ruppeiner method to probe the microstructure of spherically symmetric AdS black hole in the parameter space of temperature and volume is discussed.

Chapter 4: The connection between thermodynamic phase transition and gravity is investigated using null geodesics. The study is carried out for Hayward AdS black hole analytically and for Bardeen AdS black hole numerically. The orbit parameters of the photon orbits are shown to be the order parameters that characterise the black hole phase transition.

Chapter 5: Here, the phase structure of a regular Hayward black hole is studied. The small-large black hole phase transition analogous to the first order van der Waals liquid-gas transition is understood from the Landau theory of phase transition. The phase transition is understood as a transition between different potential phases of the black hole.

Chapter 6: The microstructure of the Hayward AdS black hole is investigated using the novel Ruppeiner geometry method. The nature and strength of the black hole microstructure interaction are phenomenologically understood from the Ruppeiner curvature scalar.

Chapter 7: The reentrant phase transition in the Born-Infeld black hole is studied in detail. The underlying microstructure is investigated by using the Ruppeiner geometry method. We show that the reentrant phase transition arises from a different microstructure than that of a standard phase transition (van der Waals like).

Chapter 8: The thesis is summarised here with a discussion on results and future research.

Chapter 2

Ingredients of Black Hole Chemistry

If I have seen further, it is by standing on the shoulders of giants.

Isaac Newton

Summary

In this chapter, we outline the fundamentals of black hole chemistry. The basics of black hole thermodynamics in AdS spacetime is presented.

In physics, thermodynamics is a general and powerful tool to understand the physical properties of a system and a wide range of phenomena. The simplicity of thermodynamics lies in its inherent property that the microscopic details are not necessary to explore macroscopic physics. This property is particularly useful in dealing with the systems for which the microscopic details are not well understood, such as quantum gravity. Therefore, the lack of complete knowledge of the quantum aspects of a black hole offers a perfect scenario for the application of thermodynamics to probe its microscopic details.

Black holes being thermodynamic systems, exhibit a rich class of phase transitions, which are the key tools in probing their properties in black hole chemistry. The quite interesting facet of black hole thermodynamics is the phase transition and related phenomenon in AdS spaces. In recent times the interest in AdS black hole thermodynamics aroused among the researchers after the identification of the cosmological constant with the thermodynamic pressure and the modification in the first law by including the corresponding variations ([Kastor et al., 2009](#); [Dolan, 2011b](#)). With this association, it was demonstrated that the phase transition features of AdS black holes could be seen as van der Waals like and/or reentrant phase transitions (RPT) ([Kubiznak and Mann, 2012a](#); [Gunasekaran et al., 2012](#); [Kubiznak](#)

et al., 2017).

The purpose of this chapter is to sketch the foundations of black hole chemistry. To begin with, we will briefly review the conventional black hole thermodynamics. The Smarr relation for asymptotically flat and asymptotically AdS black holes are presented. With the motivation of the inclusion of dynamical cosmological constant in black hole thermodynamics, we will discuss the methods to obtain the first law of black hole mechanics in AdS spacetime. The rich thermodynamic properties that emerge from this extended version of thermodynamics are presented in the black hole chemistry section. The presentation in this chapter is inspired by Ref. (Hennigar, 2018; Mbarek, 2019; Mann, 2015)

2.1 Standard Black Hole Thermodynamics

The laws of black hole mechanics can be summarised as follows (Bardeen et al., 1973):

- **Zeroth law:** The surface gravity κ of a stationary black hole is constant over the event horizon.
- **First law:** When a black hole system changes from one stationary state to another, the differences in mass is equal to differences in area times the surface gravity plus additional work terms.

$$dM = \frac{\kappa}{8\pi}dA + \Omega dJ + \Phi dQ + \dots \quad (2.1)$$

Where M is mass, Q is the charge, A is event horizon area, J is angular momentum, $\Phi = \Phi_+ - \Phi_\infty$ is conjugate potential, $\Omega = \Omega_+ - \Omega_\infty$ is the angular velocity of the black hole. The subscripts $+$ and ∞ corresponds to black hole horizon and infinity, respectively.

- **Second law:** The area of the event horizon of a black hole never decreases through any classical process, i.e. $dA \geq 0$.
- **Third law:** No procedure can reduce the surface gravity to zero by a finite number of steps. i.e. $\kappa_n > \kappa_{n+1} > 0, n < \infty$. In other words, it is impossible to create an extremal black hole in a finite number of steps.

Classically speaking, the above laws demonstrate the connection between ordinary thermodynamics and black hole mechanics. In fact, the first such connection was developed as

a result of the works due to Hawking and Bekenstein (Hawking, 1975; Bekenstein, 1972, 1973). In his pioneering work, Bekenstein argued that a black hole does possess entropy, which is proportional to the area of the event horizon via the area law. However, the constant of proportionality was fixed later by Hawking, in his demonstration that a black hole can emit radiation. Using the quantum field theory calculations in curved spacetime, Hawking showed that the radiating black hole has a characteristic temperature,

$$T = \frac{\hbar\kappa}{k_B 2\pi c}, \quad (2.2)$$

where the physical constants have the usual meaning. The comparison of $\kappa\delta A$ term in the first law of black hole mechanics with the $T\delta S$ term in ordinary thermodynamics yields the identification of entropy with the area, which turns out to be,

$$S = \frac{Ac^3}{4\hbar G}. \quad (2.3)$$

The presence of \hbar in the above expressions for temperature and entropy, indeed a clear indication of the quantum mechanical nature of the black holes.

In short, in standard black hole we have the following parallels

Energy	E	\longleftrightarrow	M	Mass
Temperature	T	\longleftrightarrow	κ	Surface gravity
Entropy	S	\longleftrightarrow	A	Horizon area

2.2 Smarr Relations for Black Holes

In formulating the laws of black hole mechanics, one of the key elements that was used is Smarr relation, the integral mass formula. For the Kerr black hole, Smarr observed that (Smarr, 1973), the first law of black hole mechanics, which is the differential mass formula,

$$dM = \mathcal{T} dA + \Omega dJ + \Phi dQ, \quad (2.4)$$

where \mathcal{T} is the effective surface tension, can be written in the integral form as,

$$M = 2TS + 2\Omega J + \Phi Q. \quad (2.5)$$

The Smarr formula is analogous to the Gibbs-Duhem relation in conventional thermodynamics. The integration of Eq. 2.4 to obtain Eq. 2.5 was possible as the black hole mass M is a homogeneous function of (A, J, Q) , and is done using the Euler's homogeneous function theorem. In conventional thermodynamics, this procedure is carried out by regarding energy as a homogeneous function of extensive thermodynamic variables. It is also worth noting that the Smarr formula is not restricted to a particular black hole solution, say Kerr, or dimension. Bardeen, Carter and Hawking have shown that this relation is valid for generic black hole solutions, and it arises from the basic geometry of the black holes. Myers and Perry later demonstrated that this relation exists even in higher dimensions (Myers and Perry, 1986).

2.2.1 Smarr Formula for Asymptotically Flat Black Holes

Smarr formula can be derived in two methods, a simple scaling argument method using dimensional analysis and Euler's theorem, and a rigorous geometric method using the Komar integrals. We will demonstrate both methods in this subsection.

Method 1

For a D dimensional stationary black hole of mass $M = M(S, J)$, the simple dimensional analysis yields the following length dimensions for its parameters,

$$M \propto [L]^{D-3}, \quad S \propto [L]^{D-2}, \quad J \propto [L]^{D-2}. \quad (2.6)$$

Under the scaling $L \rightarrow \alpha L$, we have

$$M \rightarrow \alpha^{D-3} M, \quad S \rightarrow \alpha^{D-2} S, \quad J \rightarrow \alpha^{D-2} J. \quad (2.7)$$

With these scale transformation law, the relation $M = M(S, J)$ read as,

$$\alpha^{D-3} M = M(\alpha^{D-2} S, \alpha^{D-2} J), \quad (2.8)$$

which, after differentiating with respect to α gives,

$$(D-3)\alpha^{D-4}M = (D-2)\frac{\partial M}{\partial(\alpha^{D-2}S)}\alpha^{D-3}S + (D-2)\frac{\partial M}{\partial(\alpha^{D-2}J)}\alpha^{D-3}J. \quad (2.9)$$

By setting $\alpha = 1$ we have the Smarr formula,

$$(D-3)M = (D-2)TS + (D-2)\Omega J, \quad (2.10)$$

where,

$$T = \frac{\partial M}{\partial S}, \quad \text{and} \quad \Omega = \frac{\partial M}{\partial J}. \quad (2.11)$$

Method 2

We begin by considering a black hole solution which is stationary and axisymmetric, so that the spacetime has two Killing vectors, say t^α and φ^α . The combination of Killing vectors,

$$\zeta^\alpha = t^\alpha + \Omega\varphi^\alpha, \quad (2.12)$$

is a null vector on the event horizon of the black hole, where Ω is its angular velocity. Let's denote the surface gravity as κ , which is constant all over the event horizon. The quantity ζ^α satisfies the relation,

$$\zeta_\beta \zeta^{\alpha;\beta} = \kappa \zeta^\alpha, \quad (2.13)$$

on the event horizon. Consider a spatial slice Σ , extending from the event horizon to spacial infinity, which has future directed normal n^α . On this hyper surface Σ we integrate,

$$I = \int_\Sigma d\Sigma_\alpha \nabla_\beta \nabla^\beta \zeta^\alpha. \quad (2.14)$$

We evaluate the above integration in two ways. In the first approach we use the relation $\nabla_\beta \nabla^\beta \zeta^\alpha = -R^\alpha_{\beta\gamma} \zeta^\gamma$, which follows from the fact that ζ^α is a Killing vector. Assuming that the vacuum Einstein equations hold, this leads to,

$$\int_\Sigma d\Sigma_\alpha \nabla_\beta \nabla^\beta \zeta^\alpha = - \int_\Sigma d\Sigma_\alpha R^\alpha_{\beta\gamma} \zeta^\gamma = 0. \quad (2.15)$$

In the second approach, we make use of Stokes' theorem. For an anti-symmetric tensor $B^{\alpha\beta}$, the Stokes' theorem is given by (Poisson, 2009),

$$\int_{\Sigma} dA_{\alpha} \nabla_{\beta} B^{\alpha\beta} = \frac{1}{2} \oint_{\partial\Sigma} dS_{\alpha\beta} B^{\alpha\beta}. \quad (2.16)$$

The integration over $\partial\Sigma$ includes two $(D-2)$ dimensional surfaces, S_{∞} and \mathcal{H} . Where, the boundary of the spatial slice Σ at the spacial infinity is denoted as S_{∞} , and at the event horizon as \mathcal{H} . Combining the results of two approaches, we have,

$$0 = \oint_{\mathcal{H}} dS_{\alpha\beta} \nabla^{\alpha} \zeta^{\beta} - \oint_{S_{\infty}} dS_{\alpha\beta} \nabla^{\alpha} \zeta^{\beta}. \quad (2.17)$$

The integration at the spatial infinity can be expressed in terms of the total mass and angular momentum, by exploiting the fact that we are assuming a vacuum solution. The total mass and angular momentum of the spacetime are given by the Komar integrals, which in D dimensions read as, (Poisson, 2009),

$$M = -\frac{1}{16\pi G_N} \left(\frac{D-2}{D-3} \right) \oint_{S_{\infty}} dS_{\alpha\beta} \nabla^{\alpha} t^{\beta}, \quad (2.18)$$

$$J = \frac{1}{16\pi G_N} \oint_{S_{\infty}} dS_{\alpha\beta} \nabla^{\alpha} \varphi^{\beta}. \quad (2.19)$$

where, G_N is the Newton's constant in D dimensions. Using these Komar integrals, the integration at the spacial infinity S_{∞} reduces to the following form,

$$\oint_{S_{\infty}} dS_{\alpha\beta} \nabla^{\alpha} \zeta^{\beta} = 16\pi \left[\Omega_{HJ} - \left(\frac{D-3}{D-2} \right) M \right]. \quad (2.20)$$

Now we turn to evaluate the integral on the horizon. Here, we make use of the fact that, $dS_{\alpha\beta} = 2\zeta_{[\alpha} N_{\beta]} \sqrt{\sigma} d^{D-2}x$, wherein N^{α} normalised null vector on the horizon such that $\zeta_{\alpha} N^{\alpha} = -1$ and σ is the determinant of the induced metric on the event horizon. With these inputs, we have

$$\oint_{\mathcal{H}} dS_{\alpha\beta} \nabla^{\alpha} \zeta^{\beta} = 2 \oint_{\mathcal{H}} \sqrt{\sigma} d^{D-2}x \zeta_{\alpha} N_{\beta} \nabla^{\alpha} \zeta^{\beta} \quad (2.21)$$

$$= 2\kappa \oint_{\mathcal{H}} \sqrt{\sigma} d^{D-2}x N_{\beta} \zeta^{\beta} \quad (2.22)$$

$$= -2\kappa A. \quad (2.23)$$

In simplifying the above equations first we used the relation $\nabla^\alpha \zeta^\beta = -\nabla^\beta \zeta^\alpha$, since ζ^α is a Killing vector, which simplifies the contraction with the surface element. After that we used the earlier relation $\zeta_\alpha \nabla^\alpha \zeta^\beta = \kappa \zeta^\beta$, which brings the surface gravity term κ . Finally, the remaining integration is carried out by using the relation $N_\beta \zeta^\beta = -1$ which gives the area of the event horizon. Combining the integrations that we evaluated over S_∞ and \mathcal{H} we get,

$$(D-3)M = (D-2) \frac{\kappa A}{8\pi} + (D-2)\Omega_H J. \quad (2.24)$$

Identifying the terms $T = \kappa/2\pi$ and $S = A/4$, we have the Smarr formula, which is the same as that we obtained using scaling arguments.

2.2.2 Smarr Formula for AdS Black Holes

In obtaining the Smarr formula for an asymptotically flat black hole, via the geometric method, we have made use of the assumption of vacuum Einstein equations with a vanishing cosmological constant. This suggests that there may arise issues when we consider a non zero cosmological constant in deriving the Smarr formula, which we will address in this subsection.

We will first show how the difference arises and then we will present the correct Smarr formula using both the scaling argument and geometric method. For simplicity we consider the four dimensional Schwarzschild-AdS black hole, which has the metric

$$ds^2 = -f(r)dt^2 + \frac{dr^2}{f(r)} + r^2 d\Omega^2. \quad (2.25)$$

The metric function is given by

$$f(r) = 1 - \frac{m}{r} + \frac{r^2}{l^2} \quad (2.26)$$

where l is the AdS length, which is related to the cosmological constant as $\Lambda = -\frac{3}{l^2}$. The temperature and entropy of the black hole can easily be obtained as

$$T = \frac{1}{4\pi r_+} \left[1 + \frac{3r_+^2}{l^2} \right], \quad S = \pi r_+^2, \quad (2.27)$$

where r_+ is the horizon radius. However the calculation of mass requires more detailed consideration.

What we expect naturally is that the conserved quantity corresponding to the Killing vector $t^\alpha = \delta_t^\alpha$ to be the mass, but that is an issue with that natural assumption. To calculate the conserved charge, we note the non vanishing components of the entity $\nabla^\alpha t^\beta$, which is

$$\nabla^t t^r = -\nabla^r t^t = -\frac{m}{2r^2} - \frac{r}{l^2}. \quad (2.28)$$

The usual definition of the Komar integral gives a diverging result,

$$M = -\frac{1}{8\pi} \oint_{S_\infty} dS_{\alpha\beta} \nabla^\alpha t^\beta = \frac{1}{4} \lim_{R_0 \rightarrow \infty} \oint_{S_{R_0}} R_0^2 \left(\frac{m}{2R_0^2} + \frac{R_0}{l^2} \right) \sin\theta d\theta d\varphi \rightarrow \infty. \quad (2.29)$$

The above divergence is clearly due to the inclusion of cosmological constant, which contributes an infinite amount of energy. We can overcome this issue by terminating the integral at a finite region R_0 , and then subtract the $m = 0$ contribution, and then take the finite cutoff to infinity. This calculation yields,

$$M = \frac{m}{2}. \quad (2.30)$$

However, the mass, temperature and entropy we obtained do not satisfy the Smarr formula we obtained in the previous subsection, as,

$$M - 2TS = -\frac{r_+^3}{l^2} \neq 0. \quad (2.31)$$

This discrepancy of Smarr formula in AdS spacetime calls for a reconsideration with a careful analysis of the cosmological constant term. We will obtain the modified Smarr formula using two methods as follows.

Method 1

The failure of the Smarr formula in the AdS spacetime that we encountered is due to abandoning the role of the cosmological constant. Caldarelli, Cognola and Klemm were the first group of researchers to verify the extended Smarr formula via scaling arguments for spinning AdS black holes in the context of AdS/CFT correspondence (Caldarelli et al., 2000). Using the scaling arguments with the consideration of cosmological constant, we obtain the extended Smarr relation,

$$(D-3)M = (D-2)TS + (D-2)\Omega J - 2VP, \quad (2.32)$$

where we have defined a pressure term, which is associated with the cosmological constant as,

$$P = -\frac{\Lambda}{8\pi}. \quad (2.33)$$

The scaling argument with cosmological constant gives another additional quantity, which is conjugate to the pressure term and termed as thermodynamic volume due to its dimension,

$$V := \frac{\partial M}{\partial P}. \quad (2.34)$$

For the case of the 4-dimensional Schwarzschild-AdS black hole we have,

$$P = \frac{3}{8\pi l^2}, \quad \text{and} \quad V = \frac{4\pi}{3} r_+^3. \quad (2.35)$$

The Smarr relation for this spacetime has the form,

$$M = 2(TS - PV). \quad (2.36)$$

Having obtained the extended Smarr relation using scaling arguments, it is natural to seek the geometrical construction for the same, as we have done in the case of the asymptotically flat black hole, which sets our next task.

Method 2

The main ingredient of the geometric method in AdS spacetime is to introduce a Killing potential, which is done by [Kastor \(2008\)](#), using which the extended Smarr formula can be obtained ([Kastor et al., 2009](#)). We begin by considering a static black hole solution for simplicity. As the relation $\nabla_\alpha \zeta^\alpha = 0$ is satisfied by a Killing vector ζ^α , from the Poincare lemma we can write the vector ζ^α as,

$$\zeta^\alpha = \nabla_\beta \omega^{\beta\alpha}, \quad (2.37)$$

wherein, the anti symmetric tensor $\omega^{\alpha\beta} = \omega^{[\alpha\beta]}$ is the Killing potential. With this definition of Killing potential and the assumption of vacuum Einstein equations, one can easily show that,

$$\int_{\partial\Sigma} dS_{\alpha\beta} \left(\nabla^\alpha \zeta^\beta + \frac{2}{D-2} \Lambda \omega^{\alpha\beta} \right) = 0, \quad (2.38)$$

where the integration is performed on the boundary of a hyper-surface Σ . As in the previous calculations the integration is the sum of two contributions, one from the sphere at infinity S_∞ and the other at a cross section of the event horizon \mathcal{H} .

The evaluation of the integral at infinity requires the knowledge of asymptotic behaviour of the AdS spacetime, which is studied by Henneaux and Teitelboim (Henneaux and Teitelboim, 1985). Detailed discussion on this is also presented in Ref. (Ashtekar and Magnon, 1984; Ashtekar and Das, 2000). The asymptotic behaviour for a static black hole is given by,

$$ds^2 = \left(-f_0 + \frac{c_t}{r^{D-3}}\right) dt^2 + \frac{1}{f_0} \left(1 - \frac{(D-1)(D-2)c_r}{2\Lambda r^{D-1}}\right) dr^2 + \left(1 + \frac{2\Lambda}{(D-1)(D-2)} \frac{c_\theta}{r^{D-1}}\right) r^2 d\Omega_{D-2}^2, \quad (2.39)$$

with

$$f_0 = 1 - \frac{2\Lambda}{(D-1)(D-2)} r^2. \quad (2.40)$$

If we consider the case of Einstein equations with negative Λ and localised stress energy source with no angular momentum, we can show that $c_t = c_r = m$ and $c_\theta = 0$. Then the large r behaviour of the metric reduces to the Schwarzschild AdS black hole metric,

$$ds^2 = -f(r) dt^2 + \frac{1}{f(r)} dr^2 + r^2 d\Omega_{D-2}, \quad (2.41)$$

with the metric function,

$$f(r) = 1 - \frac{m}{r^{D-3}} - \frac{2\Lambda r^2}{(D-1)(D-2)}. \quad (2.42)$$

The non zero components of the Killing potential now reads as

$$\omega_{r \rightarrow \infty}^{rt} = -\omega_{r \rightarrow \infty}^{tr} = \frac{r}{D-1}, \quad (2.43)$$

and

$$\nabla^r \zeta^t = -\nabla^t \zeta^r = \frac{(D-3)m}{2r^{D-2}} - \frac{2\Lambda r}{(D-1)(D-2)}. \quad (2.44)$$

With the aid of these, the integration at the infinity simplifies, as the term with Killing potential and the divergence term. The remaining part of the integral is,

$$\int_{S_\infty} dS_{\alpha\beta} \left(\nabla^\alpha \zeta^\beta + \frac{2}{D-2} \Lambda \omega^{\alpha\beta} \right) = -16\pi \frac{D-3}{D-2} M. \quad (2.45)$$

The integration on the cross section of the horizon gives,

$$\int_{\mathcal{H}} dS_{\alpha\beta} \left(\nabla^{\alpha} \zeta^{\beta} + \frac{2}{D-2} \Lambda \omega^{\alpha\beta} \right) = -2\kappa A + \frac{2\Lambda}{D-2} \left(\int_{\mathcal{H}} dS_{\alpha\beta} \omega^{\alpha\beta} \right), \quad (2.46)$$

where the first term is obtained as in the case of asymptotically flat spacetime. Putting all the above results together, we have the extended Smarr formula,

$$(D-3)M = (D-2)TS - 2PV, \quad (2.47)$$

where we have identified the pressure and volume terms as,

$$P = -\frac{\Lambda}{8\pi G_N}, \quad \text{and} \quad V = -\frac{1}{2} \int_{\mathcal{H}} dS_{\alpha\beta} \omega^{\alpha\beta}. \quad (2.48)$$

The generalisation of the above derivation to include angular momentum is straightforward (Cvetič et al., 2011).

2.3 Black Hole Thermodynamics in AdS Spacetime

We follow the Hamiltonian formalism to derive the first law of black hole mechanics in AdS spacetime (Mann, 2015). It follows from considering the Killing vector l^a to be the generator of a Killing horizon and taking an appropriate space-like hyper-surface Σ . We begin with the relation, $g_{\alpha\beta} = -n_{\alpha}n_{\beta} + h_{\alpha\beta}$ where $n_{\alpha}n^{\alpha} = -1$ and $n^{\alpha}h_{\alpha\beta} = 0$. The contraction of Einstein tensor with a unit normal yields,

$$H = -16\pi G_N T_{\alpha\beta} n^{\alpha} n^{\beta}, \quad H_{\alpha} = -16\pi G_N T_{\sigma\beta} n^{\sigma} h_{\alpha}^{\beta}. \quad (2.49)$$

Considering the cosmological constant Λ as the only source of stress energy, we get $H = -2\Lambda$ and $H_{\alpha} = 0$. If we consider the evolution of the system along the vector field $\xi^{\alpha} = Nn^{\alpha} + N^{\alpha}$, where $n_{\alpha}N^{\alpha} = 0$, then the total gravitational Hamiltonian is $\mathcal{H} = \sqrt{h}[N(H + 2\Lambda) + N^{\alpha}H_{\alpha}]$. $N = -\zeta \cdot n$ denotes the lapse function and N^{α} the shift, which is tangential to Σ . These functions tell how to relate coordinates between two slices: the lapse measures the proper time, while the shift measures changes in the spatial coordinates. Considering the perturbation $h_{\alpha\beta} \rightarrow h_{\alpha\beta} + s_{\alpha\beta}$, $\pi^{\alpha\beta} \rightarrow \pi^{\alpha\beta} + p^{\alpha\beta}$ ($\pi^{\alpha\beta}$ is the conjugate momentum) and $\Lambda \rightarrow \Lambda + \delta\Lambda$, and performing

a straightforward calculation, we get,

$$N\delta H + N^\alpha \delta H_\alpha = -D_\alpha B^\alpha = -2N\delta\Lambda, \quad (2.50)$$

where

$$B^\alpha = N\left(D^\alpha s - D_\beta s^{\alpha\beta}\right) - sD^\alpha N + s^{\alpha\beta}D_\beta N + \frac{1}{\sqrt{h}}N^\beta\left(\pi^{\sigma\rho}s_{\sigma\rho}h_\beta^\alpha - 2\pi^{\alpha\sigma}s_{\beta\sigma} - 2p_\beta^\alpha\right). \quad (2.51)$$

Since $N = -n_\alpha \zeta^\alpha = -n_\alpha \nabla_\beta \omega^{\beta\alpha} = -D_\beta(n_\alpha \omega^{\beta\alpha})$, we have,

$$D_\alpha\left(B^\alpha + 2\omega^{\alpha\beta}n_{\alpha\beta}\delta\Lambda\right) = 0 \Rightarrow I := \oint_{\partial\Sigma} dA_\alpha\left(B^\alpha + 2\omega^{\alpha\beta}n_\beta\delta\Lambda\right) = 0. \quad (2.52)$$

The anti-symmetric tensor $\omega^{\alpha\beta}$ is called the Killing potential. The integration over $\partial\Sigma$ includes two boundaries, one at the black hole horizon and the other at infinity. The evaluation of the integral at infinity, with suitable arguments, leads to,

$$\oint_{S_\infty} dA_\alpha B^\alpha = -16\pi G_N \delta M - \lim_{r \rightarrow \infty} \left(\frac{2r^{D-1}\Omega_{D-2}}{D-1}\right) \delta\Lambda \quad (2.53)$$

and

$$\oint_{S_\infty} dA_\alpha\left(2\omega^{\alpha\beta}n_\beta\delta\Lambda\right) = \lim_{r \rightarrow \infty} \left(\frac{2r^{D-1}\Omega_{D-2}}{D-1}\right) \delta\Lambda. \quad (2.54)$$

We note that the term due to the Killing potential exactly cancels the divergence arising from the variation in Λ . At the black hole horizon, we obtain

$$\oint_h dA_\alpha B^\alpha = 2\kappa\delta A, \quad (2.55)$$

where A is horizon area and κ is the surface gravity. We re-write the term with Killing potential as,

$$\oint_h dA_\alpha\left(2\omega^{\alpha\beta}n_\beta\delta\Lambda\right) = 2\left(\oint_h dA_\alpha 2\omega^{\alpha\beta}n_\beta\right) \delta\Lambda. \quad (2.56)$$

Combining the above results we obtain the first law of black hole thermodynamics as,

$$\delta M = \frac{\kappa}{2\pi} \frac{\delta A}{4} + V\delta P = T\delta S + V\delta P, \quad (2.57)$$

where we have identified the pressure and volume terms as,

$$P = -\frac{\Lambda}{8\pi G_N} \quad \text{and} \quad V = -\oint_h dA_\alpha \omega^{\alpha\beta} n_\beta. \quad (2.58)$$

This is consistent with the Smarr relation, $M = 2(TS - PV)$, which we obtained in previous section. Recalling from classical thermodynamics that the enthalpy $H = E + PV$ satisfies $\delta H = T\delta S + V\delta P$, we note that, in extended thermodynamics, the mass of the black hole should be regarded as enthalpy rather than internal energy.

2.4 Black Hole Chemistry

The inclusion of thermodynamic pressure and volume terms into black hole thermodynamics leads to extended black hole thermodynamics, which enables us to see black hole phase transitions parallel to everyday thermodynamic phenomena. The familiar phase transitions such as van der Waals like, solid/liquid transition, triple point transition, reentrant transition have replicas in the context of black hole phase transition. In this section, we present some of the classic examples for the above. We work in a canonical ensemble, where the black hole charge Q or the angular momentum J is fixed. In this scenario, the thermodynamic potential turn out to be the Gibbs free energy G , and the thermodynamic stability of the system is given by the specific heat C_P , which are defined as follows,

$$G = M - TS = G(P, T, J, Q), \quad \text{and} \quad C_P = T \left(\frac{\partial S}{\partial T} \right)_{P, J, Q}. \quad (2.59)$$

In the following sections we will present Hawking-Page and van der Waals like phase transitions. A detailed discussion on reentrant phase transition will be presented in chapter 7.

Hawking-Page Phase Transition

This is the simplest phase transition exhibited by a black hole. Let us consider the metric of a four dimensional spherically symmetric black hole,

$$ds^2 = -f(r)dt^2 + \frac{dr^2}{f(r)} + r^2 d\Omega^2, \quad (2.60)$$

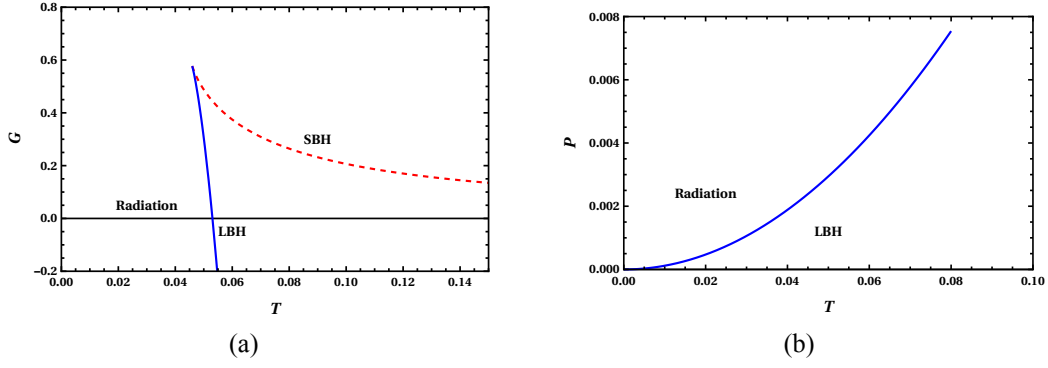


Figure 2.1: Gibbs free energy plot and coexistence diagram for Hawking Page transition

where,

$$f(r) = 1 - \frac{2M}{r} + \frac{r^2}{l^2}. \quad (2.61)$$

The corresponding thermodynamic quantities are,

$$M = \frac{r_+}{2} \left(1 + \frac{r_+^2}{l^2} \right), \quad S = \pi r_+^2, \quad T = \frac{l^2 + 3r_+^2}{4\pi l^2 r_+}, \quad P = \frac{3}{8\pi l^2}, \quad V = \frac{4}{3}\pi r_+^2. \quad (2.62)$$

The Gibbs free energy can be obtained as,

$$G = M - TS = \frac{4}{3}\pi P r_+^3 - \pi r_+^2 T + \frac{r_+}{2}. \quad (2.63)$$

The Gibbs free energy plotted in Fig 2.1(a) has a discontinuity in its first derivative, implying a first-order phase transition. The system undergoes a first-order phase transition between a radiation state and a large black hole state. This phase transition is known as Hawking-Page transition (Hawking and Page, 1983). The specific heat of the SBH (small black hole) branch is negative and hence corresponds to a thermodynamically unstable state. On the other hand, the LBH (large black hole) branch has a positive specific heat, and it is thermodynamically stable. The coexistence between the radiation and black hole states can be obtained by the condition $G = 0$, which is represented in Fig 2.1(b). The coexistence line of radiation/black hole resembles that of solid/liquid phase transition (Kubiznak and Mann, 2015).

Van der Waals Phase Transition

Charged black holes show phase transition which is analogous to Van der Waals system (Chamblin et al., 1999a; Kubiznak and Mann, 2012b). Consider the metric of four dimen-

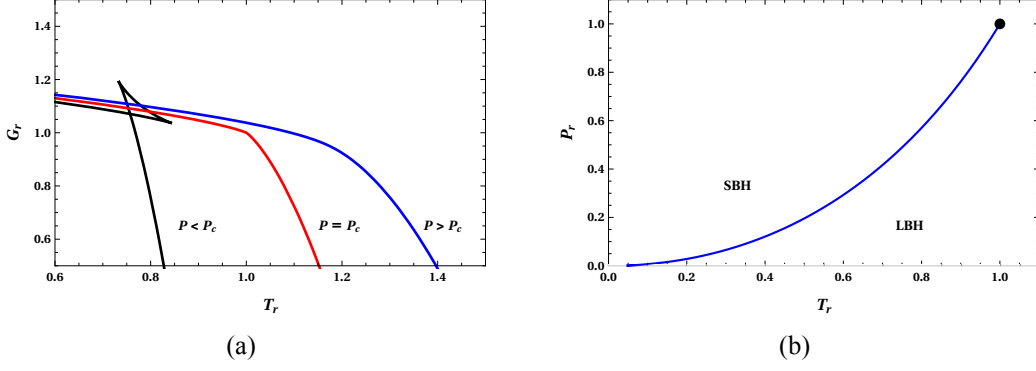


Figure 2.2: Gibbs free energy plot and coexistence diagram for vdW like phase transition of charged AdS black hole

sional charged AdS black hole,

$$ds^2 = -f(r)dt^2 + \frac{dr^2}{f(r)} + r^2 d\Omega^2, \quad (2.64)$$

where,

$$f(r) = 1 - \frac{2M}{r} + \frac{Q^2}{r^2} + \frac{r^2}{l^2}. \quad (2.65)$$

The corresponding thermodynamic quantities are (Kubiznak and Mann, 2012b; Dolan, 2011b),

$$M = \frac{4}{3}\pi Pr^3 + \frac{Q^2}{2r} + \frac{r}{2}, \quad S = \pi r_+^2, \quad T = \frac{l^2(r_+^2 - Q^2) + 3r_+^2}{4\pi l^2 r_+^3}, \quad P = \frac{3}{8\pi l^2}, \quad V = \frac{4}{3}\pi r_+^2, \quad \varphi = \frac{Q}{r_+}. \quad (2.66)$$

The Gibbs free energy in the canonical ensemble can be obtained as,

$$G = M - TS = -\frac{1}{3}2\pi Pr^3 + \frac{3Q^2}{4r} + \frac{r}{4}. \quad (2.67)$$

The behaviour of this thermodynamic potential G is shown in Fig 2.2(a). The observed swallow tail behaviour is the signature of a vdW like first-order phase transition. The black hole undergoes a transition between the small black hole and large black hole phases. This behaviour disappears at the critical point, which is characterised by,

$$P_c = 1/96\pi Q^2, \quad T_c = \sqrt{6}/18\pi Q, \quad v_c = 2\sqrt{6}Q. \quad (2.68)$$

At this point the the phase transition becomes second order. The coexistence of SBH and LBH phases is depicted in Fig 2.2(b), which is analogous to liquid-gas states coexistence of a vdw fluid.

Chapter 3

Ruppeiner Geometry and Black Hole Microstructures

Let no one ignorant of geometry enter.

Engraved at the door of Plato's Academy

Summary

This chapter outlines the elements of Ruppeiner geometry. The construction of the Ruppeiner curvature scalar and its connection to black hole microstructure is discussed.

In the pioneering work of Hawking and Bekenstein, it was shown that a black hole is not only a gravity system but also a thermal system. A black hole possesses temperature and entropy, which are related to its surface gravity and event horizon area, respectively. The success of black hole thermodynamics in understanding various aspects of the black hole prompts us to formulate some relation between micro-dynamics and thermodynamics. Inspired by this, several approaches have been developed to probe the microscopic origin of black hole thermodynamics, which we will sketch in this section. Unlike a conventional thermodynamic system, where the macroscopic quantities are constructed from the microscopic knowledge of the system, the statistical investigation of the black hole is carried out in a reverse order. The microstructure of the black hole is scrutinised from its macroscopic thermodynamic quantities by studying the phase transitions.

It is a well-established notion that the geometrical methods can serve as a tool to understand microscopic interaction in a thermal system. It was Weinhold who constructed the first thermodynamic geometry method by considering internal energy as the thermodynamic

potential (Weinhold, 1975a). Later, by choosing entropy as the thermodynamic potential, another nifty geometrical method was introduced by Ruppeiner, starting from Boltzmann entropy formula (Ruppeiner, 1995). Essentially, the geometrical methods were developed from Gaussian thermodynamic fluctuation theory, in which a metric is constructed by choosing a suitable thermodynamic potential in a phase space which constitutes other thermodynamic variables; the corresponding curvature scalar encodes details about phase transitions and critical points. This method was used in analysing the conventional thermal systems like ideal fluids, van der Waals (vdW) systems, Ising models, quantum gases etc. (Ruppeiner, 1979; Janyszek, 1990; Ruppeiner, 1981; Janyszek and Mrugala, 1989, 1990; Oshima et al., 1999; Mirza and Mohammadzadeh, 2008; May et al., 2013a). The results so obtained give a very clear picture of the applicability of the geometrical methods in understanding microscopic details. The two main aspects of Ruppeiner geometry is the revelation of correlation and the interaction type of the microstructure. The sign of the curvature scalar is an indicator of the nature of the interaction, positive/negative for repulsive/attractive interaction and zero for no interaction. On the other hand, the magnitude of the curvature scalar is the measure of the correlation length of the system. As the correlation length diverges near the critical point of the system, so does the curvature scalar.

As the entropy is taken to be the thermodynamic potential in Ruppeiner geometry, the application of it to the black hole system is straight forward and interesting (see Ref. (Ruppeiner, 2014) for a recent review on this). An early accomplishment of this method is to the BTZ black holes (Cai and Cho, 1999). Later, the nature of microstructure of the Reissner-Nordstrom (RN) black hole was sought for using this method (Aman et al., 2003), where the curvature scalar R vanishes and no interaction was found. However, a non-vanishing R was expected as the spacetime is curved. This problem was re-examined by considering a complete set of thermodynamic variables, to begin with, including the angular momentum and cosmological constant, and taking appropriate limit for RN black hole (Mirza and Zamani-Nasab, 2007), which led to a non-vanishing R . In subsequent developments, the vdW like behaviour of the black hole and the underlying microscopic details were investigated using the geometrical methods (Sahay et al., 2010; Chaturvedi et al., 2017; Wei et al., 2017; Chaturvedi et al., 2018). In this so-called R -crossing method, the coordinates of the parameter space are taken as temperature and fluid density, and the diverging behaviour of R can be observed. However mismatch in the divergence of curvature scalar and specific heat

in some cases using this method, led to the proposal of several other geometrical methods (Quevedo, 2007; Liu et al., 2010; Niu et al., 2012; Wei and Liu, 2013; Banerjee and Roychowdhury, 2012; Mansoori and Mirza, 2014; Mo et al., 2013; Mansoori et al., 2015; Hendi and Naderi, 2015; Dolan, 2015; Mansoori et al., 2016; Hosseini Mansoori and Mirza, 2019; Banerjee et al., 2011a,b).

As we mentioned in the introductory chapter, combining the idea of the dynamic cosmological constant in black hole chemistry with the thermodynamic geometry, a new method of investigating the black hole microstructure was proposed by Wei et al. (Wei and Liu, 2015). The parameter space was constructed by using the fluctuation coordinates, mass and pressure. For the first time, the concept of black hole molecule was introduced here, and the number density of black hole molecules were found to be an order parameter for the phase transition. The most important finding of this construction was the finding of a repulsive interaction in the microstructure of a charged AdS black hole. Soon, this method was adopted to investigate various aspects of black hole microstructure by several researchers (Guo et al., 2019; Du et al., 2020; Dehyadegari et al., 2017; Chabab et al., 2018; Deng and Huang, 2017; Kord Zangeneh et al., 2018; Miao and Xu, 2018, 2019; Chen et al., 2019; Xu et al., 2020a; Naveena Kumara et al., 2019, 2021b). However, the interdependence of thermodynamic variables temperature and volume was not addressed here, requiring more serious intervention.

The application of Ruppeiner geometry to spherically symmetric black holes in AdS background poses some serious challenges compared to those in asymptotically flat spacetimes. This is because of the interdependence of the thermodynamic variables, entropy (S) and volume (V), via the horizon radius, which results in a vanishing heat capacity at constant volume and adiabatic compressibility. These vanishing quantities cause a singularity in the line element and thus, resulting in a diverging curvature scalar in Ruppeiner geometry. To address this issue, an efficient method is to introduce a normalised curvature scalar by considering the vanishing response function as a constant whose value is close to zero (see Ref. (Xu et al., 2020b) for an alternate approach). This restores the missing information in the curvature scalar associated with the microstructure and critical phenomena of the black hole. A first of such remedy was presented by Wei et al. (2019a), where a normalised universal metric was constructed to study the microstructure interaction by choosing the fluctuation coordinates as temperature and volume. When applied to a conventional van der

Waals system, this method gives expected results, where the dominant interaction among the fluid molecules is always attractive in all of the phases. Surprisingly RN-AdS black holes showed deviation from this behaviour, wherein a repulsive dominant interaction was also observed for certain physical conditions (Wei et al., 2019a,b). Subsequent studies show that the black hole microstructure exhibits richer properties than a conventional thermodynamic system. Therefore this novel method promptly captured much attention (Wei and Liu, 2020b; Naveena Kumara et al., 2020b; Wei and Liu, 2020a; Wu et al., 2020; Xu et al., 2020b; Ghosh and Bhamidipati, 2020b,a; Yerra and Bhamidipati, 2020; Dehyadegari et al., 2020). In this chapter, we present this novel method, following the pioneering articles (Wei et al., 2019a,b)

3.1 First Laws and Ruppeiner Geometry

We begin by considering the Boltzmann's entropy formula,

$$S = k_B \ln \Omega, \quad (3.1)$$

where k_B is Boltzmann constant, and Ω is the number of microstates of the thermodynamic system under consideration. The inverse relation of the above equation is the starting point of the thermodynamic fluctuation theory.

Consider a thermodynamic system which has two independent variables, say x^0 and x^1 . Then the probability that the system can be found in a state which is characterised by the coordinates in the intervals $x^0 + dx^0$ and $x^1 + dx^1$ is proportional to the number of microscopic states Ω ,

$$P(x^0, x^1) dx^0 dx^1 = C \Omega(x^0, x^1) dx^0 dx^1, \quad (3.2)$$

where C is a normalisation constant. From Eqs. 3.1 and 3.2 we have,

$$P(x^0, x^1) \propto e^{S/k_B}. \quad (3.3)$$

To set up the Ruppeiner geometry, we consider two subsystems of an isolated thermodynamic system having a total entropy S . The smaller subsystem is assigned with an entropy S_B and the larger subsystem with entropy S_E . Viewing the larger subsystem as a thermal

bath, we can take $S_B \ll S_E \approx S$. Therefore, if the system is described by a set of independent variables x^0 and x^1 ,

$$S(x^0, x^1) = S_B(x^0, x^1) + S_E(x^0, x^1). \quad (3.4)$$

When the system is in thermal equilibrium, the entropy S is in its local maximum S_0 . Taylor expanding the entropy in the neighbourhood of the local maximum $x^\mu = x_0^\mu$, we obtain

$$S = S_0 + \left. \frac{\partial S_B}{\partial x^\mu} \right|_{x_0^\mu} \Delta x_B^\mu + \left. \frac{\partial S_E}{\partial x^\mu} \right|_{x_0^\mu} \Delta x_E^\mu + \frac{1}{2} \left. \frac{\partial^2 S_B}{\partial x^\mu \partial x^\nu} \right|_{x_0^\mu} \Delta x_B^\mu \Delta x_B^\nu + \frac{1}{2} \left. \frac{\partial^2 S_E}{\partial x^\mu \partial x^\nu} \right|_{x_0^\mu} \Delta x_E^\mu \Delta x_E^\nu + \dots \quad (3.5)$$

Since the first derivatives vanish for the equilibrium condition, we have

$$\begin{aligned} \Delta S = S - S_0 &= \frac{1}{2} \left. \frac{\partial^2 S_B}{\partial x^\mu \partial x^\nu} \right|_{x_0^\mu} \Delta x_B^\mu \Delta x_B^\nu + \frac{1}{2} \left. \frac{\partial^2 S_E}{\partial x^\mu \partial x^\nu} \right|_{x_0^\mu} \Delta x_E^\mu \Delta x_E^\nu + \dots \\ &\approx \frac{1}{2} \left. \frac{\partial^2 S_B}{\partial x^\mu \partial x^\nu} \right|_{x_0^\mu} \Delta x_B^\mu \Delta x_B^\nu, \end{aligned} \quad (3.6)$$

where we have truncated the higher order terms and the second term. The second term is negligible compared to the first term, as the entropy S_E of the thermal bath is close to that of the whole system, and its second derivative with respect to the intensive variables x^μ are smaller than those of S_B .

In Ruppeiner geometry, the entropy S is taken as the thermodynamical potential, and its fluctuation ΔS is related to the line element Δl^2 , which is the measure of the distance between two neighbouring fluctuation states of the thermodynamic system (Ruppeiner, 1995). The Ruppeiner line element is given by,

$$\Delta l^2 = -\frac{1}{k_B} g_{\mu\nu}^R \Delta x^\mu \Delta x^\nu, \quad (3.7)$$

where k_B is the Boltzmann constant and the metric $g_{\mu\nu}^R$ is,

$$g_{\mu\nu}^R = \frac{\partial^2 S_B}{\partial x^\mu \partial x^\nu}. \quad (3.8)$$

Since the line element is related to the distance between the neighbouring fluctuation states, the metric $g_{\mu\nu}^R$ must be encoded with the microscopic details of the system.

Riemannian Geometry

Under the transformation $x^\mu \rightarrow x'^\mu$ the entity $g_{\mu\nu}^R$ (we will drop the superscript R now onwards) transforms as follows (Landau and Lifshitz, 1980),

$$g_{\mu\nu} = \frac{\partial x^\rho}{\partial x'^\mu} \frac{\partial x^\sigma}{\partial x'^\nu} g_{\rho\sigma}. \quad (3.9)$$

This is exactly like the transformation of the metric tensor in Riemannian geometry. Which implies that the distance between two neighbouring fluctuating states, Δl^2 can be treated as the distance between two neighbouring states in the state space. This motivates us to calculate the curvature scalar in the parameter space, as the information in Riemannian geometry is contained in scalar curvature. We have the following conventional definitions,

$$\Gamma_{\mu\nu}^\lambda = \frac{1}{2} g^{\rho\lambda} (\partial_\mu g_{\rho\nu} + \partial_\nu g_{\mu\rho} - \partial_\rho g_{\mu\nu}) \quad (3.10)$$

$$R_{\alpha\beta\gamma}^\rho = \partial_\beta \Gamma_{\alpha\gamma}^\rho - \partial_\gamma \Gamma_{\alpha\beta}^\rho + \Gamma_{\alpha\gamma}^\delta \Gamma_{\beta\delta}^\rho - \Gamma_{\alpha\beta}^\delta \Gamma_{\gamma\delta}^\rho \quad (3.11)$$

$$R_{\mu\nu} = R_{\mu\alpha\nu}^\alpha, \quad R = g^{\mu\nu} R_{\mu\nu}. \quad (3.12)$$

In a two dimensional space, the curvature scalar R is given by,

$$R = -\frac{1}{\sqrt{g}} \left[\frac{\partial}{\partial x^0} \left(\frac{g_{01}}{g_{00}\sqrt{g}} \frac{\partial g_{00}}{\partial x^1} - \frac{1}{\sqrt{g}} \frac{\partial g_{11}}{\partial x^0} \right) + \frac{\partial}{\partial x^1} \left(\frac{2}{\sqrt{g}} \frac{\partial g_{01}}{\partial x^1} - \frac{1}{\sqrt{g}} \frac{\partial g_{00}}{\partial x^1} - \frac{g_{01}}{g_{00}\sqrt{g}} \frac{\partial g_{00}}{\partial x^0} \right) \right], \quad (3.13)$$

where g is the determinant of the metric $g_{\mu\nu}$. For a diagonal metric the above expression reduces to,

$$R = \frac{1}{\sqrt{g}} \left[\frac{\partial}{\partial x^0} \left(\frac{1}{\sqrt{g}} \frac{\partial g_{11}}{\partial x^0} \right) + \frac{\partial}{\partial x^1} \left(\frac{1}{\sqrt{g}} \frac{\partial g_{00}}{\partial x^1} \right) \right]. \quad (3.14)$$

In the following sections we will show that this scalar curvature plays an important role in probing the microstructure of a thermodynamic system.

First law and Ruppeiner geometry

In this subsection, we will exploit the Ruppeiner geometry from the perspective of the first law of thermodynamics. We begin by considering the first law for a thermodynamic system,

$$dU = TdS - PdV + \sum_i y_i dx^i, \quad (3.15)$$

where x^i and y^i are the thermodynamic variables and conjugate potentials, respectively. Absorbing the PdV term into the summation we have,

$$dU = TdS + \sum_i y_i dx^i. \quad (3.16)$$

In Ruppeiner geometry, the entropy S is taken as the thermodynamical potential, therefore we change the above relation to,

$$dS = \frac{1}{T}dU - \sum_i \frac{y_i}{T}dx_i, \quad (3.17)$$

With the intensive and extensive quantities being, respectively,

$$x^\mu = (U, V, \dots), \quad y_i = (-P, \dots), \quad (3.18)$$

where the indices run as $\mu = 0, 1, 2, 3..$ and $i = 1, 2, 3, \dots$. From equation 3.17 we have the quantity $z_\mu = \frac{\partial S}{\partial x^\mu}$, which reads as,

$$z_\mu = \left(\frac{1}{T}, -\frac{y_i}{T} \right), \quad (3.19)$$

using which Eq. 3.17 can be written as,

$$dS = z_\mu dx^\mu. \quad (3.20)$$

And the line element Δl^2 can now be expressed as,

$$\Delta l^2 = -\Delta z_\mu \Delta x^\mu. \quad (3.21)$$

Using Eq. 3.19 we have,

$$\Delta z_0 = \Delta \left(\frac{1}{T} \right) = -\frac{1}{T^2} \Delta T, \quad (3.22)$$

$$\Delta z_i = \Delta \left(-\frac{y_i}{T} \right) = \frac{y_i}{T^2} \Delta T - \frac{1}{T} \Delta y_i. \quad (3.23)$$

Substituting these, the line element Δl^2 takes the form,

$$\Delta l^2 = \frac{1}{T} \Delta T \Delta S + \frac{1}{T} \Delta y_i \Delta x^i. \quad (3.24)$$

We have two choices to consider the fluctuation coordinates, (T, x^i) and (T, y_i) . We will consider these two cases separately.

(T, x^i) as fluctuation coordinates

The typical examples for this case are the parameter space of (T, V) and (T, ρ) , where ρ is the density of the system. We will first investigate the appropriate potential for the description of these parameter spaces, and then we will obtain the specific form of the line element. As the fluctuation coordinates are T and x^i , the thermodynamic potential must be the Helmholtz free energy $F = U - TS$. We have,

$$dF = -SdT + y_i dx^i, \quad (3.25)$$

and the relation,

$$\frac{\partial S}{\partial x^i} = -\frac{\partial y_i}{\partial T}. \quad (3.26)$$

We can express ΔS and Δy_i in terms of the independent variables as,

$$\Delta S = \left(\frac{\partial S}{\partial T}\right) \Delta T + \left(\frac{\partial S}{\partial x^i}\right) \Delta x^i, \quad (3.27)$$

$$\Delta y_i = \left(\frac{\partial y_i}{\partial T}\right) \Delta T + \left(\frac{\partial y_i}{\partial x^j}\right) \Delta x^j. \quad (3.28)$$

Combining the Eqs. 3.24, 3.26, 3.27 and 3.28 we have,

$$\Delta l^2 = \frac{1}{T} \left(\frac{\partial S}{\partial T}\right) \Delta T^2 + \frac{1}{T} \left(\frac{\partial y_i}{\partial x^j}\right) \Delta x^i \Delta x^j. \quad (3.29)$$

This can be expressed in terms of the Helmholtz free energy, by using the relations $S = -\partial_T F$ and $y_i = \partial_{x^i} F$ which are evident from Eq.3.25, as

$$\Delta l^2 = -\frac{1}{T} \left(\frac{\partial^2 F}{\partial T^2}\right) \Delta T^2 + \frac{1}{T} \left(\frac{\partial^2 F}{\partial x^i \partial x^j}\right) \Delta x^i \Delta x^j. \quad (3.30)$$

The corresponding curvature scalar can be easily obtained from this line element for the fluctuation coordinates (T, V) and (T, ρ) .

(T, y^i) as fluctuation coordinates

The typical example for this choice is (T, P) parameter space. For this case, the thermodynamic potential of the geometry is,

$$W = U - TS - y_i x^i, \quad (3.31)$$

and the differential reads as,

$$dW = -SdT - x^i dy_i. \quad (3.32)$$

From the above expression we have,

$$S = -\frac{\partial W}{\partial T}, \quad x^i = -\frac{\partial W}{\partial y_i}. \quad (3.33)$$

Then the expansions of ΔS and Δx^i in terms of the independent coordinates T and y_i are,

$$\Delta S = \left(\frac{\partial S}{\partial T}\right) \Delta T + \left(\frac{\partial S}{\partial y_i}\right) \Delta y_i \quad (3.34)$$

$$\Delta x^i = \left(\frac{\partial x^i}{\partial T}\right) \Delta T + \left(\frac{\partial x^i}{\partial y_j}\right) \Delta y_j \quad (3.35)$$

Using these results, the line element takes the form,

$$\Delta l^2 = -\frac{1}{T} \left(\frac{\partial^2 W}{\partial p_\mu \partial p_\nu}\right) \Delta p_\mu \Delta p_\nu, \quad (3.36)$$

where $p_\mu = (T, y_i)$.

3.2 Scalar Curvature and Phase Transition

In this section, we develop the connection between the Ruppeiner curvature scalar and phase transition. For a fluid system, the Ruppeiner curvature scalar diverges at the critical point of phase transition. While applying the Ruppeiner geometry method to a black hole system, we expect this behaviour. Therefore the investigation of black hole microstructure properties develops through the study of black hole phase transition. Apart from this, the sign of the curvature scalar tells the nature of interaction in the microstructure. A positive sign indicates

repulsive interaction, and a negative sign signifies an attractive interaction.

Here we consider the fluctuation coordinates T and x for simplicity. The extensive variable x can be the volume V , charge Q or angular momentum J of the black hole. For this choice, the metric is diagonal and from Eq. 3.30 we have,

$$g_{\mu\nu} = \frac{1}{T} \begin{pmatrix} -\left(\frac{\partial^2 F}{\partial T^2}\right)_x & 0 \\ 0 & \left(\frac{\partial^2 F}{\partial x^2}\right)_T \end{pmatrix} = \frac{1}{T} \begin{pmatrix} -\left(\frac{\partial S}{\partial T}\right)_x & 0 \\ 0 & \left(\frac{\partial y}{\partial x}\right)_T \end{pmatrix}. \quad (3.37)$$

In fact, the line element can be expressed in terms of the specific heat,

$$C_x = T \left(\frac{\partial S}{\partial T} \right)_x, \quad (3.38)$$

as

$$dl^2 = \frac{C_x}{T^2} dT^2 + \frac{(\partial_{xy})_T}{T} dx^2. \quad (3.39)$$

From Eq. 3.14, the corresponding scalar curvature can be easily obtained as,

$$R = \frac{1}{2C_x^2 (\partial_{xy})^2} \{ T(\partial_{xy}) [(\partial_T C_x)(\partial_{xy} - T\partial_{T,xy})] + C_x [(\partial_{xy})^2 + T((\partial_x C_x)(\partial_{x,xy}) - T(\partial_{T,xy})^2) + 2T(\partial_{xy})(-(\partial_{x,x} C_x) + T(\partial_{T,T,xy}))] \}. \quad (3.40)$$

From the above expression it is clear that, the scalar curvature R diverges when $C_x = 0$ or $(\partial_{xy})_T = 0$. For a van der Waals like phase transition, the critical point is given by,

$$(\partial_{xy})_T = (\partial_{x,xy})_T = 0. \quad (3.41)$$

Therefore the divergence of the scalar curvature at the critical point is always guaranteed. This behaviour gives a possible connection between the Ruppeiner curvature scalar and the correlation length, which goes to infinity at the critical point.

Taking temperature T and volume V as the fluctuation coordinates the, i.e. $x = V$ and $y = -P$, the line element 3.39 takes the form,

$$dl^2 = \frac{C_V}{T^2} dT^2 - \frac{(\partial_V P)_T}{T} dV^2. \quad (3.42)$$

where C_V is the heat capacity at constant volume. The Ruppeiner curvature scalar can be

obtained directly from Eq. 3.42 by using the conventional definitions of Riemannian geometry.

However, the metric associated with the line element (3.42) is not invertible as $g_{TT} = 0$ or $g^{TT} = \infty$. This is due to the fact that the heat capacity C_V vanishes for a spherically symmetric AdS black hole system. This, in turn, arises from the interdependence of the thermodynamic variables, namely entropy and volume. To overcome this issue, a normalised Ruppeiner scalar is defined as (Wei et al., 2019a),

$$R_N = C_V R \tag{3.43}$$

where R is the curvature scalar calculated from Eq. 3.42. The normalised curvature scalar diverges at the critical point of phase transition.

The normalised curvature scalar R_N can be now used to probe the microstructure of the black hole. Before concluding this section, we reiterate the following.

- The sign of R_N reveals the nature of dominant interaction in the black hole microstructure. Positive/negative for repulsive/attractive and zero for no interaction.
- The absolute value of R_N is the measure of the average number of correlated constituents, in general. For a black hole system, this could be the average number of correlated black hole molecules.

Chapter 4

Photon Orbits and Thermodynamic Phase Transition of AdS Black Holes

When you have to shoot, shoot, don't talk!

Tuco, *The Good, the Bad, and the Ugly*

Summary

This chapter is based on our published work in Phys. Rev. D. ([Naveena Kumara et al., 2020a](#)). We probe the phase structure of the regular anti-de Sitter (AdS) black holes using the null geodesics. The radius of photon orbit and minimum impact parameter shows a nonmonotonous behaviour below the critical values of the temperature and the pressure, corresponding to the phase transition in extended phase space. The respective differences of the radius of unstable circular orbit and the minimum impact parameter can be seen as the order parameter for the small-large black hole phase transition, with a critical exponent $1/2$. Our study shows that there exists a close relationship between the gravity and thermodynamics for the regular AdS black holes.

4.1 Introduction

The characteristic features of the material particle in the very vicinity of the event horizon can be utilized to unveil the information encoded in the concerned black hole. This motivation leads us to directly link the analysis of the particle motions, that are affected by the strong gravity near the compact objects such as a black hole, neutron stars etc., to the black hole properties. The study of geodesics of a test particle plays a vital role in the understanding of some observational effects such as the strong gravitational lensing and black

hole silhouette, as well as quasinormal modes (Cardoso et al., 2009; Stefanov et al., 2010). Attempts to unravel the vdW phase transition of a black hole through astrophysical observations has its roots in quasinormal mode (QNM) studies (Liu et al., 2014). In these studies, it was reported that during the SBH-LBH phase transition, the slope of the quasinormal mode changes drastically.

Prompted by the study relating the dynamics and thermodynamics, in the context of AdS black holes, recently there were attempts to establish a relationship between the gravity and thermodynamics (Wei and Liu, 2018; Wei et al., 2019c). The correlation between the gravity and the critical behaviour is seen through the unstable null geodesic, which is encoded with the phase transition details. The radius of the photon sphere and the minimum impact parameter of the photon orbit exhibits an oscillatory behaviour during the vdW phase transition. Above the critical point of phase transition, the behaviour of these quantities become monotonous. This is analogous to the behaviour of Hawking temperature with horizon radius and entropy. Another significant result is that the respective differences in the radius and the minimum impact parameters act as an order parameter for SBH-LBH phase transition with a critical exponent $1/2$. The phase transition is scrutinised using photon orbit method for several black holes in different spacetime backgrounds (Xu et al., 2019; Chabab et al., 2020; Li et al., 2020; Han et al., 2018; Hegde et al., 2020). Studies related to null geodesics in other contexts have also appeared in subsequent works (Zhang et al., 2019; Chandrasekhar and Mohapatra, 2019; Wei and Liu, 2019).

The Penrose censorship conjecture states the existence of singularity dressed by an event horizon (Hawking and Penrose, 1970; Hawking and Ellis, 2011). Therefore all the electrovacuum solutions of Einstein general relativity are in accordance with such point of view. However, such conjectures do not forbid us to consider the regular black hole spacetimes free from the singularity. Regular black holes were proposed to overcome such singular points, where the central singularity is replaced by a repulsive de-Sitter core. In this regard, motivated by the ideas of Sakharov (Sakharov, 1966) and Gliner (Gliner, 1966), Bardeen proposed first regular black hole solution (Bardeen, 1968). The subsequent study of all the regular black holes was inspired by Bardeen's idea (Hayward, 2006; Ayon-Beato and Garcia, 1998, 2000). Later Ayon-Beato-Garcia found the first exact regular black hole solution of Einstein field equations coupled to a nonlinear electrodynamic source. Various properties such as the black hole thermodynamics (Man and Cheng, 2014, 2013), the rotating black hole

shadows (Abdujabbarov et al., 2016; Amir and Ghosh, 2016), quasinormal modes (Flachi and Lemos, 2013) as well as the strong gravitational lensing (Eiroa and Sendra, 2011) have been investigated in the background of regular black hole spacetimes. Some regular black hole solutions were also considered in alternative theories of gravity such as Lovelock gravity (Aros and Estrada, 2019) and massive gravity theories (Nam, 2018). Regular black holes have also been extended to higher dimensions, to study its horizon structure and thermodynamical properties (Ali and Ghosh, 2018; Kumar et al., 2019). In our recent work, we have investigated the microstructure of the regular Hayward black hole using the Ruppeiner geometry method, where we have reported the existence of repulsive interaction in the black hole microstructure (Naveena Kumara et al., 2021b, 2020b). In the present work, we study the phase transition of regular black holes in AdS spacetime by considering the correspondence between photon orbits and the extended phase space thermodynamics. We show the parametric effect induced in the black hole solution due to the presence of nonlinear charge.

The organisation of the chapter is as follows. In section 4.2, we discuss the phase transition of regular Hayward AdS black hole using the photon orbits. In section 4.3 we carry out a similar investigation for the regular Bardeen AdS black hole. Finally, we conclude the chapter in section 4.4.

4.2 Regular Hayward Black Hole

4.2.1 Thermodynamics of Regular Hayward Black Hole

The regular black hole solutions can be derived from Einstein gravity minimally coupled to nonlinear electrodynamics with negative cosmological constant Λ given by the action (Fan and Wang, 2016),

$$\mathcal{I} = \frac{1}{16\pi G} \int d^4x \sqrt{-\hat{g}} [R - \mathcal{L}(\mathcal{F}) + 2\Lambda], \quad (4.1)$$

where R and \hat{g} are the Ricci scalar and the determinant of the metric tensor, respectively. $\mathcal{L}(\mathcal{F})$ is the Lagrangian density of nonlinear electrodynamics which is a function of $\mathcal{F} = F_{\mu\nu}F^{\mu\nu}$ with $F_{\mu\nu} = 2\nabla_{[\mu}A_{\nu]}$, the strength tensor of nonlinear electrodynamics. The regular Hayward black hole solution can be obtained from the Lagrangian density,

$$\mathcal{L}(\mathcal{F}) = \frac{12}{\alpha} \frac{(\alpha\mathcal{F})^{3/2}}{(1 + (\alpha\mathcal{F})^{3/4})^2}, \quad (4.2)$$

with $\alpha > 0$ which has the dimension of length squared. For a spherically symmetric space-time, $F_{\mu\nu}$ admits two non-vanishing components, F_{tr} and $F_{\theta\phi}$. For a pure magnetic charge only $F_{\theta\phi}$ survives. The resulting Maxwell tensor reads with only component,

$$F_{\theta\phi} = -F_{\phi\theta} = -Q_m \sin\theta, \quad (4.3)$$

and hence the gauge potential and the Maxwell invariant for this field turn out to be,

$$A_\mu = Q_m \cos\theta \delta_\mu^\phi, \quad \mathcal{F} = \frac{2Q_m^2}{r^4}. \quad (4.4)$$

Here the constant Q_m is identified with the magnetic monopole charge of the nonlinear electrodynamics. The metric for a regular Hayward AdS black hole in four-dimensional space-time reads (Fan and Wang, 2016),

$$ds^2 = -f(r)dt^2 + \frac{1}{f(r)}dr^2 + r^2 d\Omega_2^2, \quad (4.5)$$

where $d\Omega_2^2 = d\theta^2 + \sin^2\theta d\phi^2$, is a 2-dimensional unit sphere, and the metric function,

$$f(r) = \left(1 - \frac{2Mr^2}{r^3 + g^3} - \frac{\Lambda r^2}{3}\right), \quad (4.6)$$

where M the mass of the black hole and g the free integration constant that is related to the magnetic charge Q_m through the relation $Q_m = g^2 / \sqrt{2\alpha}$.

Now, we briefly present the extended thermodynamics of the regular Hayward black hole. In extended phase space description, the pressure P is related to the cosmological constant Λ as (Kastor et al., 2009; Dolan, 2011b),

$$P = -\frac{\Lambda}{8\pi}. \quad (4.7)$$

The horizon of the black hole is characterised by the condition, $f(r_+) = 0$. Using this condition we get,

$$M = \frac{r_+}{2} + \frac{4}{3}\pi P(g^3 + r_+^3) + \frac{g^3}{2r_+^2}. \quad (4.8)$$

The Hawking temperature of the black hole which is associated to the surface gravity κ is

obtained as,

$$T = \frac{\kappa}{2\pi} = \frac{f'(r)}{4\pi} \Big|_{r=r_+} = \frac{2Pr_+^4}{g^3 + r_+^3} - \frac{g^3}{2\pi r_+(g^3 + r_+^3)} + \frac{r_+^2}{4\pi(g^3 + r_+^3)}. \quad (4.9)$$

With these, the first law of thermodynamics reads as,

$$dM = TdS + \Psi dQ_m + VdP + \Pi d\alpha, \quad (4.10)$$

where Ψ and Π are the variables conjugate to the magnetic charge Q_m and parameter α , respectively. The entropy and volume of the black hole have the following non trivial profile,

$$S = \int \frac{dM}{T} = 2\pi \left(\frac{r_+^2}{2} - \frac{g^3}{r_+} \right), \quad (4.11)$$

$$V = \left(\frac{\partial M}{\partial P} \right)_{S, Q_m, \alpha} = \frac{4}{3}\pi (g^3 + r_+^3). \quad (4.12)$$

We also note that the definition of entropy S for regular black hole is not unique, another choice of S from area law is also possible. Then we have to give up with the above first law, which is to be modified with a modified mass M (Ma and Zhao, 2014). However these do not alter the phase transition and related properties of the black hole. The equation of state reads as,

$$P = \frac{g^3}{4\pi r_+^5} + \frac{g^3 T}{2r_+^4} - \frac{1}{8\pi r_+^2} + \frac{T}{2r_+}. \quad (4.13)$$

The regular black hole exhibits a vdW like critical behaviour, which has been studied extensively in the literature (Fan, 2017). The first order phase transition takes place between a small black hole (SBH) phase and a large black hole (LBH) phase. The critical point of this phase transition is given by,

$$T_{cH} = \frac{(5\sqrt{2} - 4\sqrt{3})(3\sqrt{6} + 7)^{2/3}}{4 \times 2^{5/6} \pi g}, \quad (4.14)$$

$$P_{cH} = \frac{3(\sqrt{6} + 3)}{16 \times 2^{2/3} (3\sqrt{6} + 7)^{5/3} \pi g^2}, \quad (4.15)$$

$$S_{cH} = \left(6\sqrt{6} + 14\right)^{2/3} \pi g^2. \quad (4.16)$$

It is clear that the critical values of the thermodynamic variables depend on the parameter g . Using this, the reduced thermodynamic variables are defined as,

$$\tilde{T} = \frac{T}{T_{cH}} \quad \tilde{P} = \frac{P}{P_{cH}} \quad \tilde{V} = \frac{V}{V_{cH}}. \quad (4.17)$$

4.2.2 Geodesic equations of motion

To obtain the relationship between the null geodesics and the phase transition of the black hole we consider a free photon orbiting around the black hole on the equatorial plane, i.e., $\theta = \pi/2$. Then the Lagrangian is,

$$2\mathcal{L} = -f(r)\dot{t}^2 + \frac{\dot{r}^2}{f(r)} + r^2\dot{\phi}^2. \quad (4.18)$$

The dots over variables stand for the differentiation with respect to an affine parameter. The generalised momenta corresponding to this Lagrangian can easily be obtained as,

$$p_t = -f(r)\dot{t} \equiv E \quad (4.19)$$

$$p_\phi = r^2\dot{\phi} \equiv L \quad (4.20)$$

$$p_r = \dot{r}/f(r). \quad (4.21)$$

In the above, E and L are the energy and orbital angular momentum of the photon, respectively, which are the constants of motion. The t motion and ϕ motion can be written as,

$$\dot{t} = \frac{E}{f(r)} \quad (4.22)$$

$$\dot{\phi} = \frac{L}{r^2 \sin^2 \theta}. \quad (4.23)$$

The Hamiltonian for the system is,

$$2\mathcal{H} = -E\dot{t} + L\dot{\phi} + \dot{r}^2/f(r) = 0. \quad (4.24)$$

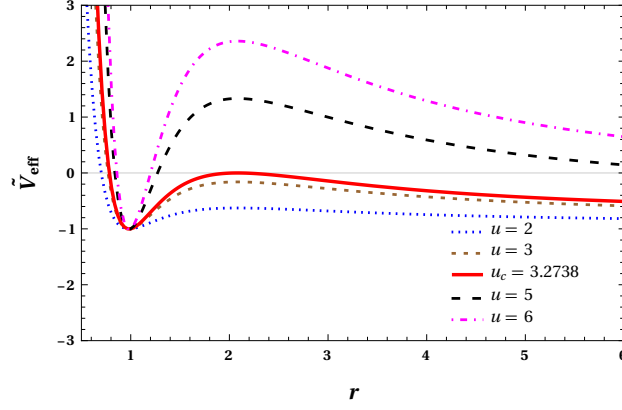


Figure 4.1: The effective potential for the regular Hayward black hole. Here we take black hole horizon $r_+ = 1$, charge parameter $g = 0.8$ and pressure $P = 0.003$. The thick red line corresponds to the critical angular momentum L_c (corresponding critical impact parameter u_c)

The expression for the radial r motion is rewritten as,

$$\dot{r}^2 + V_{eff} = 0 \quad (4.25)$$

where V_{eff} is the effective potential, which has the following explicit form,

$$V_{eff} = \frac{L^2}{r^2} f(r) - E^2. \quad (4.26)$$

The behaviour of $\tilde{V}_{eff} = V_{eff}/E^2$ is shown in Fig. 4.1 for different values of impact parameter $u = L/E$.

The accessible region for the photon is $V_{eff} < 0$, since $\dot{r}^2 > 0$. From the Fig. 4.1 it is clear that, the photon fall into the black hole for small values of u , whereas it is reflected for large values of u , as it approaches the black hole. Between these two conditions there is an unstable circular photon orbit which corresponds to the critical angular momentum (red thick line in Fig. 4.1). At the peak of that particular effective potential the radial velocity of the photon is zero. The corresponding value of r at the peak is the radius of the photon sphere. The unstable circular orbit is characterised by,

$$V_{eff} = 0 \quad , \quad V'_{eff} = 0 \quad , \quad V''_{eff} < 0, \quad (4.27)$$

where the prime denotes the differentiation with respect to r . Expanding the second equation ($V'_{eff} = 0$),

$$2f(r_{ps}) - r_{ps} \partial_r f(r_{ps}) = 0. \quad (4.28)$$

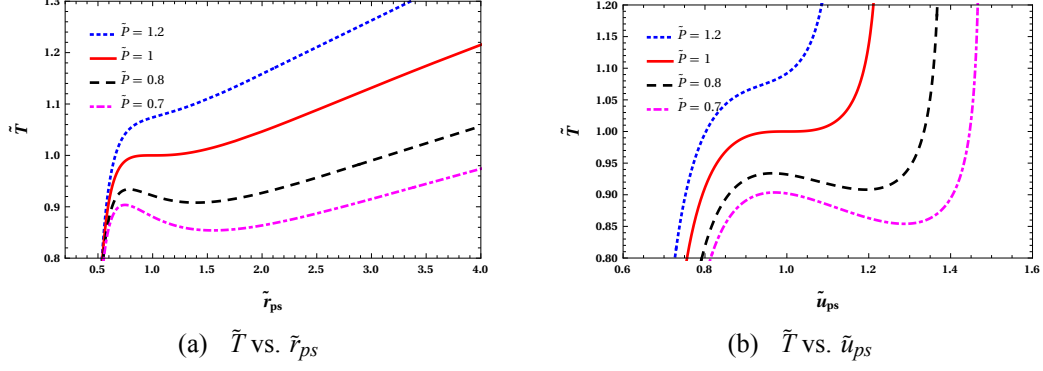


Figure 4.2: The behaviour of photon sphere radius r_{ps} and minimum impact parameter u_{ps} with temperature in reduced space for Hayward case. These plots are for the reduced pressure $\tilde{P} = 0.7, 0.8, 1, 1.2$

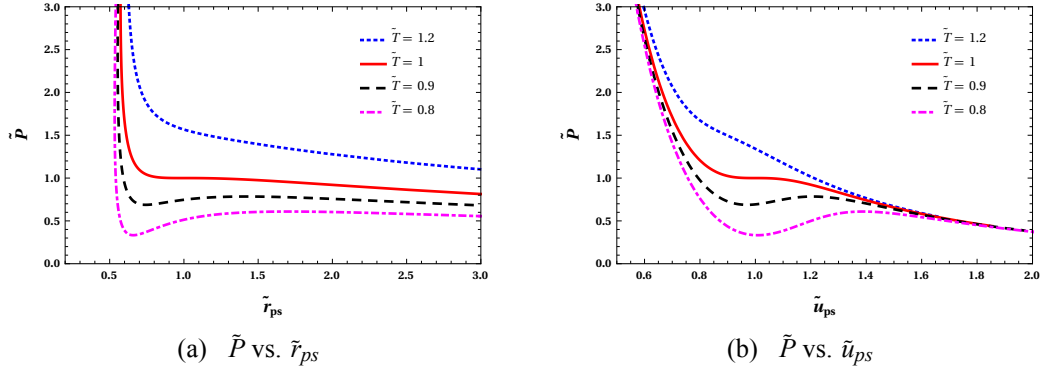


Figure 4.3: The behaviour of photon sphere radius r_{ps} and minimum impact parameter u_{ps} with pressure in reduced space for Hayward case. These plots are for the reduced temperature $\tilde{T} = 0.8, 0.9, 1, 1.2$

The solution of this gives the radius of photon sphere r_{ps} ,

$$r_{ps} = \frac{1}{4} \left(2 \sqrt{-\frac{8g^3M}{\sqrt[3]{Y}} + \frac{9M^2}{2} + \frac{27M^3}{4\sqrt{\frac{9M^2}{4} + X + \sqrt[3]{Y}}}} - \sqrt[3]{Y} + \sqrt{9M^2 + 4(X + \sqrt[3]{Y})} + 3M \right), \quad (4.29)$$

where,

$$X = \frac{8g^3M}{\sqrt[3]{27g^3M^3 + \sqrt{729g^6M^6 - 512g^9M^3}}}, \quad (4.30)$$

and

$$Y = 27g^3M^3 + \sqrt{729g^6M^6 - 512g^9M^3}. \quad (4.31)$$

The solution of the first equation, ($V_{eff} = 0$), gives the minimum impact parameter of the photon,

$$u_{ps} = \frac{L_c}{E} = \left. \frac{r}{\sqrt{f(r)}} \right|_{r_{ps}}. \quad (4.32)$$

The explicit form of this can be obtained by using Eq. (4.29).

The insight of using the photon sphere parameters r_{ps} and u_{ps} to probe the details of the small-large black hole phase transition, stems from the phenomenon of black hole lensing (Wei and Liu, 2018). In black hole lensing, the impact parameter of the photon u has a close connection with the deflection angle. Larger the impact parameter smaller is the deflection angle. However, under the limit $u \rightarrow u_{ps}$ the deflection angle is unbounded (Bozza, 2002). We can relate these key quantities, r_{ps} and u_{ps} , to the thermodynamic variables P and S by using the expression for mass of the black hole M . $r_{ps}(P, S)$ is a complicated expression which we have not written here. The behaviour r_{ps} and u_{ps} against the temperature is studied in reduced parameter space, Fig. 4.2(a) and 4.2(b). The similar study is carried out for $\tilde{P} - \tilde{r}_{ps}$ and $\tilde{P} - \tilde{u}_{ps}$ plots for a fixed value of reduced temperature, Fig. 4.3(a) and 4.3(b).

In Fig. 4.2, both the photon sphere radius and the critical impact parameter shows non-monotonous behaviour below the critical pressure. All the isobars for $\tilde{P} < 1$ have one minimum and a maximum. There is an inflexion point for the isobar $\tilde{P} = 1$. For all the values above $\tilde{P} = 1$, the oscillating behaviour disappears. This behaviour of $\tilde{T} - \tilde{r}_{ps}$ and $\tilde{T} - \tilde{u}_{ps}$ is quite similar to the isobars in $\tilde{T} - \tilde{S}$ plane for the vdW fluid. On the other hand the $\tilde{P} - \tilde{r}_{ps}$ and $\tilde{P} - \tilde{u}_{ps}$ plots shown in Fig. 4.3 have similarity with the isotherms of the vdW system in the $P - V$ plane. These connections indicate that there is a relationship between the photon orbits and the critical behaviour of the black hole.

4.2.3 Critical behaviour from unstable photon orbits

We have constructed the equal area law for the $\tilde{T} - \tilde{r}_{ps}$ and $\tilde{T} - \tilde{u}_{ps}$ isobars, similar to the isobars in the $\tilde{T} - \tilde{S}$ plane of vdW system. Using those results, we obtained the behaviour of the radius of the circular orbit and the minimum impact parameter along the coexistence curve (Fig. 4.4). The \tilde{r}_{ps} and \tilde{u}_{ps} has two branches corresponding to SBH and LBH phases of the black hole. With the increase in temperature, both the r_{ps} and u_{ps} decreases for the LBH branch, whereas increases for SBH branch. At the critical value $\tilde{T} = 1$ both branches share the same value. The differences $\Delta\tilde{r}_{ps}$ and $\Delta\tilde{u}_{ps}$ are plotted against the reduced temperature \tilde{T} , which is shown in Fig. 4.5. A sudden change in $\Delta\tilde{r}_{ps}$ and $\Delta\tilde{u}_{ps}$ exists in the regions corresponding to the first order phase transitions, i.e., for $\tilde{T} < 1$. The difference becomes zero as the critical value of \tilde{T} is approached, where the second order phase transition is observed. The behaviour of $\Delta\tilde{r}_{ps}$ and $\Delta\tilde{u}_{ps}$ near the critical point is observed in the insets of Fig. 4.5(a) and 4.5(b). We

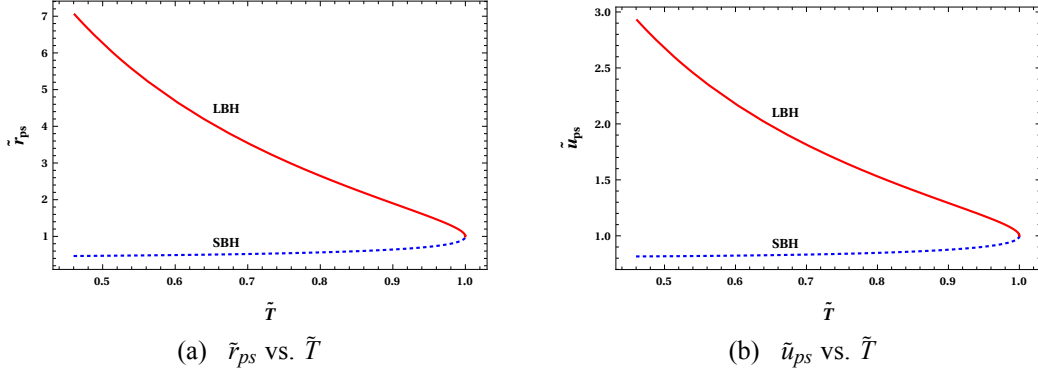


Figure 4.4: The behaviour of photon sphere radius r_{ps} and minimum impact parameter u_{ps} of the photon orbit along the coexistence curve for Hayward case

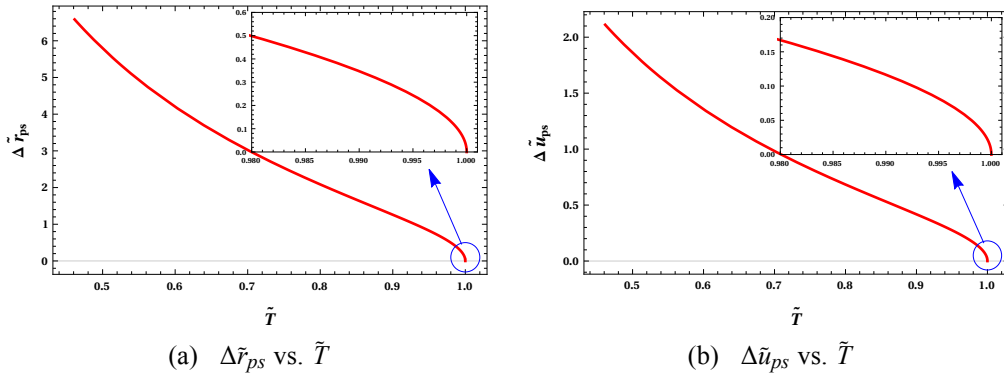


Figure 4.5: The behaviour of difference of the radii of the circular orbit $\Delta\tilde{r}_{ps}$ and the difference of the minimum impact parameter $\Delta\tilde{u}_{ps}$ along the coexistence curve for Hayward case. The change of concavity near the critical point is shown in the insets

also note that, near the critical point the concavity of the curve changes. The behaviour near the critical point can be assumed to be of the following form,

$$\Delta\tilde{r}_{ps}, \quad \Delta\tilde{u}_{ps} \sim a \times (1 - \tilde{T})^\delta. \quad (4.33)$$

Taking logarithm on both side, we have,

$$\ln \Delta\tilde{r}_{ps}, \quad \ln \Delta\tilde{u}_{ps} \sim \delta \ln(1 - \tilde{T}) + \ln a. \quad (4.34)$$

This implies that $\ln \Delta\tilde{r}_{ps}$ and $\ln \Delta\tilde{u}_{ps}$ are linearly varies with $\ln(1 - \tilde{T})$. We numerically fit the curve by varying \tilde{T} from 0.99 to 0.9999. The numerically obtained results along with the fitting results are shown in Fig. 4.6. The numerical study reveals that, in the vicinity of critical point,

$$\Delta\tilde{r}_{ps} = 3.42124(1 - \tilde{T})^{0.500003}, \quad (4.35)$$

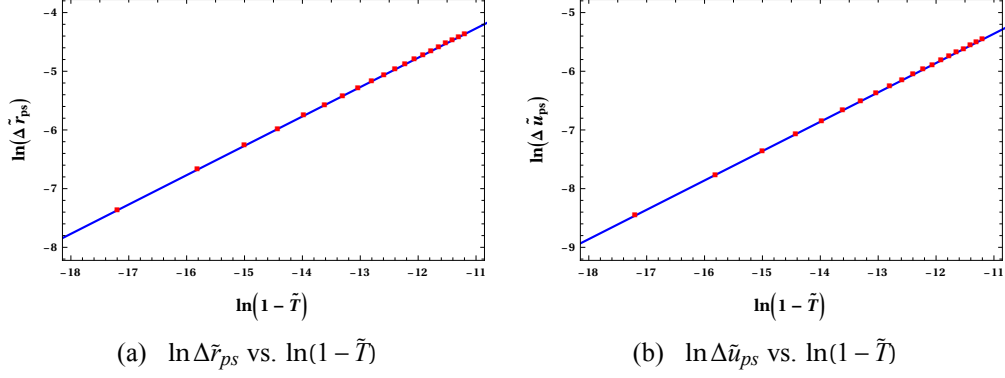


Figure 4.6: Near critical point behaviours of the change of the photon orbit radius $\Delta \tilde{r}_{ps}$ and the minimum impact parameter $\Delta \tilde{u}_{ps}$ during the black hole phase transition for Hayward case. Red square dots are the numerical results and blue solid lines are our fitting results.

and

$$\Delta \tilde{u}_{ps} = 1.15021(1 - \tilde{T})^{0.500003}. \quad (4.36)$$

This behaviour, i.e. $\Delta \tilde{r}_{ps} \sim (1 - \tilde{T})^{1/2}$ and $\Delta \tilde{u}_{ps} \sim (1 - \tilde{T})^{1/2}$, suggests that $\Delta \tilde{r}_{ps}$ and $\Delta \tilde{u}_{ps}$ can serve as the order parameters to characterise the phase transition. This, once again confirms our earlier observation on the connection between the photon orbits and thermodynamic phase transitions. The result shows that the numerical error in the calculation is negligible.

4.3 Regular Bardeen Black Hole

In this section, we establish the connection between thermodynamic phase transition and the null geodesic for the Bardeen case. The regular Bardeen AdS black hole can be obtained by using the following Lagrangian density in the action (4.1),

$$\mathcal{L}(\mathcal{F}) = \frac{12}{\alpha} \frac{(\alpha \mathcal{F})^{5/4}}{(1 + (\alpha \mathcal{F})^{1/2})^{5/2}}. \quad (4.37)$$

The Bardeen solution of the black hole in AdS spacetime has the following form (Fan and Wang, 2016),

$$ds^2 = -f(r)dt^2 + \frac{1}{f(r)}dr^2 + r^2 d\Omega^2 \quad (4.38)$$

with

$$f(r) = 1 - \frac{2Mr^2}{(g^2 + r^2)^{3/2}} + \frac{8}{3}\pi Pr^2. \quad (4.39)$$

As before, the pressure P is related to the cosmological constant Λ as $P = -\Lambda/8\pi$. The condition $f(r_+) = 0$ yields the mass of the black hole as,

$$M = \frac{(g^2 + r_+^2)^{3/2} (8\pi P r_+^2 + 3)}{6r_+^2}. \quad (4.40)$$

The Hawking temperature can be easily obtained as,

$$\begin{aligned} T &= \frac{\kappa}{2\pi} = \frac{f'(r)}{4\pi} \Big|_{r=r_+} \\ &= \frac{2Pr_+^3}{g^2 + r_+^2} + \frac{r_+}{4\pi(g^2 + r_+^2)} - \frac{g^2}{2\pi r_+(g^2 + r_+^2)}. \end{aligned} \quad (4.41)$$

The first law of thermodynamics has the same form as that of Hayward case,

$$dM = TdS + \Psi dQ_m + VdP + \Pi d\alpha, \quad (4.42)$$

with the variables having same meaning. In fact this is the generic form of the first law in the extended phase space for black holes with nonlinear electric/magnetic charges, which can be derived using a covariant approach (Zhang and Gao, 2018). The entropy of the black hole is,

$$S = \int \frac{dM}{T} = -\frac{2\pi g^3}{r_+} {}_2F_1\left(-\frac{3}{2}, -\frac{1}{2}; \frac{1}{2}; -\frac{r_+^2}{g^2}\right), \quad (4.43)$$

where ${}_2F_1$ is the Hyper-geometric function. The volume V can be obtained as,

$$V = \left(\frac{\partial M}{\partial P}\right)_{S, Q_m, \alpha} = \frac{4}{3}\pi (g^2 + r_+^2)^{3/2}. \quad (4.44)$$

Inverting the expression of Hawking temperature (Eq. 4.41) for pressure we have the equation of state,

$$P = \frac{g^2}{4\pi r_+^4} + \frac{g^2 T}{2r_+^3} - \frac{1}{8\pi r_+^2} + \frac{T}{2r_+}, \quad (4.45)$$

from which an oscillatory behaviour of isotherms below critical temperature and hence the phase transition is evident, which is well studied (Tzikas, 2019). The critical values of the thermodynamic variables for this phase transition are determined, which are,

$$T_{cB} = -\frac{(\sqrt{273} - 17) \sqrt{\frac{1}{2}(\sqrt{273} + 15)}}{24\pi g}, \quad (4.46)$$

$$P_{cB} = \frac{\sqrt{273} + 27}{12(\sqrt{273} + 15)^2 \pi g^2}, \quad (4.47)$$

$$S_{cB} = \frac{1}{2} (\sqrt{273} + 15) \pi g^2. \quad (4.48)$$

As earlier, the critical values depend on the parameter g . The reduced thermodynamics variables can be defined from these critical variables as before. The study of coexistent physics is not trivial compared to Hayward black hole case as the analytical expression for the coexistence curve is not feasible. Therefore we investigate the critical behaviour of the black hole numerically in the next section. The coexistent curve which separates the SBH and LBH phases of the black hole can be obtained numerically by using the swallow tail behaviour of the Gibbs free energy, $G = M - TS$.

Photon Orbit and Phase transition

The geodesic for the photon moving in the equatorial plane of regular Bardeen AdS black hole is analysed in the same line as in Hayward case. The behaviour of $\tilde{V}_{eff} = V_{eff}/E$ is similar to that of Hayward case. There exists a critical impact parameter u_c which defines the unstable photon orbit. The photon approaching the black hole with impact parameter $u > u_c$ will be scattered and photon with $u < u_c$ will be absorbed by the black hole. However, quantitatively there is a difference in the effective potential, for example height of the potential barrier is different in Bardeen and Hayward case for a given value of g .

The expression for the photon orbit radius is obtained by solving the second relation in Eq. (4.28) for the Bardeen background, which has a relatively simple form,

$$r_{ps} = \frac{2^{2/3} M^2}{\sqrt[3]{Z}} + M + \frac{\sqrt[3]{Z}}{2^{2/3}}, \quad (4.49)$$

where,

$$Z = -15g^2 M + \sqrt{15} \sqrt{15g^4 M^2 - 8g^2 M^4 + 4M^3}. \quad (4.50)$$

With the use of Eq. (4.49) and Eq. (4.32) we obtain the minimum impact parameter u_{ps} for the Bardeen case. As argued earlier, the photon sphere radius and minimum impact parameter are the key quantities in probing the phase transition of the black hole. The isobars in \tilde{T} vs. \tilde{r}_{ps} and \tilde{T} vs. \tilde{u}_{ps} and isotherms in \tilde{P} vs. \tilde{r}_{ps} and \tilde{P} vs. \tilde{u}_{ps} planes show the corresponding vdW like phase transition in regular Bardeen black hole (Fig. 4.7 and Fig. 4.8).

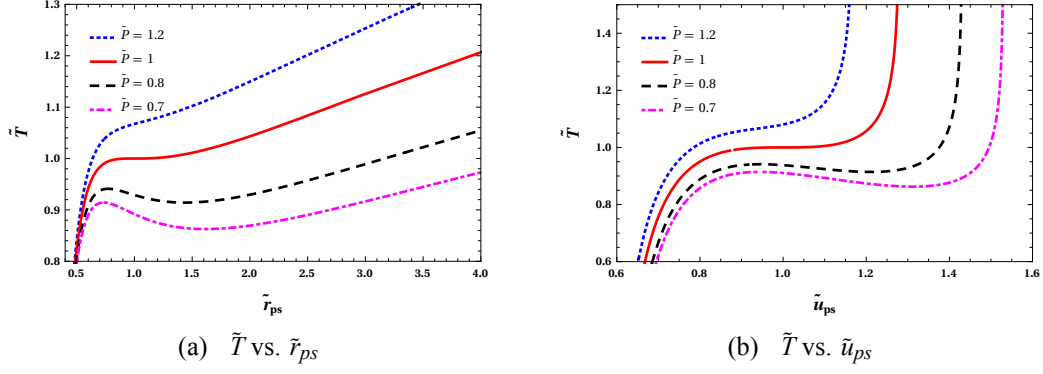


Figure 4.7: The behaviour of photon sphere radius r_{ps} and minimum impact parameter u_{ps} with temperature in reduced space for Bardeen case. These plots are for the reduced pressure $\tilde{P} = 0.7, 0.8, 1, 1.2$

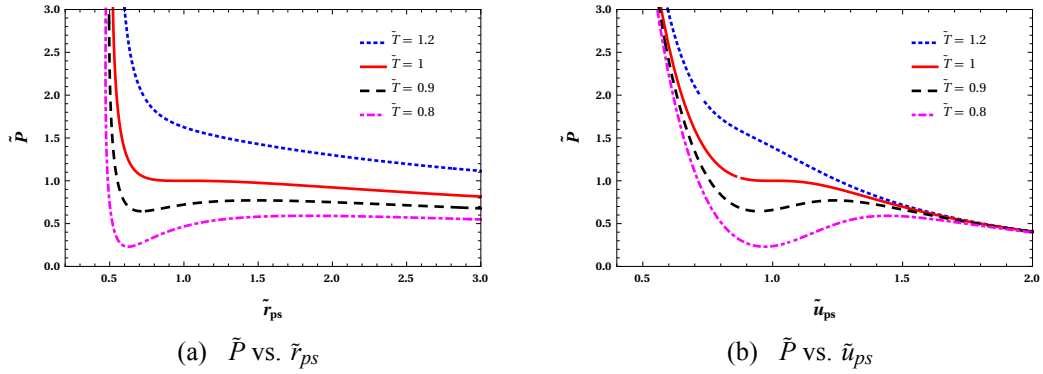


Figure 4.8: The behaviour of photon sphere radius r_{ps} and minimum impact parameter u_{ps} with pressure in reduced space for Bardeen case. These plots are for the reduced temperature $\tilde{T} = 0.8, 0.9, 1, 1.2$

Unlike Hayward black hole case, it is not possible to solve the equal area law analytically for the isobars of the Bardeen black hole case. We have performed a numerical calculation to obtain the result. Using the result we studied the behaviour of photon orbit radius r_{ps} and minimum impact parameter u_{ps} along the coexistence line (Fig. 4.9). Here too, as in Hayward case, there is a sudden change for r_{ps} and u_{ps} during the phase transition. The changes Δr_{ps} and Δu_{ps} along the coexistence line is also studied numerically (Fig. 4.10). The behaviour of the curve is as before. Using the curve fit formula of the form Eq. (4.33), the numerical fit yields,

$$\Delta \tilde{r}_{ps} = 4.04741(1 - \tilde{T})^{0.507242}, \quad (4.51)$$

and

$$\Delta \tilde{u}_{ps} = 1.51445(1 - \tilde{T})^{0.508615}. \quad (4.52)$$

This shows that Δr_{ps} and Δu_{ps} serve as order parameter of the phase transition with crit-

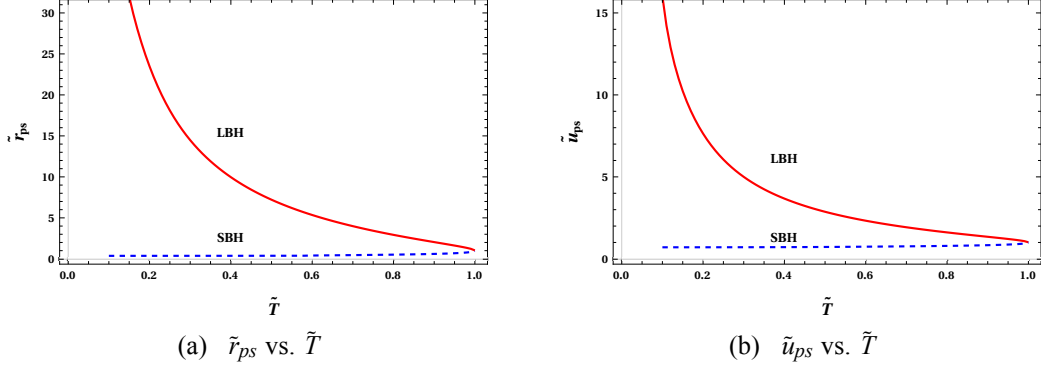


Figure 4.9: The behaviour of photon sphere radius r_{ps} and minimum impact parameter u_{ps} of the photon orbit along the coexistence curve for Bardeen case

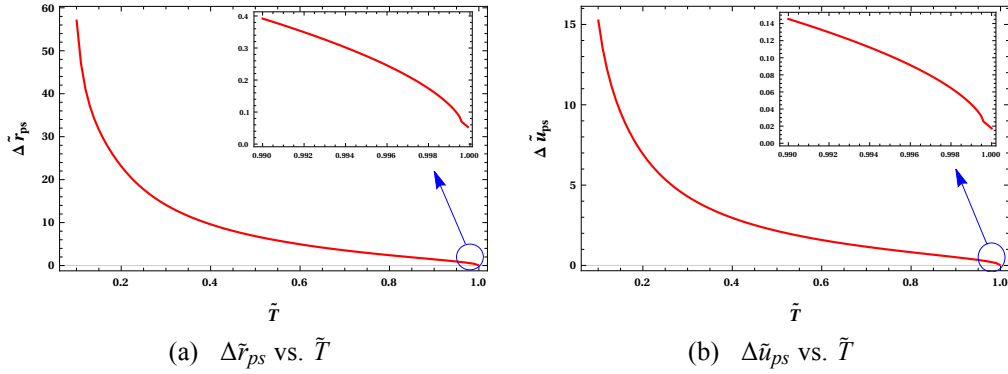


Figure 4.10: The behaviour of difference of the radii of the circular orbit $\Delta \tilde{r}_{ps}$ and the difference of the minimum impact parameter $\Delta \tilde{u}_{ps}$ along the coexistence curve for Bardeen case. The change of concavity near the critical point is shown in the insets

ical exponent $1/2$. The numerical data and fitting results are shown in Fig. 4.11. In this case the numerical errors are within 1.72%. Unlike Hayward case a finite tiny error present here as the coexistence curve also obtained numerically. From the connection between null geodesics and thermodynamic phase transition of Bardeen and Hayward cases, we can ascertain that the result is apparent for any regular spacetime background.

4.4 Discussions

One of the most intriguing aspect of gravitational theories is the presence of physical singularity at the centre of black holes. Among the several ways of avoiding the black hole singularity, the non linear electrodynamics (NED) coupled to general relativity is widely discussed. One of the simple NED model which gives well defined magnetically charged black holes is the generic regular black holes (Fan and Wang, 2016). The interesting sub

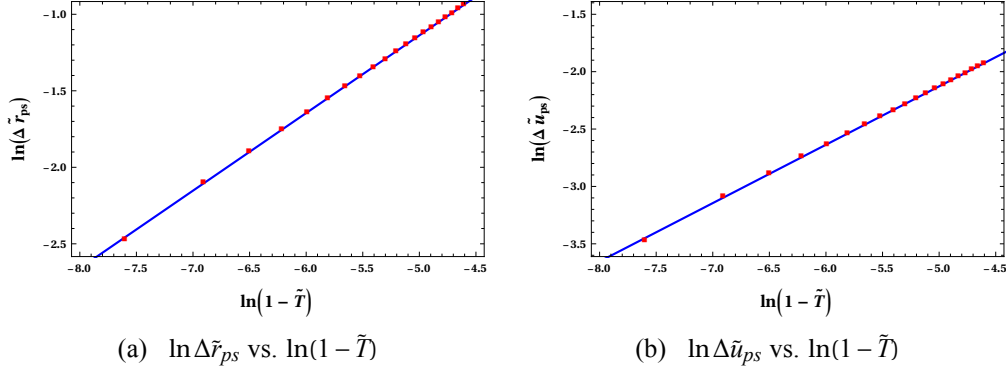


Figure 4.11: Near critical point behaviours of the change of the photon orbit radius $\Delta \tilde{r}_{ps}$ and the minimum impact parameter $\Delta \tilde{u}_{ps}$ during the black hole phase transition for the Bardeen case. Red square dots are the numerical results and blue solid lines are our fitting results

classes of this model are the Hayward and Bardeen black holes. Naturally, it is compelling to study the physical properties associated with the regular generic black holes and compare the differences and similarities to the generic black holes which exhibit a physical singularity.

In this chapter, using the formalism of unstable circular null geodesics for a class of regular black holes including Hayward-AdS and Bardeen-AdS spacetimes, we find a close connection between the gravity and thermodynamics in the extended phase space. The well-known van der Waals-like phase structure is probed via the photon orbit radius r_{ps} and minimum critical impact parameter u_{ps} . In the reduced parameter space, the isobars and isotherms in each of these key parameters' plots show oscillatory behaviour below the critical values of the temperature \tilde{T} and the pressure \tilde{P} , respectively. Such behaviours are in accordance with the van der Waals-like phase transition of the black holes. The disappearance of the first-order phase transition above the critical point is clearly seen in the isobar and isotherm plots of r_{ps} and u_{ps} . Moreover, the differences Δr_{ps} and Δu_{ps} serve as order parameters for the critical behaviour. Furthermore, near the second-order phase transition points, these differences exhibit a change of concavity with critical exponents $\delta = 1/2$. We studied the behaviour of Δr_{ps} and Δu_{ps} along the coexistence curve analytically for Hayward-AdS black hole, whereas, due to the difficulty in solving Bardeen case we adopted numerical method. The behaviour of Δr_{ps} and Δu_{ps} near the critical point are probed numerically in both the cases, with a negligible error in Hayward case and a mere 1.72% in Bardeen case. In both cases we are lead to the same inference, from which we expect that the generic regular black holes are characterised by the same observed feature.

Our results show that regular black holes are in close proximity with charged AdS black holes, in phase transition perspectives. Thus a regular modification to the electrovacuum solutions of Einstein field equations could be a possible candidate for probing its thermal properties. The thermal properties connecting the photon orbits may be useful to distinguish the regular black holes from Kerr one in AdS spacetimes and to test whether or not the regular black hole candidates are the black holes predicted by Einstein's relativity. This is one more interesting peripheral aspect of circular photon orbit which can disclose the observational signature of the thermodynamic phase transition. Our speculation is on the ground that photon orbit has strong astrophysical interest, and its ability to reflect the black hole phase transition.

Chapter 5

Microstructure and Continuous Phase Transition of AdS Black Holes

If you can heat it, it has microscopic structure.

Ludwig Boltzmann

Summary

This chapter is based on our article [Naveena Kumara et al. \(2021b\)](#). We study the phase transition of a regular Hayward-AdS black hole by introducing a new order parameter, the potential conjugate to the magnetic charge due to the non-linearly coupled electromagnetic field. We use Landau continuous phase transition theory to discuss the van der Waals like critical phenomena of the black hole. The popular interpretation of the AdS black hole phase transition as between a large and a small black hole is reinterpreted as the transition between a high potential phase and a low potential phase. The underlying microstructure for this phase transition is probed using the Ruppeiner geometry. By investigating the behaviour of the Ruppeiner scalar curvature, we find that the charged and uncharged (effective) molecules of the black hole have distinct microstructures analogous to fermion and boson gas.

5.1 Introduction

For a charged AdS black hole, choosing a parameter space with coordinates as mass and pressure, the Ruppeiner curvature scalar can be written in terms of the molecular density of the black hole microstates ([Wei and Liu, 2015](#)). Here, by introducing the concept of black hole molecules, the authors have studied the phase transition and the interaction between

the black hole molecules in two distinct phases. The molecular number density measures the microscopic degrees of freedom, using which the order parameter is constructed. However, recently it was shown that for RN-AdS black hole the phase transition is regulated by the electric potential (Guo et al., 2019). Black hole can exist in any of the three potential phases, namely, high potential phase, low potential phase and neutral potential phase. The neutral potential phase of the black hole is analogous to the liquid-vapour coexistence phase found in a vdW system. The potential due to the charge Q serves as the order parameter. The microscopic and phase transition study is carried out by using the Landau continuous phase transition theory. The influence of charge, the key entity in phase transition as it was conjectured, on the microstructure is investigated via Ruppeiner geometry. In this regard, one of the motivations for our research stems from the curiosity about the phase structure of the black holes which are composed of magnetic charges.

It is more reasonable to rephrase the question we posed in the beginning as, ‘‘Does a black hole without a singularity have a microstructure?’’ In this work, we investigate the phase structure of regular Hayward black hole in AdS background. The chapter is organized as follows. In section 5.2, the phase transition is studied using the Landau theory of continuous phase transition, followed by probing the microstructure using Ruppeiner geometry in section 5.3. Results are presented in section 5.4.

5.2 Phase Transition of Regular Hayward Black Hole

5.2.1 Thermodynamics of the Black Hole

We recall the thermodynamic quantities of Hayward AdS black hole, which we have presented in section 4.2. The Hawking temperature of the black hole, which is related to the surface gravity κ , is obtained as

$$T = \frac{f'(r_+)}{4\pi} = \frac{2Pr_+^4}{g^3 + r_+^3} - \frac{g^3}{2\pi r_+(g^3 + r_+^3)} + \frac{r_+^2}{4\pi(g^3 + r_+^3)}. \quad (5.1)$$

With this temperature, we can write the first law of thermodynamics in the conventional form,

$$dM = TdS + \Psi dQ_m + VdP + \Pi da. \quad (5.2)$$

Where Ψ is the conjugate potential for the magnetic charge Q_m , Π is conjugate to the parameter α . The volume and entropy of the black hole have the following non trivial profile,

$$V = \frac{4}{3}\pi(g^3 + r_+^3) \quad \text{and} \quad S = 2\pi\left(\frac{r_+^2}{2} - \frac{g^3}{r_+}\right). \quad (5.3)$$

The Potential reads as,

$$\Psi = \left(\frac{\partial M}{\partial Q_m}\right)_{S,P,\alpha} = \frac{3g^4}{\sqrt{2\alpha}(g^3 + r_+^3)}. \quad (5.4)$$

Rearranging Eq. (5.1) we have the equation of state,

$$P = \frac{g^3}{4\pi r_+^5} + \frac{g^3 T}{2r_+^4} - \frac{1}{8\pi r_+^2} + \frac{T}{2r_+}. \quad (5.5)$$

The critical behaviour of regular Hayward black hole can be studied by choosing a pair of conjugate variables like $(P - V)$ or $(T - S)$. Choosing the pair (P, V) we have the Maxwell's equal area law in the following form,

$$P_0(V_2 - V_1) = \int_{V_1}^{V_2} P dV. \quad (5.6)$$

With Eq. (5.6) and using corresponding expressions for $P_0(V_1)$ and $P_0(V_2)$ from equation of state, we obtain,

$$r_2 = g \left[\frac{x(x^3 + 6x^2 + 6x + 1) + \sqrt{y}}{x^4} \right]^{1/3}, \quad (5.7)$$

$$P_0 = 3 \left[\frac{\sqrt{y} + x(x^3 + 6x^2 + 6x + 1)}{x^4} \right]^{1/3} \left(\frac{[(-2x^4 - 11x^3 - 20x^2 - 11x - 2)\sqrt{y} + z]}{16\pi g^2 x(x^2 + 4x + 1)(3x^2 + 4x + 3)^2} \right), \quad (5.8)$$

$$T_0 = \frac{\left[\frac{\sqrt{y} + x(x^3 + 6x^2 + 6x + 1)}{x^4} \right]^{2/3} [u - (x^3 + 4x^2 + 4x + 1)\sqrt{y}]}{4\pi g x (3x^4 + 16x^3 + 22x^2 + 16x + 3)}. \quad (5.9)$$

Where

$$y = x^2 (x^6 + 12x^5 + 54x^4 + 82x^3 + 54x^2 + 12x + 1), \quad (5.10)$$

$$z = x (2x^7 + 23x^6 + 104x^5 + 213x^4 + 213x^3 + 104x^2 + 23x + 2), \quad (5.11)$$

$$u = x (x^6 + 10x^5 + 37x^4 + 54x^3 + 37x^2 + 10x + 1). \quad (5.12)$$

We have taken $x = r_1/r_2$, where r_1 and r_2 are the radii of black hole for first-order phase

transition points. $x = 1$ gives critical values of temperature T and pressure P ,

$$T_c = \frac{(5\sqrt{2} - 4\sqrt{3})(3\sqrt{6} + 7)^{2/3}}{4 \cdot 2^{5/6} \pi g} \quad (5.13)$$

$$P_c = \frac{3(\sqrt{6} + 3)}{16 \cdot 2^{2/3} (3\sqrt{6} + 7)^{5/3} \pi g^2}. \quad (5.14)$$

During the phase transition, a system undergoes a sudden change in its physical properties which is controlled by external thermodynamic variables. A familiar example in day-to-day life is the solid-liquid-gas transition due to a change in the temperature or pressure. A common feature of these transitions is that the order or symmetry of the system changes at the transition point. At the phase transition point of the black hole, there is a sudden change in the potential Ψ , which is controlled by the pressure and temperature. This indicates that the black hole microstructure is in different phases at different potentials. The two phases of the black hole with different symmetry and order are determined by the potentials,

$$\Psi_1 = \frac{3g^4}{\sqrt{2\alpha}(g^3 + r_1^3)} \quad \text{and} \quad \Psi_2 = \frac{3g^4}{\sqrt{2\alpha}(g^3 + r_2^3)}, \quad (5.15)$$

where r_1 and r_2 can be written in terms of x using Eq. (5.7), and the critical value of the potential Ψ_C can be obtained by setting $x = 1$. We define the following order parameter to characterize the phase transition,

$$\varphi(T) = \frac{\Psi_1 - \Psi_2}{\Psi_C}. \quad (5.16)$$

The behaviour of the order parameter is shown in Fig. 5.1, where we have defined $\chi = T/T_C$. We examine the mechanism of black hole phase transition from the perspective of black hole magnetic charge, since the conjugate potential of magnetic charge serves as the order parameter.

5.2.2 Phase Transition of the Black Hole

In Landau theory, a continuous phase transition is associated with a broken symmetry. In other words, the phase transition is the spontaneous breaking of the symmetry, where the system chooses one state during this. Landau realized that an approximate form for the

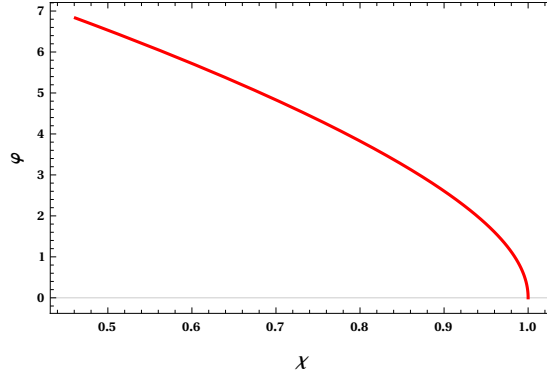


Figure 5.1: The order parameter vs reduced temperature ($\phi - \chi$) plot of regular Hayward AdS black hole

free energy could be constructed without prior knowledge about the microscopic states. In this theory, it is always possible to ascertain an order parameter which vanishes on the high-temperature side of the phase transition and has a non-zero value on the low-temperature side of the phase transition. That is, in one phase, the order parameter has a non-zero value; in another phase, it vanishes. The order parameter describes the nature and extent of symmetry breaking. At the second-order phase transition, the order parameter grows continuously from the null value at the critical point. Since the order parameter approaches zero at the phase transition, one can Taylor expand the free energy as a power series of the order parameter. The symmetries of the theory govern the form of this expansion.

The phase transition in a black hole system can also be characterized by the symmetry and order degrees as in a conventional thermodynamic system. In a black hole system, we can identify two phases with different potentials below the critical point (for $T < T_C$). The system in higher potential phase ϕ_1 possesses a relatively ordered state with lower symmetry. This corresponds to a certain orientation of black hole molecules under the action of the strong potential ϕ_1 . Whereas, the system is in a lower potential state ϕ_2 possesses relatively lower order degree and a higher symmetry than the phase ϕ_1 . This is due to the weakened orientation of the black hole molecules. The black hole molecules will have a certain orientation for all the values of temperature below critical value T_C . When the temperature is above the critical value ($T > T_C$), the thermal motion of molecules increases and causes the black hole molecules to attain random orientation. The system now has a higher symmetry than all the states below the critical temperature. For the less symmetrical phase (below the critical temperature with higher-order) the order parameter ϕ is non-zero. For the more symmetrical phase (above critical temperature with lower order) the order parameter ϕ is zero.

Near the critical point T_C , the order parameter φ is small and hence the free energy can be expanded in terms of the order parameter. The symmetry of the spacetime under the transformation $\varphi \rightleftharpoons -\varphi$ removes the odd powers in that perturbation series.

$$G(\varphi, T) = G_0(T) + \frac{1}{2}a(T)\varphi^2 + \frac{1}{4}b(T)\varphi^4 + \dots \quad (5.17)$$

where G_0 is the Gibbs free energy at $\varphi(T) = 0$, which describes the temperature dependence of the high temperature phase near the critical point.

In Landau theory, it is presumed that $b > 0$ so that the free energy G has a minimum for finite values of the order parameter φ . For $a > 0$, there is only one minimum at $\varphi = 0$, which corresponds to the symmetrical phase (more symmetrical phase). Whereas for $a < 0$ there are two minima with $\varphi \neq 0$ in the unsymmetrical phase (less symmetrical phase). The transition point is governed by the condition of $a = 0$. One of the assumptions of the theory is that $a(T)$ has no singularity at the transition point so that it can be expanded in the neighbourhood of the critical point as integral powers of $(T - T_C)$. To first order,

$$a = a_0(T - T_C) \quad a_0 > 0. \quad (5.18)$$

The coefficient $b(T)$ may also be replaced by $b(T_C) = b$. The expansion of free energy, therefore, becomes,

$$G(\varphi, T) = G_0(T) + \frac{1}{2}a_0(T - T_C)\varphi^2 + \frac{1}{4}b\varphi^4 + \dots \quad (5.19)$$

In the unsymmetrical phase, the dependence of the order parameter φ on the temperature near the critical point is determined by the condition that G which is a function of φ be a minimum. In a stable equilibrium state, $G(T)$ has a vanishing first derivative and a positive second derivative.

$$\frac{\partial G}{\partial \varphi} = a_0(T - T_C)\varphi + b\varphi^3 = 0 \quad (5.20)$$

$$\frac{\partial^2 G}{\partial \varphi^2} = a_0(T - T_C) + 3b\varphi^2 > 0. \quad (5.21)$$

The solutions of Eq. (5.20) are,

$$\varphi = 0 \quad \text{and} \quad \varphi = \pm \sqrt{-\frac{a_0(T-T_C)}{b}} \quad (5.22)$$

The solution $\varphi = 0$, when $a > 0$, renders a disordered state in the temperature range $T > T_C$. The non-zero solution corresponds to the ordered state, where the configuration of the phases on the temperature scale depends on the sign of a_0 . For $a_0 > 0$ and $a_0 < 0$, the ordered state corresponds to the temperatures $T < T_C$ and $T > T_C$, respectively. From Eq. (5.22) we have $\varphi \propto (T-T_C)^{1/2}$ near the critical point, which gives the critical exponent $\beta = 1/2$.

Substituting these solutions (5.22) back to the Eq. (5.19) we get the reliance of free energy on the temperature near the phase transition point,

$$G(T, \varphi) = G_0, \quad T > T_C \quad (5.23)$$

$$G(T, \varphi) = G_0 - \frac{a_0^2}{2b}(T-T_C)^2, \quad T < T_C. \quad (5.24)$$

These solutions match at $T = T_C$, i.e., the free energy is continuous at the critical point. At constant pressure the total differential of the Gibbs free energy is

$$dG = -SdT - Q_m d\Psi - \alpha d\Pi. \quad (5.25)$$

The expression for entropy is,

$$S = -\left(\frac{\partial G}{\partial T}\right) = \frac{a_0^2}{b}(T-T_C). \quad (5.26)$$

This is the difference of entropy between the ordered and disordered states. If the entropy of the disordered phase is S_0 , and that of ordered phase is $S_0 + \frac{a_0^2}{b}(T-T_C)$. The black hole entropy is also continuous at the phase transition point. The specific heat can be calculated as

$$C = T\left(\frac{\partial S}{\partial T}\right). \quad (5.27)$$

The specific heat has a jump at the critical point,

$$C(T < T_C)|_{T=T_C} - C(T > T_C)|_{T=T_C} = \frac{a_0^2}{b} T_C. \quad (5.28)$$

From this it is clear that the heat capacity of the ordered state is greater than that of the disordered state. This expression also indicates that the critical exponent α is zero. From Eq. (5.25) we have,

$$-Q_m = \left(\frac{\partial G}{\partial \varphi} \right)_T = a_0(T - T_C)\varphi + b\varphi^3. \quad (5.29)$$

Which gives,

$$-\left(\frac{\partial \varphi}{\partial Q_m} \right)_T = \frac{1}{a_0(T - T_C) + 3b\varphi^3}. \quad (5.30)$$

Using Eq. (5.22) gives two branches,

$$-\left(\frac{\partial \varphi}{\partial Q_m} \right)_T = \begin{cases} \frac{1}{a_0(T - T_C)} & \text{for } T > T_C \\ \frac{-1}{2a_0(T - T_C)} & \text{for } T < T_C \end{cases} \quad (5.31)$$

From this we can infer that the critical exponent $\gamma = 1$. At the phase transition point $a = 0$, therefore, from Eq. (5.30) we can obtain the relation,

$$Q_m \propto \varphi^3. \quad (5.32)$$

Which simply tells that the critical exponent $\delta = 3$.

5.3 Ruppeiner Geometry and Microstructure

Landau theory, being universal, does not give the phase structure of the system. However, the symmetry or order of degree of the system arises from the underlying microstructure. The parameters a and b in the theory are related to the system characteristics. However, they do not appear in the identification of critical exponents. This discrepancy persists even for a conventional thermodynamic system. This is because, in the continuous phase transition theory, the fluctuation of the order parameter is not considered near the transition point. This can be addressed by using a fluctuation theoretical tool, namely the Ruppeiner geometry. The black hole microstructure can be analyzed by studying the nature of Ruppeiner

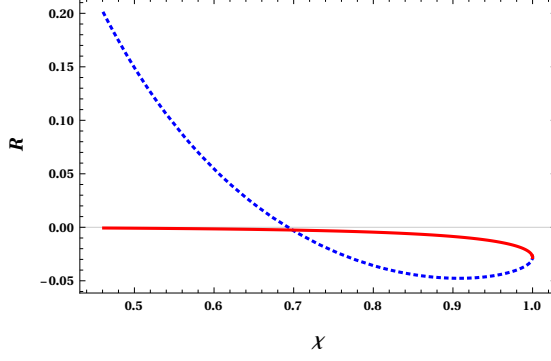


Figure 5.2: The Ruppeiner scalar curvature vs reduced temperature ($R - \chi$) plot for regular Hayward AdS black hole

curvature scalar R . The thermodynamic invariant curvature scalar R is calculated by using the definition in the Weinhold energy form (Weinhold, 1975b),

$$g_{\alpha\beta} = \frac{1}{T} \frac{\partial^2 M}{\partial X^\alpha \partial X^\beta} \quad (5.33)$$

in the (S, P) parametric space. The exact expression for the curvature scalar is complicated. Using the earlier results (equations 5.7, 5.8 and 5.9) we obtain the curvature scalar for the two phases of the black hole. The obtained R is plotted against χ to study the nature of the interaction between the black hole molecules (Fig. 5.2). We also note that in the limit $g/r_+ \ll 1$, the Ruppeiner scalar takes the following simple form,

$$R = \frac{5\pi^{3/2}g^3\sqrt{S} - S^2}{(\pi^{3/2}g^3 + S^{3/2})(S^{3/2}(8PS + 1) - 2\pi^{3/2}g^3)}. \quad (5.34)$$

The behaviour of R does not change in this approximation. This simply means that the correction to entropy in a regular black hole does not impact the nature of microscopic interactions. In a magnetically charged black hole, there are two distinct types of molecules; charged and uncharged, which contributes to the microscopic degrees of freedom of the entropy. The black hole phase transition can be seen as a manifestation of the phase structure of a two-fluid system with magnetically charged and uncharged molecules.

The ordered and disordered phase of the black hole can be attributed to the relative degree of freedom of the magnetically charged molecules. If the d.o.f. of charged molecules is N_g and the total d.o.f. of the black hole is N , the black hole can have three different situations depending on N_g/N ratio. $N_g/N = n_0$ is moderately ordered, $N_g/N > n_0$ highly ordered and $N_g/N < n_0$ less ordered phases, due to the action of the magnetic potential Ψ .

At a given temperature the magnetic potential corresponding to the R_1 and R_2 branches are different. Since $\Psi_2 < \Psi_1$, R_2 represents the symmetric phase of the black hole where the molecules are in a disordered state. In other words R_2 stands for the low potential phase of the black hole. Therefore R_2 branch always represents the situation $N_g/N < n_0$. Whereas the phases corresponding to R_1 have three different cases. $R_1 > 0$ phase ($N_g/N < n_0$) has less symmetry and higher order, $R_1 = 0$ phase ($N_g/N = n_0$) has both moderate symmetry and order, $R_1 < 0$ phase ($N_g/N > n_0$) has more symmetry and lower order.

5.4 Discussions

From several recent developments in the field of black hole thermodynamics, it is a well-established notion that black holes have microstructure like ordinary thermodynamic systems. Moreover, the degrees of freedom of these constituent black hole molecules is what counts towards the black hole entropy. The phase structure of these molecules entitles the thermodynamic and phase transition properties of the system. In this work, we have shown that the phase transition of a magnetically charged black hole is determined by the magnetic potential. However, this result is similar to that of RN-AdS black hole where the key role is played by the electric potential (Guo et al., 2019). The symmetry or the order degree of the regular black hole is governed by the magnetic potential. The changing symmetry results in different phases of the system, which is investigated using the Landau theory of continuous phase transition.

The statistical interpretation of the Ruppeiner scalar reveals the nature of the interaction of the black hole molecules. Under the limiting case $g \rightarrow 0$, we have $R < 0$, which corresponds to uncharged molecules. With the presence of charged molecules, R tends to become positive. In the context of quantum gases, $R < 0$ and $R > 0$ results are obtained for fermion gas and boson gas, respectively (Mirza and Mohammadzadeh, 2008; May et al., 2013b). For the regular Hayward black hole, magnetically charged molecules and uncharged molecules have different microstructures similar to fermion gas and boson gas.

However, in the case of anyon gas, the sign of R tells the average interaction between the constituents. Positive R stands for repulsive, and negative R corresponds to attractive interaction. Vanishing R implies zero interaction. In this view, we can think that the black hole molecules have repulsive, attractive and zero interactions depending on the curvature

scalar behaviour. Our research gives information about the microstructure of magnetically charged molecules which is similar to that of electrically charged molecules in RN-AdS black hole. This phenomenological description will help us understand the exact microstructure of the black hole in future research, and similar investigation can be done for other non-singular black holes.

Chapter 6

Repulsive Interactions in the Microstructure of AdS Black Holes

Imagination is more important than knowledge.

Albert Einstein

Summary

The present chapter is modified version of our published article ([Naveena Kumara et al., 2020b](#)). We study the interaction between the microstructures of Hayward-AdS black hole using Ruppeiner geometry. Our investigation shows that the dominant interaction between the black hole molecules is attractive in most part of the parametric space of temperature and volume, as in van der Waals system. However, in contrast to the van der Waals fluid, there exists a weak dominant repulsive interaction for small black hole phase in some parameter range. This result clearly distinguishes the interactions in a magnetically charged black hole from that of van der Waals fluid. However, these sort of interactions are characteristic for charged black holes since they do not depend on magnetic charge or temperature.

6.1 Introduction

Recently, a general Ruppeiner geometry framework was developed from the Boltzmann entropy formula, to study the black hole microstructure ([Wei et al., 2019a](#)). The fluctuation coordinates were taken as the temperature and volume, and a universal metric was constructed. When this methodology was applied to the van der Waals fluid, only a dominant attractive interaction was observed, as it should be. However, when the same methodology

is used for the RN-AdS black hole, a different result was obtained. A repulsive interaction between black hole molecules was found in a small parameter range, in addition to the dominant attractive interaction in the rest of the parameter space (Wei et al., 2019a,b). Even so, in the case of five-dimensional neutral Gauss-Bonnet black hole, only a dominant attractive interaction was discovered, which is similar to van der Waals fluid (Wei and Liu, 2020b). Therefore, in general, the nature of the black hole molecular interactions are not universal. In our recent work (Naveena Kumara et al., 2021b), we have observed that there exists a repulsive interaction in Hayward-AdS black hole, like that in the RN-AdS case. In the present work, we will make a detailed investigation of the previously observed repulsive interaction.

The primary motivation for our research is due to the great interest regarding regular black holes in black hole physics, as they do not possess any physical singularities. Wide variety of regular black holes exist, ranging from the first solution given by Bardeen (Bardeen et al., 1973), and its modifications (Ayon-Beato and Garcia, 1998, 2000), to the one in which we are interested, the Hayward black hole (Hayward, 2006). (We suggest the readers to go through our articles (Naveena Kumara et al., 2020a, 2021b) for a detailed discussion on this). Hayward black hole is a solution to Einstein gravity non-linearly coupled to an electromagnetic field which carries a magnetic charge. The secondary motivation for the present study comes from the question, what is the nature of the microstructure of a black hole with magnetically charged constituents? In this chapter, we probe the phase structure and repulsive interactions in the microstructure of this magnetically charged AdS black hole.

The chapter is organised as follows. In the following section, we discuss the phase structure of the black hole. Then the Ruppeiner geometry for the black hole is constructed for microstructure study (section 6.3). Then we present our findings in section 6.4.

6.2 Phase structure of the Hayward-AdS Black Hole

We study the phase structure in the extended phase space, where the cosmological constant Λ gives the pressure term $P = -\Lambda/8\pi$. For completeness, we briefly recall the thermodynamic quantities of the black hole presented in previous chapters. The thermodynamic quantities;

temperature, volume and entropy of the black hole are easily obtained as,

$$T = \frac{f'(r_+)}{4\pi} = \frac{2Pr^4}{g^3 + r^3} - \frac{g^3}{2\pi r(g^3 + r^3)} + \frac{r^2}{4\pi(g^3 + r^3)}; \quad (6.1)$$

$$V = \frac{4}{3}\pi(g^3 + r^3) \quad \text{and} \quad S = 2\pi\left(\frac{r^2}{2} - \frac{g^3}{r}\right). \quad (6.2)$$

These results are consistent with the first law,

$$dM = TdS + \Psi dQ_m + VdP + \Pi d\alpha, \quad (6.3)$$

and the Smarr relation,

$$M = 2(TS - VP + \Pi\alpha) + \Psi Q_m. \quad (6.4)$$

The heat capacity of the black hole system at constant volume is,

$$C_V = T\left(\frac{\partial S}{\partial T}\right)_V = 0. \quad (6.5)$$

Inverting the expression for the Hawking temperature (6.1) we get the equation of state,

$$P = \frac{g^3}{4\pi r^5} + \frac{g^3 T}{2r^4} - \frac{1}{8\pi r^2} + \frac{T}{2r}. \quad (6.6)$$

From the state equation, we can observe that the black hole shows a critical behaviour similar to that found in a van der Waals system. This is often interpreted as the transition between a small black hole (SBH) and a large black hole (LBH) phases. In our earlier study ([Naveena Kumara et al., 2021b](#)), we have shown that an alternate interpretation is possible using Landau theory of continuous phase transition, where the phase transition is between the black hole phases at different potentials. In this alternate view, the black hole phases, namely high potential, intermediate potential and low potential phases, are determined by the magnetic charge. In either of these interpretations, the phase transition can be studied by choosing a pair of conjugate variables like $(P-V)$ or $(T-S)$. With the conjugate pair (P, V) , the Maxwell's equal area law has the form,

$$P_0(V_2 - V_1) = \int_{V_1}^{V_2} PdV. \quad (6.7)$$

Since there exists no analytical expression for the coexistence curve of Hayward-AdS black hole, we usually seek numerical solutions. For that, we obtain the following key ingredient

from the Maxwell's equal area law. Using the Eq. (6.7) and expressions for $P_0(V_1)$ and $P_0(V_2)$ from equation of state (6.6) we get the solution as $P_0(x)$ and $T_0(x)$ (see Ref. (Naveena Kumara et al., 2021b)). We have taken $x = r_1/r_2$, where r_1 and r_2 are the radii of black hole for first-order phase transition points. The critical values are readily obtained by setting $x = 1$,

$$T_c = \frac{(5\sqrt{2} - 4\sqrt{3})n_1^{2/3}}{4 \times 2^{5/6}\pi g}, \quad (6.8)$$

$$P_c = \frac{3n_2}{16 \times 2^{2/3}n_1^{5/3}\pi g^2}, \quad (6.9)$$

and

$$V_c = 4n_3\pi g^3, \quad (6.10)$$

where $n_1 = 3\sqrt{6} + 7$, $n_2 = \sqrt{6} + 3$ and $n_3 = 2\sqrt{6} + 5$. The reduced thermodynamic variables are defined as,

$$T_r = \frac{T}{T_c}, \quad P_r = \frac{P}{P_c}, \quad V_r = \frac{V}{V_c}. \quad (6.11)$$

Using these we can write the equation of state in the reduced parameter space,

$$P_r = \frac{2^{2/3}n_1^{5/3} [V_r((2n_1)^{2/3} T_r(3n_3V_r - 1)^{1/3} - 2n_3) + 2]}{n_2 [3n_3V_r - 1]^{5/3}}. \quad (6.12)$$

The reduced equation of state is independent of the magnetic charge parameter g . From the reduced state equation we obtain the spinodal curve, which separates metastable phases from the unstable phase, using the condition,

$$(\partial_{V_r} P_r)_{T_r} = 0. \quad (6.13)$$

The explicit form of the spinodal curve is,

$$T_{rsp} = \frac{2^{4/3}n_3 [n_3V_r - 2]}{n_1^{2/3} [n_3V_r + 1] [3n_3V_r - 1]^{1/3}}. \quad (6.14)$$

Solving this for V_r and substituting in Eq. (6.12) we obtain the curve in $P-V$ plane. The spinodal curve along with the coexistence curve display the stable, unstable and metastable phases of the black hole. The coexistence curve is obtained numerically using the expressions $r_2(x)$, $P_0(x)$ and $T_0(x)$. The spinodal and coexistence curves are shown together in Fig. 6.1. By fitting the coexistence curve in $P-T$ plane we obtained the following expression,

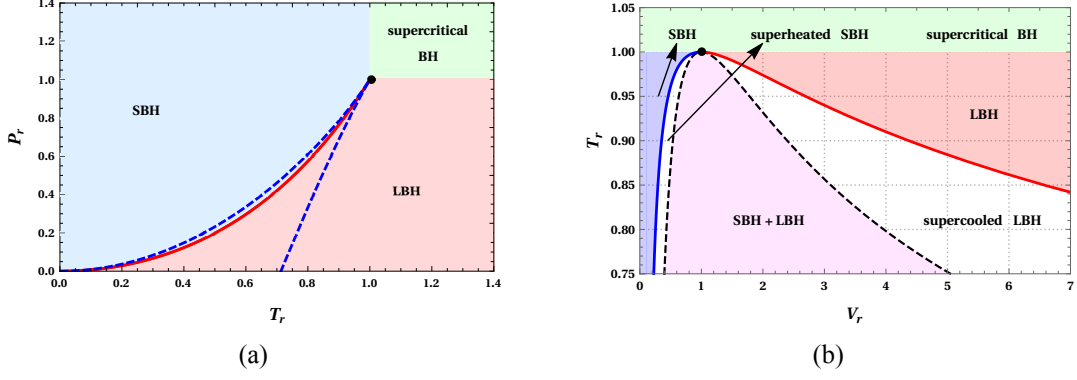


Figure 6.1: Phase structure of Hayward-AdS black hole in $P-T$ and $T-V$ diagrams. The coexistence curve is represented by a solid line and the spinodal curve is shown with a dashed line.

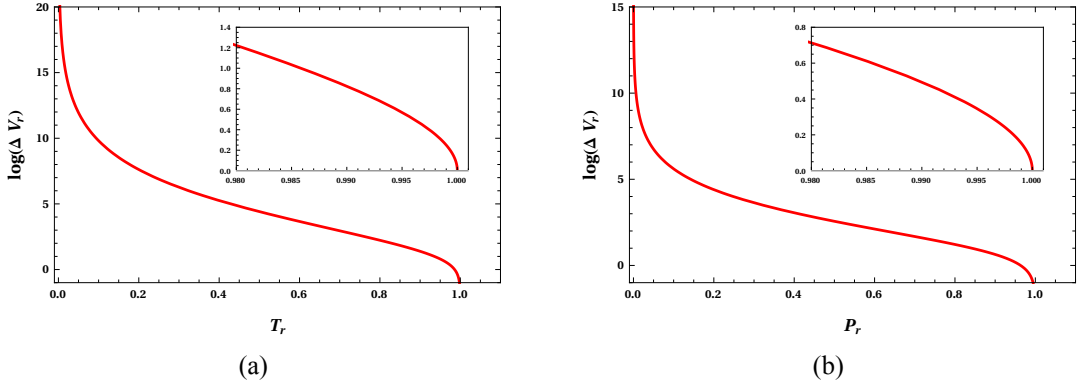


Figure 6.2: The behaviour of volume change $\Delta V_r = V_{rl} - V_{rs}$ during phase transition of the black hole. The behaviour near the critical point is shown in inlets using linear scale.

$$\begin{aligned}
 P_r = & 5.622 \times 10^{-7} - 5.539 \times 10^{-5} T_r + 0.693 T_r^2 + 0.1365 T_r^3 + 0.1966 T_r^4 \\
 & - 0.4255 T_r^5 + 1.134 T_r^6 - 1.698 T_r^7 + 1.621 T_r^8 - 0.8651 T_r^9 + 0.2085 T_r^{10}. \quad (6.15)
 \end{aligned}$$

The SBH, LBH and supercritical BH phases are depicted in Fig. 6.1(a). The coexistence curve separates the SBH and LBH phases. It terminates at the critical point, after which the distinction between the SBH and LBH states is not possible, hence this corresponds to the supercritical black holes. The region between the coexistence curve and spinodal curve corresponds to the metastable states, namely the supercooled LBH and the superheated SBH, which are shown in the $T-V$ diagram (Fig. 6.1(b)). An observable feature in these diagrams is that the spinodal and coexistence curves meet each other at the critical point.

Now, we would like to study the change in volume during the black hole phase transition as a function of temperature and pressure. Using expression of $r_2(x)$, we make the functional

change $V(r) \rightarrow V(x)$ to obtain a parametric expression for ΔV_r . The parametric expression of ΔV_r along with that of T_r and P_r ($T_0(x)$ and $P_0(x)$ expressions) are used to plot Fig. 6.2, which gives the behaviour of ΔV_r . From Fig. 6.2 it is clear that, ΔV_r decreases with increase in both temperature and pressure. It approaches zero at the critical point ($T_r = 1$ and $P_r = 1$). The numerical calculation reveals that, the behaviour near the critical point is,

$$\Delta V_r = 9.5005(1 - T_r)^{0.5296}, \quad \Delta V_r = 5.4984(1 - P_r)^{0.5216}. \quad (6.16)$$

This suggests that the change in volume ΔV_r can serve as the order parameter to characterise the black hole phase transition, with a universal critical exponent $1/2$.

6.3 Microstructure of the Hayward-AdS Black Hole

In this section we examine the microstructure of the black hole using Ruppeiner geometry in which T and V are taken as fluctuation coordinates. The line element in this parameter space has the form (Wei et al., 2019a),

$$dl^2 = \frac{C_V}{T^2} dT^2 - \frac{(\partial_V P)_T}{T} dV^2. \quad (6.17)$$

The heat capacity C_V vanishes for the Hayward-AdS black hole (Eq. 6.5). This makes the line element (6.17) singular, hence the corresponding geometry will not give the information regarding the microstructure of the black hole. Therefore the normalised scalar curvature is used for studying the microscopic interactions,

$$R_N = C_V R. \quad (6.18)$$

From a straightforward calculation, for the Hayward-AdS black hole we obtain,

$$R_N = \frac{[8\pi g^3 - V][8\pi g^3(\tau + 1) + V(2\tau - 1)]}{2[4\pi g^3(\tau + 2) + V(\tau - 1)]^2}. \quad (6.19)$$

with

$$\tau = \pi^{2/3} T (6V - 8\pi g^3)^{1/3}. \quad (6.20)$$

In terms of the reduced parameters,

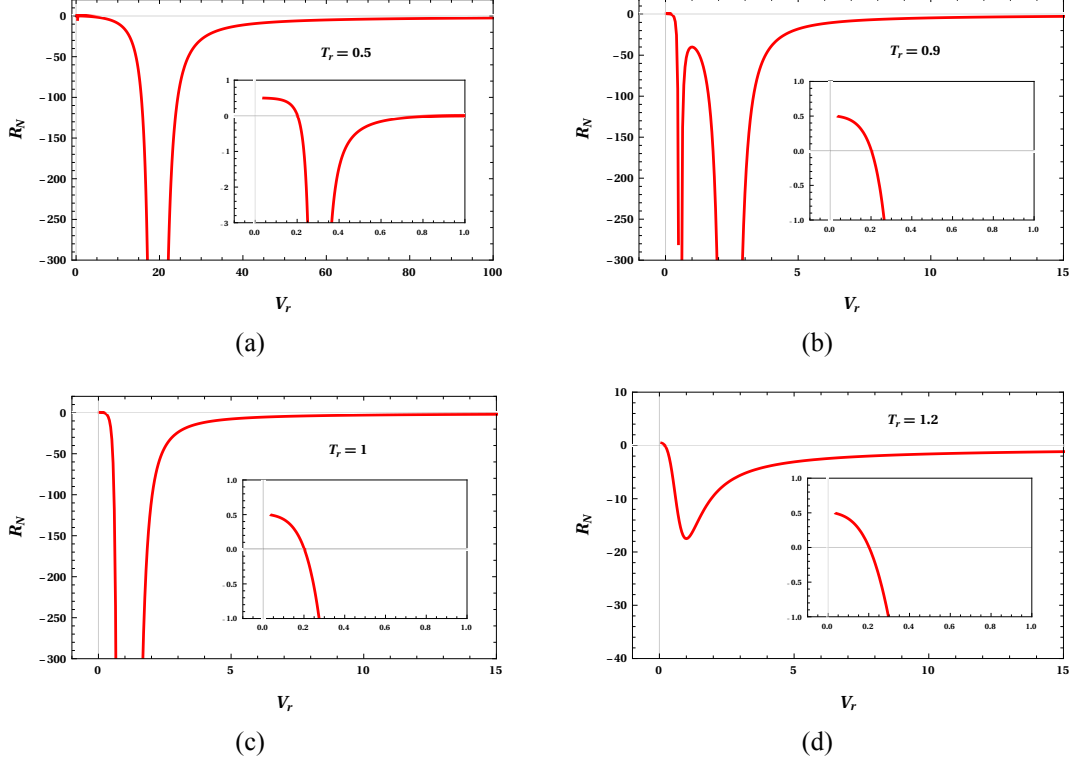


Figure 6.3: The behaviour of the normalised curvature scalar R_N against the reduced volume V_r at constant temperature.

$$R_N = \frac{4 [n_3 V_r - 2] [-A + 2n_3 V_r - 4]}{[A - 4n_3 V_r + 8]^2}, \quad (6.21)$$

where,

$$A = 2^{1/6} n_1^{2/3} T_r \left(\sqrt{2} V_r + 5\sqrt{2} - 4\sqrt{3} \right) (3n_3 V_r - 1)^{1/3}. \quad (6.22)$$

Similar to the case of charged AdS black hole and Gauss Bonnet black hole, R_N is independent of g . The normalised curvature scalar R_N diverges along the spinodal curve.

The behaviour of R_N with reduced volume V_r for a fixed temperature is studied in Fig. (6.3). For $T_r < 1$, below critical temperature, R_N has two negative divergence points. They approach each other as the temperature increases and merge together at $V_r = 1$ for $T_r = 1$. These divergences do not exist for temperatures greater than the critical value. We see that there always exists small regions where the curvature scalar is positive (shown in inlets). We need to examine whether these regions are thermodynamically stable. Setting $R_N = 0$ we get,

$$T_0 = \frac{T_{rsp}}{2} = \frac{2^{5/6} [n_3 V_r - 2]}{n_1^{2/3} \left[\sqrt{2} V_r + 5\sqrt{2} - 4\sqrt{3} \right] [3n_3 V_r - 1]}. \quad (6.23)$$

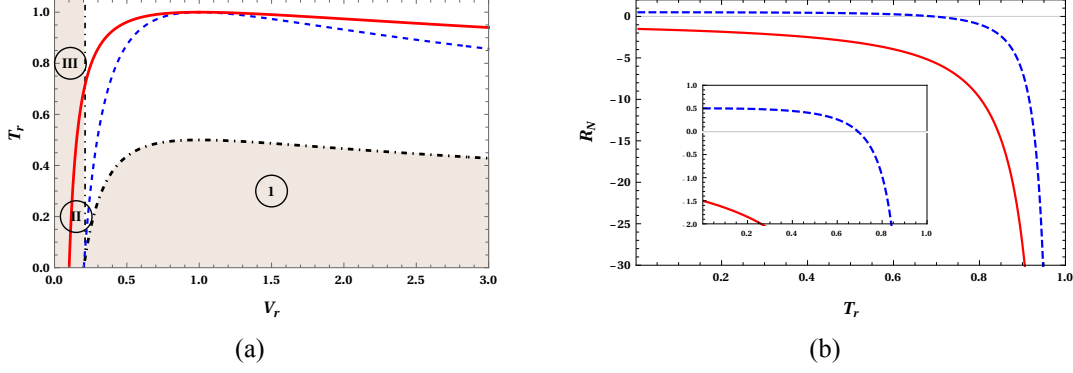


Figure 6.4: 6.4(a): The sign changing curve (dot-dashed black) of R_N along with the coexistence (solid red) and spinodal (dashed blue) curves. The vertical black (dot-dashed) line corresponds to V_0 . 6.4(b): The behaviour of normalised curvature scalar R_N along the coexistence line. The red (solid) line and blue (dashed) line corresponds to LBH and SBH, respectively. The inlet shows the region where the SBH branch takes positive R_N value.

This is the sign-changing temperature (where curvature scalar changes its sign), which is half of the spinodal curve temperature as in vdW system, RN-AdS and Gauss-Bonnet black holes. Another solution for this is, $V_r = 2/n_3 \equiv V_0$.

The spinodal, sign changing and coexistence curves are shown together in Fig. 6.4(a). The region (I) under the spinodal curve for $V_r > V_0$, R_N is positive, which corresponds to the coexistence phase of SBH and LBH, similar to van der Waals fluid's coexistence phase. Everywhere below V_0 , R_N is positive, including region above and below the coexistence curve. The region (II) under the coexistence curve is the same as the previous case, a coexistence phase. However, in the region (III) above the curve, which is a SBH phase, we can safely say that the black hole molecules possess repulsive interaction. Therefore in Hayward-AdS black hole, for a small parameter range there exist dominant repulsive interaction. This result is similar to RN-AdS black hole and in contrast to five-dimensional neutral Gauss-Bonnet black hole, where there is no repulsive interaction.

Finally, we consider the behaviour of the scalar curvature R_N along the coexistence curve. Since there exists no analytical expression for the coexistence curve, the analytical study of the curvature scalar behaviour is not possible. The numerical solution is obtained and shown in Fig. 6.4(b). Both the SBH branch and LBH branch of R_N have divergences near the critical point. For a large black hole, the sign of R_N is always negative and hence the microscopic interaction is always attractive. Interestingly, for the small black hole, there is a lower temperature range where R_N is positive (inlet of the diagram). This indicates a repulsive interaction between the black hole molecules. From this, we can conclude that

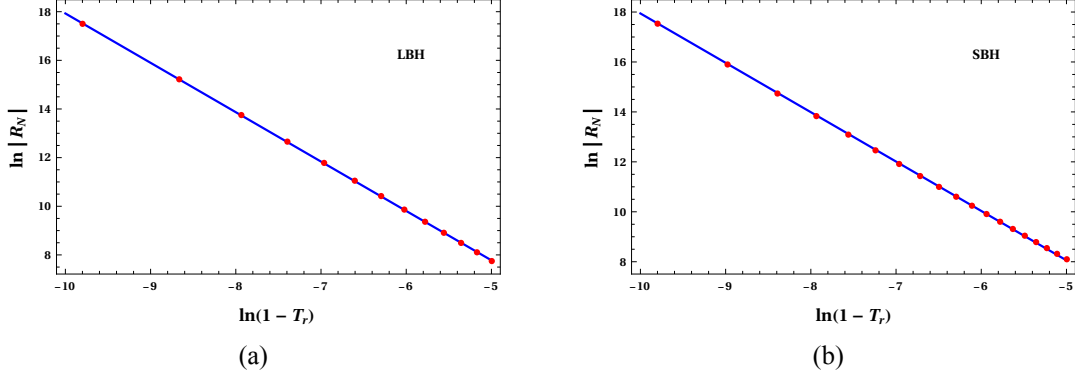


Figure 6.5: The numerical fit of $\ln |R_N|$ vs. $\ln(1 - T_r)$ for LBH (left) and SBH (right) branches. The solid blue line correspond to the plot of fitting formula and the red dots correspond to numerical data.

in the low-temperature regime, the microstructure, as well as microscopic interaction of the black hole changes drastically during the phase transition. Whereas in the high-temperature range, only microstructure changes, and the nature of interaction remains attractive in both phases. These results are strikingly different from that of van der Waals fluid, where the dominant interaction among the molecules is always attractive.

The critical phenomena associated with the Ruppeiner curvature along the coexistence curve is also studied numerically, as in Ref. (Wei et al., 2019b). The numerical fit is obtained by assuming the following behaviour near the critical point,

$$R_N \sim (1 - T_r)^p. \quad (6.24)$$

Which reduces to

$$\ln |R_N| = -p \ln(1 - T_r) + q. \quad (6.25)$$

From the numerical fit for the SBH and LBH branches we obtain,

$$SBH: \quad \ln R_N = -1.97733 \ln(1 - T_r) - 1.83058 \quad (6.26)$$

$$LBH: \quad \ln R_N = -2.03007 \ln(1 - T_r) - 2.37298 \quad (6.27)$$

These are depicted in Fig. 6.5 along with the numerical data. The results suggest that $p \approx 2$, which we set as $p = 2$ considering the numerical error. Combining Eq. (6.26) and Eq. (6.27) we construct,

$$R_N(1 - T_r)^2 = -e^{-(1.83058+2.37298)/2} = -0.122238 \approx -1/8. \quad (6.28)$$

This agrees with previously obtained results for vdW fluid and other AdS black holes (Wei et al., 2019a,b; Wei and Liu, 2020b), that R_N has a universal exponent 2 and the relation $R_N(1 - T_r)^2 = -1/8$, near the critical point.

6.4 Discussions

In this chapter, we have studied the phase transitions and microstructure of the Hayward-AdS black hole. The microscopic properties are analysed from the behaviour of Ruppeiner curvature scalar along the coexistence curve. Since an analytical expression for the coexistence curve is not feasible we have carried out our investigation numerically. In the first part of the chapter, we probed the phase structure of the black hole using the coexistence curve in $P_r - T_r$ and $T_r - V_r$ planes. Along with this, spinodal curve is also plotted, which enables us to identify the metastable phases of the black holes, namely the superheated SBH and the supercooled LBH. It is shown that the change in volume ΔV_r during the SBH - LBH phase transition can serve as an order parameter to describe the same. The behaviour of ΔV_r has a critical exponent 1/2 which is universal.

In the second part of this chapter, we have focused on the Ruppeiner geometry of the black hole. We have adopted the definition of curvature scalar given in the Ref. Wei et al. (2019a), where the fluctuation coordinates are temperature and volume. The normalised curvature scalar diverges to the negative infinity at the critical point. Also, we numerically confirm that in the vicinity of critical point R_N has a critical exponent 2 and $R_N(1 - T_r)^2 \approx -1/8$. Even though the black hole shows van der Waals like phase transition, the microstructure properties differ in some aspects. In van der Waals fluid the dominant interaction among the constituent molecules is always attractive, which does not change during the phase transition. The change in microstructure does not lead to any change in the nature of microscopic interaction. However, in Hayward-AdS black hole there exists a domain, low-temperature range for the small black hole, where the dominant interaction between the black hole molecules is repulsive, which is inferred from the positive sign of the normalised curvature scalar. During the phase transition, in this temperature range, the microscopic interaction of the black hole changes significantly. This result is similar to what is observed in RN-AdS black hole and in contrast to the five-dimensional neutral Gauss-Bonnet black hole, where the interaction is always attractive like van der Waals fluid. To conclude, the magnetic charge in

the Hayward-AdS black hole plays a similar role as the electric charge in RN-AdS black hole in contributing to the microstructure. We believe that this is another significant step in understanding black hole microstructure properties.

Chapter 7

Reentrant Phase Transition and Microstructure of AdS Black Holes

I know that I know nothing.

Plato, *Socratic paradox*

Summary

In this chapter we study the microscopic origin of this reentrant phase transition by employing a novel Ruppeiner geometry method, which is based on our published article in Phys. Rev. D. ([Naveena Kumara et al., 2021a](#)). Having in mind that the entropy and volume are interdependent in a spherically symmetric AdS black hole, the application of Ruppeiner geometry for such a system must be carried out with a special care. We have constructed the Ruppeiner curvature scalar in the parametric space where the temperature and volume are the fluctuation coordinates. we investigated the phase structure and the corresponding microscopic interactions for both the standard van der Waals (SPT) and the reentrant phase transitions (RPT), where a first-order phase transition is accompanied by a zeroth-order transition. They discovered that the microstructure that leads to RPT is distinct from that of SPT. We have shown that the Born Infeld coupling coefficient b determines the microscopic interaction of the black hole. Due to the complex structure of spacetime the authors were only able to perform numerical calculations.

7.1 Introduction

A reentrant phase transition (RPT) occurs when the system undergoes more than one phase transition when there is a monotonic change in the thermodynamic variable, such that, the

initial and final macrostates of the system are the same. In conventional thermodynamic systems, this phenomenon was first observed in the nicotine/water mixture, in a process with a fixed percentage of nicotine and an increase in the temperature, the system exhibited a reentrant phase transition from initial homogeneous mixed state to an intermediate distinct nicotine/water phases and finally to the homogeneous state (Hudson, 1904). This kind of reentrant phase transition is observed in a variety of physical systems, more commonly in multicomponent fluid systems, gels, ferroelectrics, liquid crystals, binary gases etc. (Narayanan and Kumar, 1994). This phenomenon is not limited to condensed matter physics, for example, a $(2 + 1)$ dimensional Dirac oscillator in non-commutative spacetime and magnetic field shows a similar phase transition (Panella and Roy, 2016).

In black hole physics, reentrant phase transition was first observed in four-dimensional Born Infeld AdS black holes (Gunasekaran et al., 2012), where the initial and final phases are large black holes and the intermediate phase is an intermediate black hole. For this case, LBH/IBH/LBH reentrant phase transition takes place when the temperature is decreased monotonically in a certain range of pressure. However, higher dimensional Born Infeld black holes do not show reentrant phase transitions (Zou et al., 2014). Interestingly, rotating black holes in dimensions $d \geq 6$ show reentrant phase transitions (Altamirano et al., 2013). In subsequent studies, the RPT in higher dimensional single spinning and multi spinning Kerr black holes in anti-de Sitter and de Sitter spacetime were investigated (Altamirano et al., 2014b,a; Kubiznak and Simovic, 2016). Reentrant phase transitions were also observed in gravity theories consisting of higher-curvature corrections (Frassino et al., 2014; Wei and Liu, 2014; Hennigar et al., 2015; Sherkatghanad et al., 2016; Hennigar and Mann, 2015). The reentrant phase transition of Born Infeld black hole was also analysed with a different perspective, wherein the charge of the system was varied, and the cosmological constant (pressure) was kept fixed (Dehyadegari and Sheykhi, 2018). Furthermore, the relationship between the RPT and the photon sphere of Born Infeld AdS spacetime has been studied (Xu et al., 2019). With a motivation from the famous saying by Boltzmann, ‘If you can heat it, it has microstructure’, it is reasonable to ask, what is the underlying microstructure that leads to a reentrant phase transition in a black hole?”

This chapter is organised as follows. In the next section, we discuss the thermodynamics and the phase structure of the black hole. We will consider the van der Waals case (which will be called SPT throughout the chapter which stands for standard phase transition) and RPT

case separately. Then the microstructure study is carried out by constructing the Ruppeiner geometry using the fluctuation coordinates as temperature and volume (section 7.3). In the final section (7.4) we present our results.

7.2 Thermodynamics and Phase Structure of the Black Hole

In this section we present thermodynamics and phase structure of the Born-Infeld AdS (BI-AdS) black hole. The action for Einstein gravity in the presence of Born-Infeld field has the following form (Born and Infeld, 1934; Gunasekaran et al., 2012),

$$S = \frac{1}{16\pi} \int d^4x \sqrt{-g} \left[\mathcal{R} - 2\Lambda + 4b^2 \left(1 - \sqrt{1 + \frac{F_{\mu\nu}F^{\mu\nu}}{2b^2}} \right) \right]. \quad (7.1)$$

Here \mathcal{R} and Λ are the Ricci scalar and cosmological constant, respectively. The Born Infeld parameter b with dimension of mass represents the maximal electromagnetic field strength, and is related to the string tension (the identification is motivated from string theory (Gibbons, 2001)), and $F_{\mu\nu} = \partial_\mu A_\nu - \partial_\nu A_\mu$ is the electromagnetic field tensor, where A_μ is the vector potential. We study the extended thermodynamics of the black hole, where the cosmological constant serves the role of thermodynamic pressure. Their relation to the AdS radius l are given by,

$$\Lambda = -\frac{3}{l^2}, \quad \text{and} \quad P = \frac{3}{8\pi l^2}. \quad (7.2)$$

The solution to the Einstein field equations in the static and spherically symmetric spacetime background yields (Fernando and Krug, 2003; Dey, 2004; Cai et al., 2004),

$$ds^2 = -f(r)dt^2 + f^{-1}(r)dr^2 + r^2 (d\theta^2 + \sin^2\theta d\phi^2) \quad \text{and} \quad F = \frac{Q}{\sqrt{r^4 + Q^2/b^2}} dt \wedge dr, \quad (7.3)$$

with the metric function of the form,

$$f(r) = 1 + \frac{r^2}{l^2} - \frac{2M}{r} + \frac{2b^2}{r} \int_r^\infty \left(\sqrt{r^4 + \frac{Q^2}{b^2}} - r^2 \right) dr \quad (7.4)$$

$$= 1 + \frac{r^2}{l^2} - \frac{2M}{r} + \frac{2b^2 r^2}{3} \left(1 - \sqrt{1 + \frac{Q^2}{b^2 r^4}} \right) + \frac{4Q^2}{3r^2} {}_2F_1 \left(\frac{1}{4}, \frac{1}{2}, \frac{5}{4}; -\frac{Q^2}{b^2 r^4} \right). \quad (7.5)$$

Where, ${}_2F_1$ is the hypergeometric function, the parameters M and Q are the ADM mass and the asymptotic charge of the solution, respectively. We obtain mass of the black hole by setting $f(r_+) = 0$,

$$M = \frac{r_+}{2} + \frac{r_+^3}{2l^2} + \frac{b^2 r_+^3}{3} \left(1 - \sqrt{1 + \frac{Q^2}{b^2 r_+^4}} \right) + \frac{2Q^2}{3r_+^2} {}_2F_1 \left(\frac{1}{4}, \frac{1}{2}, \frac{5}{4}; -\frac{Q^2}{b^2 r_+^4} \right). \quad (7.6)$$

The Hawking temperature and the corresponding entropy are given by,

$$T = \frac{1}{4\pi r_+} \left(1 + \frac{3r_+}{l^2} + 2b^2 r_+^2 \left(1 - \sqrt{1 + \frac{Q^2}{b^2 r_+^4}} \right) \right), \quad (7.7)$$

$$S = \frac{A}{4} = \pi r_+^2. \quad (7.8)$$

The electric potential Φ and the electric polarization B , which is conjugate to b and is referred to as ‘‘BI vacuum polarization’’, measured at infinity with respect to the event horizon they are calculated to be,

$$\Phi = \frac{Q}{r_+} {}_2F_1 \left(\frac{1}{4}, \frac{1}{2}, \frac{5}{4}; -\frac{Q^2}{b^2 r_+^4} \right) \quad (7.9)$$

$$B = \frac{2}{3} b r_+^3 \left(1 - \sqrt{1 + \frac{Q^2}{b^2 r_+^4}} + \frac{Q^2}{3b r_+} \right) {}_2F_1 \left(\frac{1}{4}, \frac{1}{2}, \frac{5}{4}; -\frac{Q^2}{b^2 r_+^4} \right) \quad (7.10)$$

Interpreting the mass M , as enthalpy rather than the internal energy of the black hole, we obtain the first law of thermodynamics as,

$$dM = TdS + VdP + \Phi dQ + Bdb, \quad (7.11)$$

where $V = \frac{4\pi r_+^3}{3}$ is the thermodynamic volume of the system. In addition to the first law of thermodynamics, the thermodynamic quantities of BI-AdS black hole satisfy the Smarr formula, which is obtained by scaling argument as,

$$M = 2(TS - VP) + \Phi Q - Bb. \quad (7.12)$$

The equation of state of the black hole system is,

$$P = \frac{T}{2r_+} - \frac{1}{8\pi r_+^2} - \frac{b^2}{4\pi} \left(1 - \sqrt{1 + \frac{Q^2}{b^2 r_+^4}} \right). \quad (7.13)$$

The black hole shows a van der Waals like phase transition, which depends on the value of the Born Infeld coupling coefficient b . The critical values corresponding to this phase transition is obtained by employing the conditions,

$$(\partial_{r_+} P)_T = (\partial_{r_+, r_+} P)_T = 0. \quad (7.14)$$

The critical values are (Gunasekaran et al., 2012; Xu et al., 2019),

$$P_c = \frac{1 - 16xQ^2}{8\pi r_{+c}^2} - \frac{b^2}{4\pi} \left(1 - \frac{1}{4xr_{+c}^2}\right), \quad T_c = \frac{1 - 8xQ^2}{2\pi r_{+c}}, \quad r_{c+} = \frac{1}{2} \left(\frac{1}{x_k^2} - \frac{16Q^2}{b^2}\right)^{\frac{1}{4}}, \quad (7.15)$$

where

$$x_k = 2\sqrt{-\frac{p}{3}} \cos\left(\frac{1}{3} \arccos\left(\frac{3q}{2p} \sqrt{\frac{-3}{p}}\right) - \frac{2\pi k}{3}\right), \quad k = 0, 1, 3, \quad (7.16)$$

and

$$p = -\frac{3b^2}{32Q^2}, \quad q = \frac{b^2}{256Q^4}. \quad (7.17)$$

Since, the critical point corresponding to x_2 is always a complex number, effectively we have only two critical points. Based on these two values we can classify the system into four different cases which depend on the value of b .

- Case 1 (no PT), $b < b_0$: For this condition, the system behaves like a Schwarzschild AdS black hole. The large black hole phase is stable and the small black hole phase is unstable. Therefore there is no van der Waals like phase transition in this case.
- Case 2 (RPT), $b_0 < b < b_1$: In this condition, the system is characterised by two critical points c_0 and c_1 . However c_0 is an unstable point as it has a higher Gibbs free energy. In this scenario, the system exhibits a zeroth-order phase transition and a van der Waals like first-order phase transition, between a large black hole phase and an intermediate black hole phase. These successive transitions are together termed as a reentrant phase transition.
- Case 3 (RPT), $b_1 < b < b_2$: This is another case of reentrant phase transition displayed by the black hole. However, here the critical point c_0 lies in the negative pressure region.

- Case 4 (SPT), $b_2 < b$: Here the black hole exhibits the typical van der Waals like phase transition with one critical point.

The values of the parameter b where the phase transition behaviour changes, are given by,

$$b_0 = \frac{1}{\sqrt{8Q}} \approx \frac{0.3536}{Q}, \quad b_1 = \frac{\sqrt{3+2\sqrt{3}}}{6Q} \approx \frac{0.4237}{Q}, \quad b_2 = \frac{1}{2Q} = \frac{0.5}{Q}. \quad (7.18)$$

For SPT situation, we introduce the reduced parameters, which are defined as,

$$P_r = \frac{P}{P_c} \quad T_r = \frac{T}{T_c} \quad V_r = \frac{V}{V_c}. \quad (7.19)$$

Since there are two critical points in the RPT case, there is no unique way of defining the reduced parameters. However, there is only one critical point which appears in the phase transition scenario of the black hole, the point where the first-order transition terminates. We define reduced parameters considering that critical point as,

$$P_r = \frac{P}{P_{c1}} \quad T_r = \frac{T}{T_{c1}} \quad V_r = \frac{V}{V_{c1}}. \quad (7.20)$$

A clear picture of phase transition of BI-AdS black hole can be understood from the behaviour of the thermodynamic potential, as it determines the globally stable states of equilibrium thermodynamics. The thermodynamic potential for the system with fixed temperature T , pressure P and charge Q is the Gibbs free energy, which is calculated from the Euclidean action (Kubiznak and Mann, 2012a; Gunasekaran et al., 2012). The stable state of the system then corresponds to the lowest Gibbs free energy. The expression for the Gibbs free energy is given by,

$$G(T, P) = \frac{1}{4} \left[r_+ - \frac{8\pi}{3} P r_+^3 - \frac{2b^2 r_+^2}{3} \left(1 - \sqrt{1 + \frac{Q^2}{b^2 r_+^4}} \right) + \frac{8Q^2}{3r_+} {}_2F_1 \left(\frac{1}{4}, \frac{1}{2}, \frac{5}{4}; -\frac{Q^2}{b^2 r_+^4} \right) \right]. \quad (7.21)$$

7.2.1 Standard Phase Transition Case

First, we study the Gibbs free energy for the SPT case by choosing $Q = 1$ and $b = 0.45$, the result is shown in Fig. 7.1. In these plots, a simple measure used for thermodynamic stability

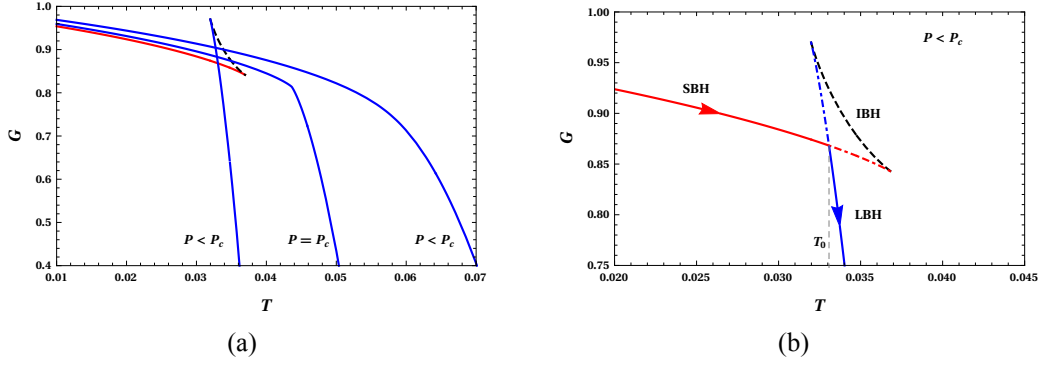


Figure 7.1: The behaviour of the Gibbs free energy G for the SPT case. Here, we take $Q = 1$ and $b = 1$. In Fig. 7.1(a), the blue and red solid lines stand for stable states, whereas black dashed line for unstable states. In Fig. 7.1(b) the direction of evolution of the system with increasing temperature T is depicted. The solid red and blue lines correspond to SBH and LBH phase of the black hole, respectively. The dot-dashed lines are the stable states not followed by the system.

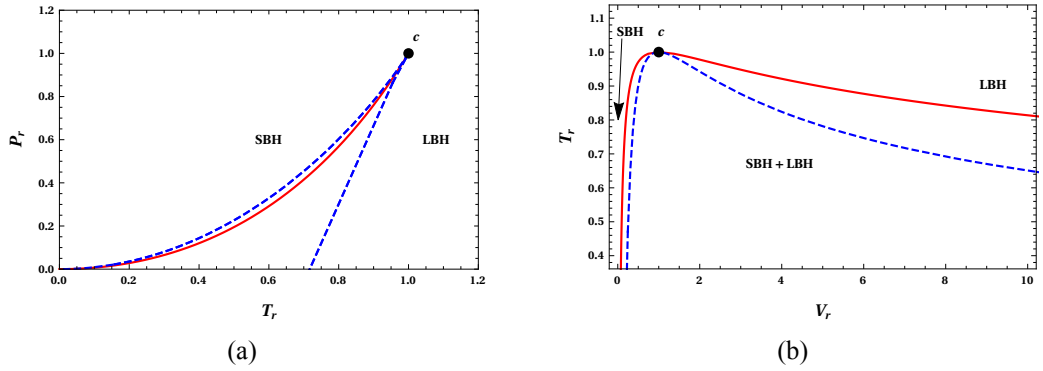


Figure 7.2: The coexistence curve (red solid line) and the spinodal curve (blue dashed line) for the SPT of the black hole. The coexistence curve separates SBH and LBH phases. The region between the coexistence curve and spinodal curves are the metastable SBH and LBH phases in respective regions. The black dot c denotes the critical point. Here we have taken $Q = 1$ and $b = 1$.

is the positivity of the specific heat. The negativity of specific heat stands for thermodynamic instability. As we are working in the canonical ensemble in an extended space the specific heat under consideration is the specific heat at constant pressure C_P . In this case (SPT), the Gibbs free energy exhibits a typical swallowtail behaviour, which is the signature of a first-order phase transition. This behaviour is seen for $P < P_c$, which disappears at $P = P_c$, shown in Fig. 7.1(a), which is a second-order phase transition point. The system always prefers a state with a low Gibbs free energy. From Fig. 7.1(b) it is clear that initially in low-temperature region, the system chooses a SBH phase as it has a lower Gibbs free energy. As the temperature increases, it follows the LBH phase branch at T_0 , as it has a lower Gibbs free energy. At this point, the system undergoes a first-order transition from SBH to LBH phase. This transition is similar to the liquid-gas phase transition of a vdW fluid.

b	0.6	0.7	0.8	0.9	1
P_c	0.003486	0.003436	0.003405	0.003385	0.003371
T_c	0.044251	0.043981	0.043815	0.043705	0.043628

Table 7.1: The critical values P_c and T_c for different values of b , with $Q = 1$, corresponding to the SPT of the black hole.

The phase structure of the black hole for the SPT case is presented in Fig. 7.2 using the coexistence and spinodal curves in the reduced parameter space. There exists no analytical expression for the coexistence curve of the system, therefore we obtain it via a numerical method by observing the swallowtail behaviour of Gibbs free energy. The coexistence curves so obtained in the $P_r - T_r$ plane are inverted for $T_r - V_r$ plane. In the $P_r - T_r$ plane, Fig. 7.2(a), the coexistence curve separates the SBH and LBH phases of the black hole. The coexistence region of SBH and LBH can be understood from $T_r - V_r$ plane, Fig. 7.2(b), which is the region under the coexistence curve. In the coexistence region, the equation of state is not applicable. To identify the metastable phases of the black hole, we find the spinodal curves, blue dashed lines in Fig. 7.2, which are defined by,

$$(\partial_V P)_T = 0 \quad \text{and} \quad (\partial_V T)_P = 0. \quad (7.22)$$

The spinodal curves meet the coexistence curve at the critical point. The region between the spinodal curve and coexistence curve corresponds to metastable phases. The region adjacent to the LBH/SBH phase is the metastable LBH/SBH phase. Beyond the critical point c , the distinction between the phases is not possible, which is termed as supercritical black hole region. In the $P_r - T_r$ plane the upper spinodal curve begins from zero, whereas lower one starts from $T_r = 0.716953$. The latter one is slightly higher than that of RN-AdS black hole, where it is $T_r = \sqrt{2}/2 \approx 0.707107$, and little less than $27/32 \approx 0.84375$ of vdW fluid (Wei et al., 2019b). In the $T_r - V_r$ plane, the curve intercepts the x -axis at $V_r = 0.163239$ for $T_r = 0$, which is comparable to $V_r = 1/3\sqrt{3} \approx 0.19245$ of RN-AdS case (Wei et al., 2019b). However it is not the exact numerical value which is of interest, but the non zero value compared to zero value for the vdW fluid. This non-zero value is related to the repulsive interactions in the microstructure, which we will study in the next section. For completeness, we mention that the spinodal curve adjacent to the LBH phase in $T_r - V_r$ plane approaches infinity. Before

concluding the SPT case, we list the critical values of pressure and temperature for different values of b in table 7.1, which we will be using to investigate the microstructure in section 7.3.

7.2.2 Reentrant Phase Transition Case

Now we focus on the reentrant phase transition exhibited by the BI-AdS black hole. Among the two cases of reentrant phase transition (case 2 and case 3), we chose case 3 ($b_1 < b < b_2$) in this chapter to demonstrate the associated properties. The results obtained are applicable for the case 2 of $b_0 < b < b_1$ also. The reentrant phase transition can be better understood from Gibbs free energy study, as shown in Fig. 7.3. In the $G-T$ plots, for pressure $P = P_{c1}$, which corresponds to the second-order phase transition point, there is no swallow tail behaviour, as seen from Fig. 7.3(a). The solid blue line represents a stable phase of the system (LBH) with positive specific heat at constant pressure C_P , while the dashed black line stands for unstable phase (SBH) of the system with negative C_P . We emphasise the fact that SBH phase in RPT case is always unstable. There is no phase transition above the critical pressure P_{c1} . For pressures $P < P_{c1}$, we begin to observe a first-order phase transition, the indication being the swallowtail, Fig. 7.3(b). Here, we identify three temperatures, designated as T_0 , T_1 and T_2 . The points in the curve corresponding to T_1 and T_2 correspondingly connect the stable LBH (blue line) and stable IBH (red line) branches to unstable branches (dashed black). The temperature T_0 , which is the intersection of the stable IBH and LBH branches, is the point where a vdW like IBH-LBH first-order phase transition occurs. As we decrease the pressure, the mere first-order phase transition situation continues till $P = P_z$, where we have $T_1 = T_2 \equiv T_z$, which is depicted in Fig 7.3(c). Further decreasing the pressure, $P < P_z$, leads to a scenario where an additional zeroth-order phase transition is also exhibited by the system, Fig 7.3(d). This happens for a range of pressures $P_l < P < P_z$, with $T_1 < T_2 < T_0$. For a fixed pressure in this range, if the system is at some temperature T_1 initially, then it stays in LBH phase as the temperature increases, till $T = T_2$. At temperature T_2 , the system finds a stable branch with lower Gibbs energy and jumps into the IBH phase. Unlike a first-order phase transition, there is a finite change in Gibbs free energy during this transition. Further, the system undergoes a secondary phase transition at $T = T_0$ from IBH to LBH phase, which is a first-order transition. In effect, the system undergoes LBH/IBH/LBH phase transition, the initial and final phases being the same. This is termed as a reentrant phase

transition. This phenomenon disappears at $P = P_t$, with $T_0 = T_2 \equiv T_t$, where the system has only LBH phase, Fig 7.3(e). There is no zeroth order or vdW like first-order phase transitions possible for the pressures $P < P_t$, Fig. 7.3(f), wherein only the LBH phase exists. In short, the system exhibits both first order and zeroth-order phase transition for the range of pressures $P \in (P_t, P_z)$ and temperatures $T \in (T_t, T_z)$, whereas only first-order phase transition for $P \in (P_z, P_{c1})$ and $T \in (T_z, T_{c1})$.

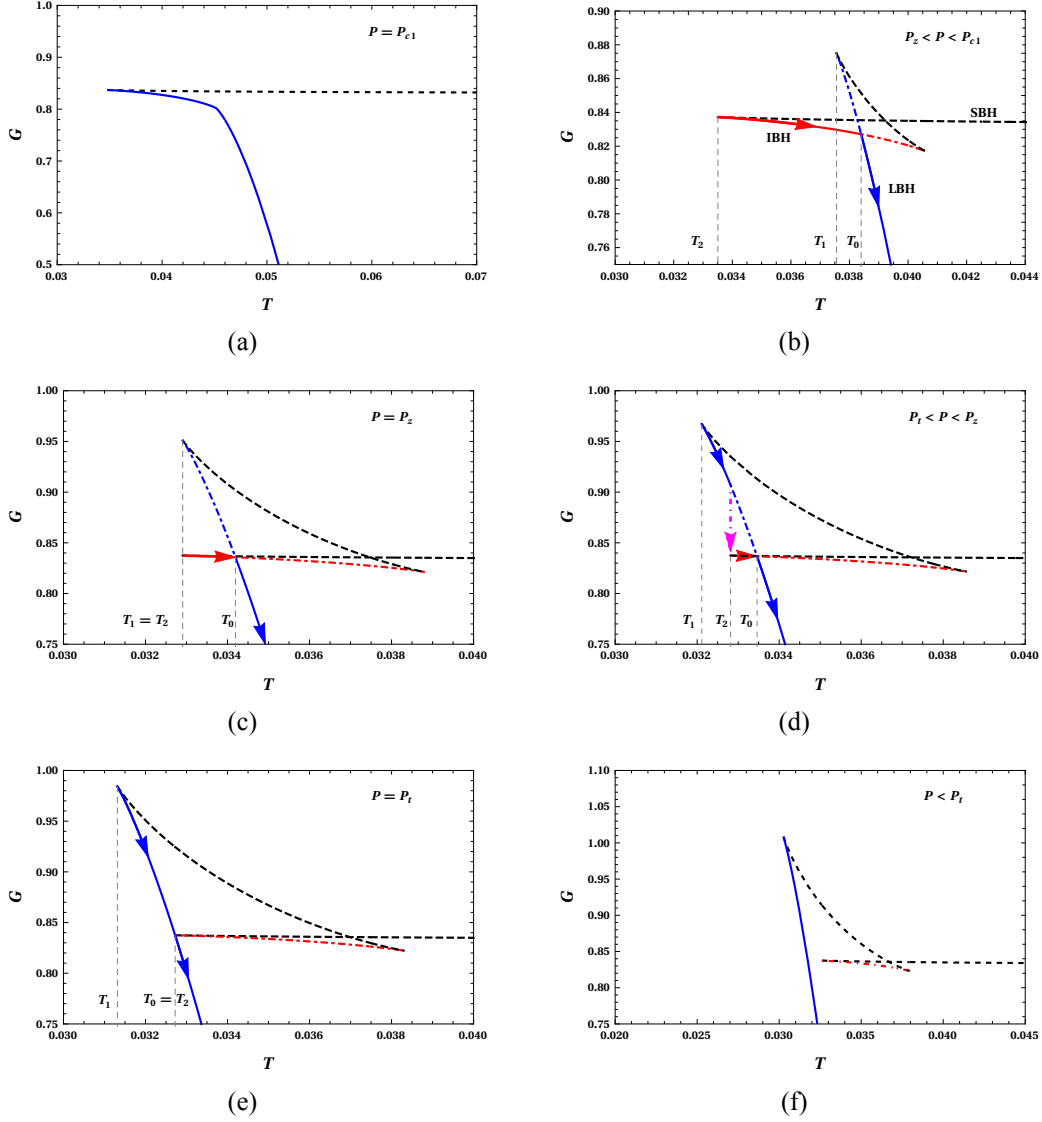


Figure 7.3: The behaviour of the Gibbs free energy G for the RPT case. We take $Q = 1$ and $b = 0.45$. The black dashed lines corresponds to negative C_P , whereas blue and red lines correspond to positive C_P . The solid red and blue lines are states preferred by the system over the dot-dashed red and blue lines.

The phase diagrams of the black hole corresponding to the reentrant phase transition case is presented in Fig. 7.4. As in SPT case, here also the results are obtained numerically by observing the behaviour of Gibbs free energy. Interestingly, for all values of pressure, we

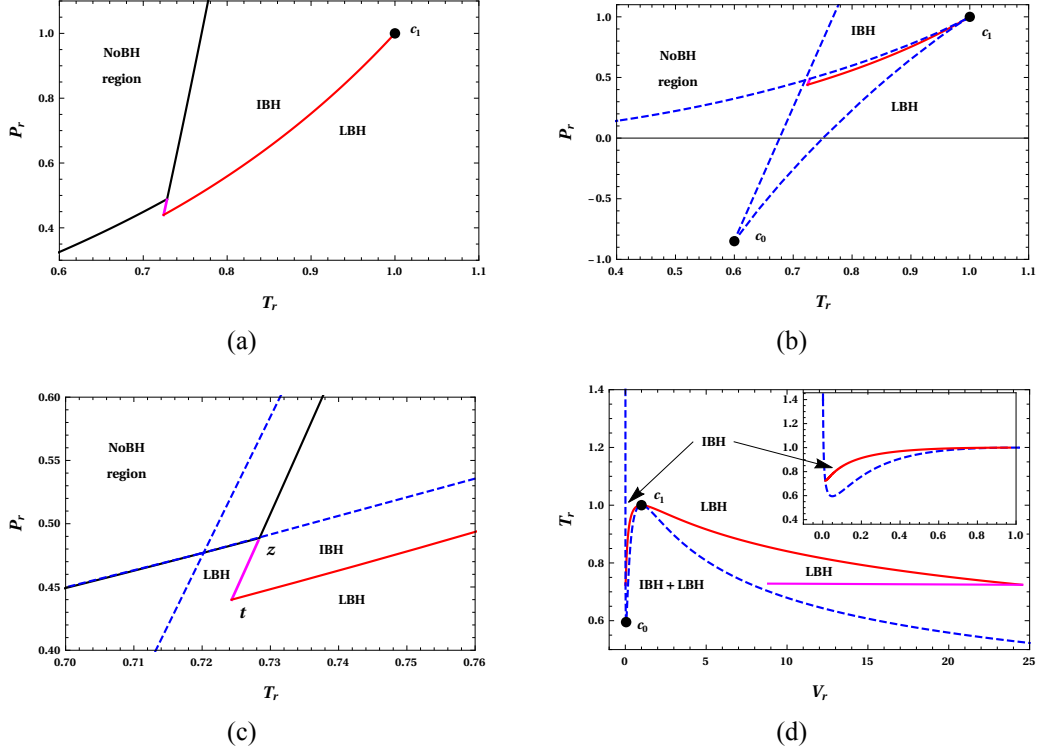


Figure 7.4: Phase diagrams for reentrant case. (a) Black line separates no black hole region from black hole region. First order coexistence curve (solid red) and zeroth order phase transition line (solid magenta) are also shown. (b) The transition lines and the spinodal curves for the RPT of the black hole. c_0 and c_1 are the two critical points. At c_1 spinodal curve meets first order coexistence curve. (c) The enlarged reentrant phase transition region. The points t and z correspond to (P_t, T_t) and (P_z, T_z) , respectively. (d) Phase structure in the $T_r = V_r$ plane. Here, the near origin behaviour is shown in the inset. In all these plots we have taken $Q = 1$ and $b = 0.45$

find that there is a lowest temperature below which there is no existence of black hole. The line which separates the black hole solutions from no black hole region is obtained by noting the temperature T_2 for pressures $P > P_z$ and T_1 for $P < P_z$ from the Gibbs free energy plots (Fig. 7.3). The result is shown in 7.4(a), where the separation line (black solid curve) has a discontinuity at (P_z, T_z) . In the same plot, the transition lines of zeroth-order and first-order phase transition are also given. As T_2 is the zeroth-order phase transition point in the pressure range $P \in (P_t, P_z)$, the corresponding transition line (solid magenta line) matches with the extension of no black hole line from P_z to P_t . The first order coexistence line (red solid line) is also obtained from the Gibbs free energy behaviour. The first order coexistence curve and zeroth-order transition line meet at (P_t, T_t) , which is the *triple point*. The zeroth order transition line terminates at (P_z, T_z) , and the other at the critical point (P_{c1}, T_{c1}) .

Here too we obtain the spinodal curves using the definition Eq. 7.22, which are shown in Fig. 7.4(b) along with the transition lines. The spinodal curve, the extremal points of the

b	0.43	0.44	0.45	0.46	0.47	0.48	0.49
P_{c0}	-0.000663	-0.00186	-0.003253	-0.004888	-0.006838	-0.009242	-0.012447
T_{c0}	0.033189	0.030199	0.026885	0.023198	0.019061	0.014328	0.008676
P_{c1}	0.003711	0.003686	0.003663	0.003643	0.003625	0.003609	0.003594
T_{c1}	0.045414	0.045289	0.045176	0.045074	0.044981	0.044895	0.044817
P_t	0.002225	0.001922	0.001612	0.001294	0.000971	0.000644	0.000318
T_t	0.037435	0.035249	0.032722	0.029762	0.026208	0.021759	0.015646
P_z	0.002395	0.002101	0.00179	0.001464	0.001122	0.000747	0.000357
T_z	0.037658	0.035457	0.032906	0.029914	0.026322	0.021821	0.015663

Table 7.2: The values of (P_{c0}, T_{c0}) , (P_{c1}, T_{c1}) , (P_t, T_t) and (P_z, T_z) for different b values, with $Q = 1$, corresponding to the RPT of the black hole.

isothermal and isobaric curves by definition, have two turning points in the reentrant case, which are marked as c_0 and c_1 . As mentioned earlier, in case 3, which we have chosen, the point c_0 lies in the negative pressure region. The region between (P_t, T_t) and (P_z, T_z) is enlarged in Fig. 7.4(c). Note that, for $\{P < P_z, T < T_z\}$ the spinodal curve and no black hole line are the same. The regions separated by first-order coexistence line and zeroth-order transition line are clearly seen here. As both zeroth-order and first-order transitions are between IBH and LBH both lines separate these two phases in their respective domains. In Fig. 7.4(d), the phase structure for the reentrant case is given in $T_r - V_r$ plane, where the coexistence region of IBH and LBH is clearly shown. The IBH region is on the left, and the LBH is on the right side of the coexistence curve. As in $P_r - T_r$ plane here also the spinodal curve has two turning points, at the critical points c_0 and c_1 . In contrast to the case of SPT, here, the spinodal curve does not intersect the V_r axis near the origin, instead shoots to infinity. On the other side, near the LBH phase, there is no change in the behaviour. The region near the origin is enlarged in the inset, where it can be seen that the IBH branch terminates when it meets the spinodal curve. Before concluding this section we list the values of (P_{c0}, T_{c0}) , (P_{c1}, T_{c1}) , (P_t, T_t) and (P_z, T_z) for different b values for the reentrant case in table 7.2.

7.3 Ruppeiner Geometry and Microstructure of the Black Hole

In this section, we investigate the microstructure of four-dimensional Born-Infeld AdS black hole using Ruppeiner geometry, constructed in the parameter space with fluctuation coordinates as temperature and volume. Particularly, we are interested in the microstructure that leads to the reentrant phase transition. As we will see, the underlying microstructure for the SPT has similarity with the RN-AdS black hole phase transition, whereas the RPT emerges due to a different nature of the black hole microstructure.

7.3.1 Standard Phase Transition Case

We obtained the normalised curvature scalar R_N for the four-dimensional Born-Infeld AdS black hole using the above definitions. The SPT and RPT cases are analysed separately. The curvature scalar R_N is expressed in terms of reduced parameters using Eq. 7.19 and Eq. 7.20 in the respective cases. First, we will analyse the SPT case. It is found that the behaviour of R_N for SPT case is similar to that of RN-AdS black hole. The functional behaviour of R_N against thermodynamic volume V_r for a fixed temperature of T_r is studied in fig. (7.5). For $T_r < 1$, below critical temperature, R_N has two negative divergences. These two divergences gradually come closer as temperature increases and merge at $T_r = 1$. The divergence at critical temperature occurs at $V_r = 1$. For temperatures above the critical value, both divergences disappear. The divergences of R_N are related to the spinodal curve. In fact, R_N diverges along the spinodal curve. Since V_r is doubly degenerate in the $T_r - V_r$ spinodal curve (Fig. 7.2(b)), below critical point, it leads to two divergences for $T_r < 1$. For low temperatures, we notice that R_N takes positive values in a very small domain (shown in the insets of Fig. 7.8(a), near the origin) as $V_r \rightarrow 0$, which is the small black hole phase. We observe positive R_N on both sides of the near origin divergence. The left side corresponds to the SBH phase (shaded yellow) and the right side corresponds to the coexistence phase (shaded green). The shaded yellow region exists for all temperatures T_r , whereas the shaded green region disappears after a particular T_r . This can be understood clearly using the sign-changing curve later (Fig. 7.6(a)). The yellow region implies that the SBH phase has a dominant repulsive interaction. On the other hand, the LBH phase is always characterised by the dominant attractive interaction. To check whether the repulsive interaction regions

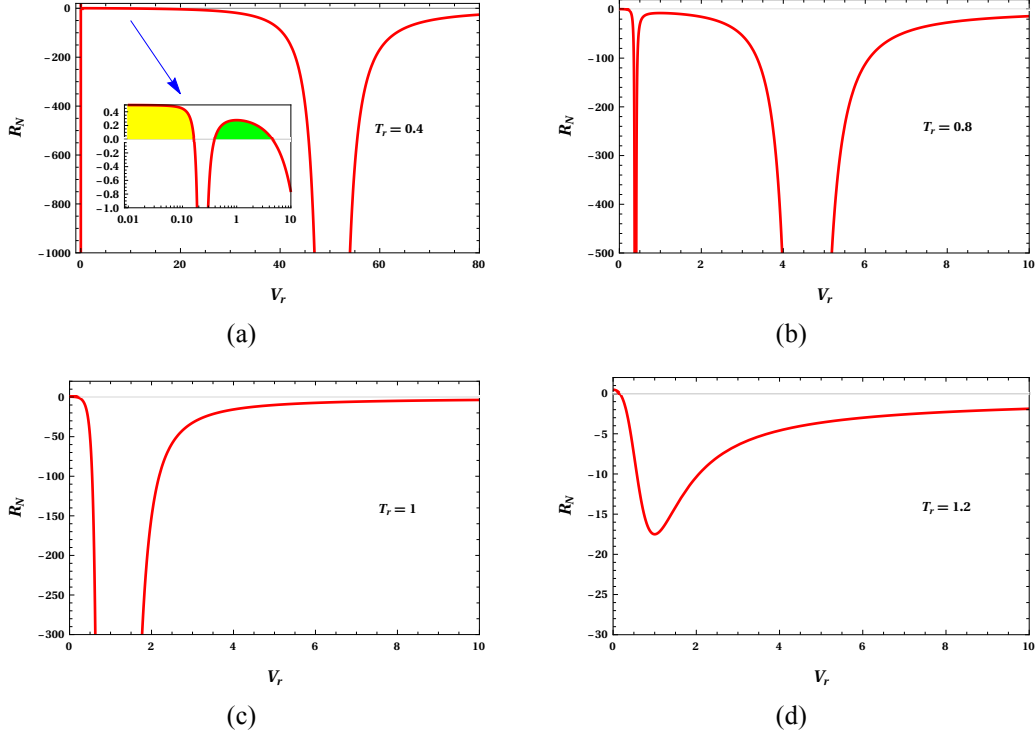


Figure 7.5: The behaviour of the normalised Ruppeiner curvature scalar R_N with the reduced volume V_r at a constant temperature for SPT. The insets show the enlarged portion near the origin. (Note that inset plot is in log scale). R_N has positive values for small values of V_r , which is depicted by shaded regions. The yellow and green shaded regions correspond to SBH and coexistence phases, respectively.

are thermodynamically stable, we present the regions of R_N with different sign in $T_r - V_r$ plane along with the coexistence and the spinodal curves (fig. 7.6(a)). The sign-changing curve of R_N is obtained by setting $R_N = 0$. The solution satisfy the condition $T_{sr} = T_{spr}/2$, where T_{0r} is the sign-changing temperature and T_{spr} temperature along the spinodal curve. In fig. 7.6(a), the shaded region corresponds to the negative sign of R_N . Region 1 is the coexistence region of SBH and LBH. Region 2 lies in the metastable phase, which is not interesting from the thermodynamic perspective. Region 3 includes part of SBH phase of the black hole, implying repulsive interactions among the small black hole constituents.

We now examine the behaviour of R_N along the coexistence curve and study the critical phenomena 7.6(b). The nature of interaction can be better understood from the behaviour of R_N along the coexistence curve. From Fig. 7.6(b) it is clear that LBH phase always has dominant attractive interaction (R_N always negative), whereas, the SBH phase switches to dominant repulsive interaction (R_N positive) from dominant attractive interaction (R_N negative) for low temperature values. The analysis for different values of Born Infeld parameter b in the SPT range was performed numerically. In the reduced coordinates, when the type of interac-

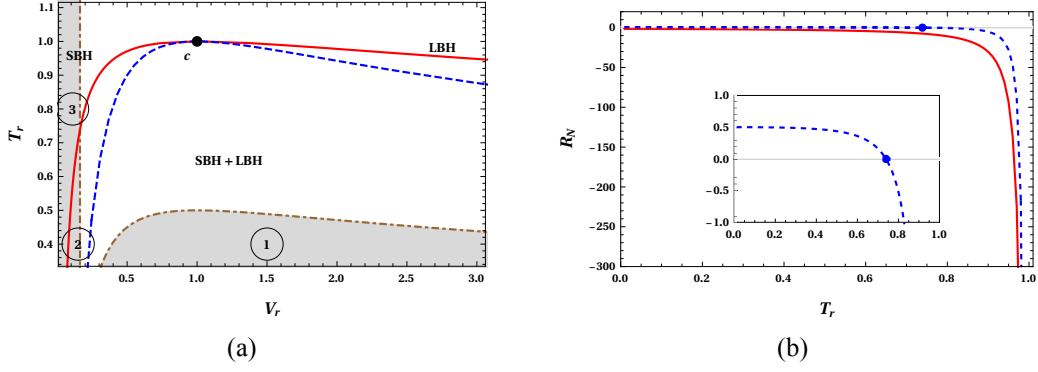


Figure 7.6: 7.6(a): The sign changing curve of R_N (brown dot-dashed line), spinodal curve (brown dashed line) and the coexistence curve (red solid line) for SPT. The shaded region (grey) corresponds to positive R_N , otherwise R_N is negative. Region 1 and (2,3) respectively correspond to green and yellow shaded regions in Fig. 7.5(a). The black dot at (1, 1) represents the critical point. 7.6(b): The behaviour of normalised Ruppeiner curvature scalar R_N along the coexistence curve. The red (solid) line and blue (dashed) line correspond to large black hole and small black hole, respectively. The change in nature of interaction of SBH is shown in inset, where R_N flips its sign. Here, the blue dot corresponds to sign changing temperature.

tion in SBH switches between attractive and repulsive interaction, for $b = (0.6, 0.7, 0.8, 0.9, 1)$ the corresponding temperatures are $(0.67063, 0.708075, 0.724286, 0.733273, 0.738949)$. For temperatures above these, the absolute value of the curvature scalar of the LBH is greater than that of the SBH. This implies that the attractive interaction in the LBH is stronger than SBH. Both the SBH and LBH branches diverge to negative infinity at the critical point. This can be seen as being due to the divergence of correlation length at the critical point. This is a universal behaviour observed in other black hole systems in AdS spacetime. We obtain the critical exponent of the normalised scalar curvature R_N at the critical point. Since the analytical expansion is not feasible, we assume that the scalar curvature has the following form near the critical point,

$$R_N \sim (1 - T_r)^{-\alpha}. \quad (7.23)$$

Taking logarithm on both sides,

$$\ln |R_N| = -\alpha \ln(1 - T_r) + \beta. \quad (7.24)$$

Along the coexistence curve, for $Q = 1$ and $b = 1$ we obtained,

$$\ln |R_N| = -2.07629 \ln(1 - T_r) - 2.67658, \quad (7.25)$$

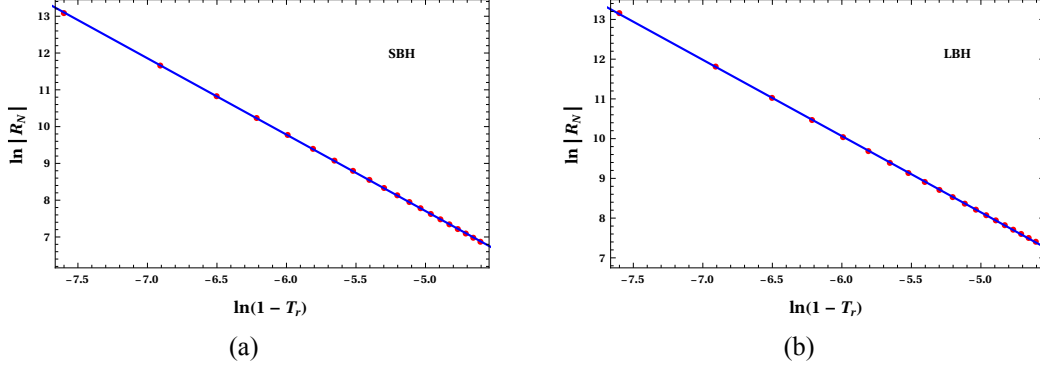


Figure 7.7: The fitting curves of $\ln R_N$ vs $\ln(1 - T_r)$ near the critical point. The red dots are numerical data and blue solid lines are obtained from fitting formulas. We have varied T_r from 0.99 to 0.9999 to obtain numerical data. (a) The coexistence saturated SBH branch (b) The coexistence saturated LBH branch

for the SBH branch and,

$$\ln |R_N| = -1.91868 \ln(1 - T_r) - 1.44762, \quad (7.26)$$

for the LBH branch. These are shown in Fig. 7.7. Considering the numerical errors we have the critical exponent $\alpha = 2$. Averaging the β values, we have,

$$R_N(1 - T_r)^2 = e^{-(2.67658+1.44762)/2} = -0.127187 \approx -\frac{1}{8}. \quad (7.27)$$

From the numerical results given in table 7.3, we have,

$$R_N(1 - T_r)^2 = -(0.130298, 0.128815, 0.128012, 0.127517, 0.127187), \quad (7.28)$$

for $b = (0.6, 0.7, 0.8, 0.9, 1)$, respectively. These values are slightly more negative than $-1/8 = -0.125$. Our results are in agreement with that of both the charged AdS black hole and vdW fluid, which have a R_N with a critical exponent of 2 and constant value of $-1/8$ for $R_N(1 - T_r)^2$, near the critical point, which is a universal behaviour.

To summarise the nature of interaction in the underlying microstructure of SPT, the LBH phase is always characterised by attractive interaction (like a bosonic gas), whereas, the SBH phase can have both attractive and repulsive interaction (like a quantum anyon gas).

b	0.6	0.7	0.8	0.9	1
α (CSSBH)	2.06414	2.06982	2.073	2.07496	2.07629
$-\beta$ (CSSBH)	2.57849	2.6243	2.64994	2.66583	2.67658
α (CSLBH)	1.9239	1.9215	1.92011	1.91926	1.91868
$-\beta$ (CSLBH)	1.49737	1.47446	1.46131	1.45317	1.44762

Table 7.3: The values of α and β obtained by numerical fit for coexistence saturated small black holes (CSSBH) and coexistence saturated large black hole (CSLBH) for different values of b , with $Q = 1$, for the SPT case.

7.3.2 Reentrant Phase Transition Case

We analyse the underlying microstructure of the black hole that results in RPT using the same method as before. The normalised Ruppeiner curvature scalar is plotted against the volume for constant temperatures in Fig. 7.8. Compared to the SPT case, here we observe an additional divergence for all temperatures $T > T_{c0}$, and only one divergence for $T < T_{c0}$. This is because, the spinodal curve has a different structure in the RPT case (Fig. 7.2(b)) compared to SPT case (Fig. 7.4(d)). For phase transition temperatures, which lie in the range $T \in (T_r, T_{c1})$, there exist three divergences as shown in Fig 7.8(a) and Fig. 7.8(b). Most general conclusions on the appearance of this divergences can be learnt from the spinodal curve. Here, the left-most divergence, say d_1 , corresponds to the spinodal curve branch that shoots to infinity after turning from c_0 in Fig. 7.4(d), which exists for temperatures $T > T_{c0}$. The middle divergence, say d_2 , corresponds to the spinodal curve between c_0 and c_1 , appearing in the temperature range $T \in (T_{c0}, T_{c1})$. And the rightmost divergence, say d_3 , is on the spinodal curve on the LBH side after c_1 , which present for all temperatures $T < T_{c1}$. At $T = T_{c1}$ divergences d_2 and d_3 merge together at $V_r = 1$, leaving only in total two divergences, Fig. 7.8(c). For completeness we mention that, at T_{c0} divergences d_1 and d_2 merge together, which is not relevant and hence not shown here. Interestingly, one divergence remains even for temperatures $T > T_{c1}$, Fig. 7.8(d). These divergences separate different phases of the black hole from each other in the $R_N - V_r$ plane, which enables us to search for the kind of interaction in each phase. The region between d_1 and d_2 corresponds to IBH phase and right side of d_3 to LBH phase. Left side of d_1 , and between d_2 and d_3 are coexistence regions. Contrary to the SPT case, R_N always takes negative values, implying only a dominant attractive interaction in all of the phases in RPT case. We search for a possible repulsive interaction at low V_r values, shown in the inset of Fig. 7.8(a), which is a

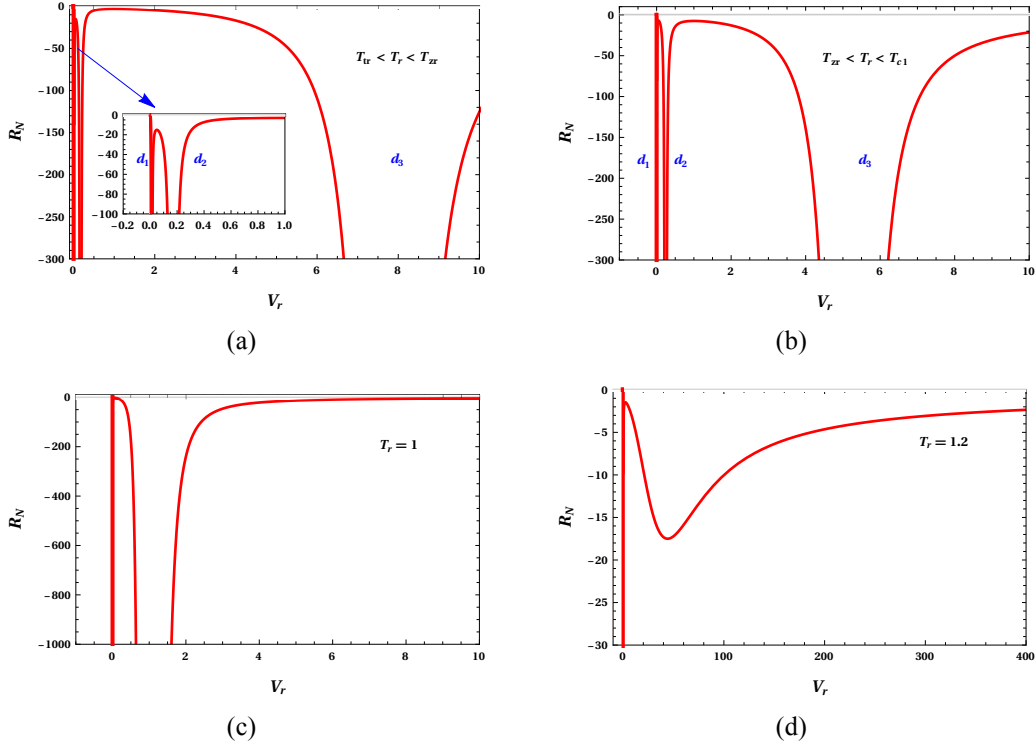


Figure 7.8: The behaviour of the normalised curvature scalar R_N against the volume V_r at constant temperature T_r for the RPT case. For $T < T_{c1}$ there are three divergences, of which two are near the origin shown in insets of (a). For temperature $T = T_{c1}$ one divergence disappears. Unlike SPT case, for temperatures $T > T_{c1}$ we still have one divergence (d). Here, we take $Q = 1$ and $b = 0.45$.

null result. This result is true for all phase transition temperatures. In short, for RPT case the black hole microstructure has only attractive interactions.

We confirm the above result by looking at the region covered by the sign-changing curve (Fig. 7.9(a)). The positive R_N values, shaded region, do not overlap with any stable state of the system. Note that the transition line of the zeroth-order phase transition (solid magenta line) also lies outside the shaded region. Near origin domain is enlarged in the inset for clarity. The behaviour of R_N along the transition curve is analysed in Fig. 7.9(b). We consider the first-order phase transition coexistence curve and the zeroth-order transition curve. As the zeroth-order transition line is not a coexistence curve, it gives only one branch. We consider only the region of temperature where the phase transition takes place, $T_t < T < T_{c1}$, as below the temperature T_t there is no phase transition. Once again, the positive sign of R_N asserts that, both IBH and LBH phases have dominant attractive interaction (like a bosonic gas). That is, during a reentrant phase transition in BI-AdS black hole, both the zeroth-order and first-order transition preserve the nature of the interaction between the microstructures. However, we notice that the correlation between the constituents changes

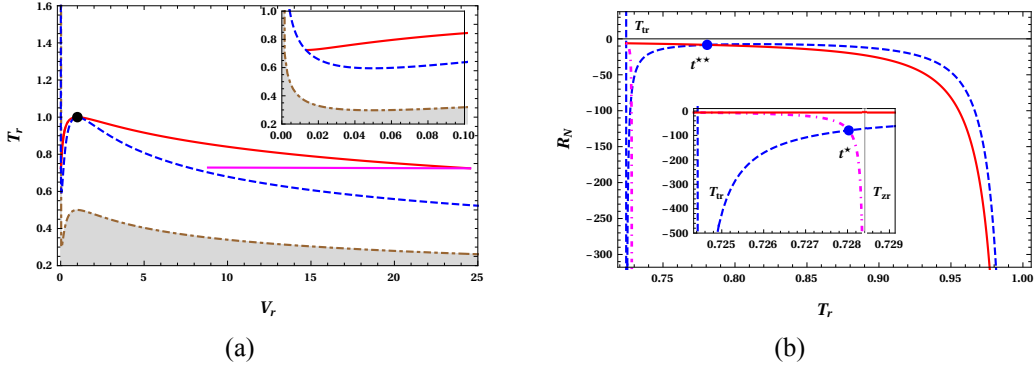


Figure 7.9: **7.9(a)**: The sign changing curve (brown dot-dashed line) of R_N , spinodal curve (blue dashed line) and the coexistence curve (red solid line) for the RPT case. The shaded region (grey) corresponds to positive R_N , elsewhere R_N is negative. All the stable phases, including near the zeroth order transition line (solid magenta line), lie outside the shaded region. The region near the origin is enlarged and shown in inset. **7.9(b)**: The behaviour of normalised curvature scalar R_N along the transition line of first-order and zeroth-order phase transition. The red (solid) line and blue (dashed) lines correspond to LBH and IBH phases, respectively. Both diverge at the critical point. The IBH branch suffers a discontinuity near the triple point T_t . The dot-dashed magenta line between T_{tr} and T_{zr} (clearly shown in the inset) corresponds to the LBH phase of zeroth-order phase transition, which is a miniature version of the other LBH branch with a divergence at T_z , which corresponds to the termination point of the transition. In the plot, the temperatures corresponding to the blue dots t^* and t^{**} are $T_r^* = 0.72803$ and $T_r^{**} = 0.780668$. We take $Q = 1$ and $b = 0.45$, respectively.

at different temperatures. The flipping temperatures are clearly shown in Fig. 7.9(b) in blue dots. For zeroth-order transition (jumping from blue dashed line to magenta dot-dashed line and vice versa), IBH phase has higher correlation strength than LBH in the temperature range $T \in (T_t, T^*)$. This property is reversed in the region $T \in (T^*, T_z)$. On the other hand, for the first-order phase transition (jumping from blue dashed line to red solid line and vice versa), IBH phase exhibits higher correlation among the constituents than LBH for temperatures $T \in (T_t, T^{**})$, which is flipped for $T \in (T^{**}, T_{c1})$. In fact, the change in the strength of the interaction is also present in SPT case. Interestingly, near the triple point, IBH phase shows a huge surge in correlation, whereas the correlation in LBH phase here, is very weak. Also, the red and magenta line merge near T_t , signifying the meeting and termination of zeroth-order and first-order transition line at that point. As in SPT case near the critical point the diverging correlation length leads to diverging R_N . For magenta line it happens at T_z , in a sense (P_z, T_z) acts as a critical point (see for example (Altamirano et al., 2013)). During a RPT, the initial and final phases are the same from the macroscopic point of view. Microscopically, this is almost true for $T < T^*$, where red and magenta line (initial and final states in RPT) are close together. However, for $T > T^*$ there is a difference in strength of interaction, which becomes considerable near T^* .

b	0.43	0.44	0.45	0.46	0.47	0.48	0.49
α (CSIBH)	1.91582	2.01262	2.07636	1.99898	2.02411	2.03111	2.03868
$-\beta$ (CSIBH)	1.68789	2.2181	2.56921	2.17032	2.31204	2.357	2.40382
α (CSLBH)	2.04466	1.9619	1.91492	1.99174	1.95724	1.9511	1.94448
$-\beta$ (CSLBH)	2.19809	1.75127	1.49509	1.8951	1.70734	1.67	1.63093

Table 7.4: The values of α and β obtained by numerical fit for coexistence saturated intermediate black holes (CSIBH) and coexistence saturated large black hole (CSLBH) for different values of b , with $Q = 1$, for the RPT case.

The critical phenomena of R_N is studied for different values of b numerically using Eq. 7.23. From the numerical results given in table 7.4, we have,

$$R_N(1 - T_r)^2 = -(0.143275, 0.137424, 0.131053, 0.13098, 0.13403, 0.13352, 0.133004), \quad (7.29)$$

for $b = (0.43, 0.44, 0.45, 0.46, 0.47, 0.48, 0.49)$, respectively. As in the case of SPT, these values are slightly more negative than $-1/8$. Within the numerical errors we have obtained the universal constant $R_N(1 - T_r)^2$ as $-1/8$ and the critical exponent 2 in RPT case too. To cut a long story short, we observe the existence of only homogeneous dominant attractive interaction in the black hole for RPT case, and both repulsive and attractive interaction in SPT case. This difference in the microstructure interaction for SPT and RPT in BI-AdS black hole tells that the microstructure is determined by the coupling parameter b .

7.4 Discussions

In this chapter, we have studied the microstructure of four-dimensional Born-Infeld AdS black hole employing a novel Ruppeiner geometry method. As the entropy and volume are interdependent in a spherically symmetric AdS black hole, the application of Ruppeiner geometry for such a system must be carried out with utmost care. Keeping this in mind, we have constructed the Ruppeiner curvature scalar in the parametric space where the temperature and volume are the fluctuation coordinates. We investigated the phase structure and the corresponding microscopic interactions for both the standard van der Waals (SPT) and the reentrant phase transitions (RPT), where a first-order phase transition is accompanied

by a zeroth-order transition. We found that the microstructure that leads to RPT is distinct from that of SPT. Our study shows that the Born Infeld coupling coefficient b determines the microscopic interaction of the black hole. Since the analytical investigation is not possible due to the complexity of the spacetime, we have carried out the study numerically.

In the first part of the chapter, we investigated the phase structure of the black hole using the spinodal and transition curves in SPT and RPT cases. The black hole has four different cases depending on the value of b , and shows the distinct RPT for certain pressure range. There are two RPT cases with two critical points in each. It is found that the phase structure associated with SPT and RPT are distinct. The phase diagrams are presented in pressure-temperature ($P - T$) and temperature-volume ($T - V$) planes, where, stable, metastable and coexistence phases are studied. In both SPT and RPT cases, we conveniently define the reduced parameters and all analyses were carried out in terms of them.

The second half of the chapter is devoted to the study of microstructure, which reveal distinct microstructure for SPT and RPT cases. Two important features, the nature of interaction and strength of correlation are sought for in this study. The microstructure that corresponds to SPT is analogous to that of RN-AdS black hole. The small black hole phase shows a dominant repulsive interaction in a certain range of parameters. As the interaction in this phase is attractive in other domains of parameter space, the interaction type resembles that of a quantum anyon gas. The large black hole phase is always characterised by the dominant attractive interaction, like a bosonic gas. These are inferred from the sign of the Ruppeiner curvature scalar R_N . For both small black hole and large black hole branches, it diverges near the critical point. The RPT case has a different microstructure compared to the SPT case, wherein no repulsive interaction is present for both the intermediate and large black hole phases. The nature of microstructure does not change during the zeroth-order and first-order phase transition in RPT, which as a dominant attractive interaction. This suggests that the nature of interaction in RPT case is always like that of a bosonic gas. Both, intermediate and large black hole, branches diverge near the physically meaningful critical point. The signature of RPT is reflected in the behaviour of curvature scalar, through its anomalies near the termination points of the zeroth-order phase transition. The strength of interaction depends on temperature, which is inferred from the magnitude of the curvature scalar, the high correlation phases are flipped at certain temperatures for both zeroth-order and first-order transition. In fact, this reversal of correlation strength is true for SPT case too.

The critical phenomenon of the system is investigated via curvature scalar. The universal properties, critical exponent-2 and the constant $R_N(1 - T_r)^2 = -1/8$, are obtained for SPT and RPT cases over a range of b values. We believe that this study will help us shed more light on the black hole microstructure in general.

Chapter 8

Final Remarks

Stay hungry stay foolish.

Steve Jobs, *originally took from the Whole Earth Catalog (1974)*

8.1 Conclusions

The aim of this research was to study the aspects of black hole chemistry, particularly the phase transitions and microstructures. With that objective, we have accomplished the following results.

1. We have shown that the phase transition of a magnetically charged black hole is determined by the magnetic potential. The symmetry or the order degree of the regular black hole is governed by the magnetic potential. The changing symmetry results in different phases of the system, which is investigated using the Landau theory of continuous phase transition.
2. Using the formalism of unstable circular null geodesics for a class of regular black holes, we find a close connection between gravity and thermodynamics in the extended phase space. The well-known van der Waals-like phase structure is probed via the photon orbit radius r_{ps} and minimum critical impact parameter u_{ps} . The differences Δr_{ps} and Δu_{ps} serve as order parameters for the critical behaviour, with critical exponents $\delta = 1/2$. Our results show that regular black holes are in close proximity with charged AdS black holes in phase transition perspectives.
3. We studied the microstructure of the AdS black holes by employing a novel Ruppeiner

geometry method. Even though the black hole shows van der Waals like phase transition, the microstructure properties differ in some aspects. In van der Waals fluid, the dominant interaction among the constituent molecules is always attractive, which does not change during the phase transition. The change in microstructure does not lead to any change in the nature of microscopic interaction. However, in Hayward-AdS black hole, there exists a domain, low-temperature range for the small black hole, where the dominant interaction between the black hole molecules is repulsive.

4. We have studied the microstructure associated with the reentrant phase transition of four-dimensional Born-Infeld AdS black hole. We found that the microstructure that leads to reentrant phase transition (RPT) is distinct from that of standard phase transition (SPT). Our study shows that the Born Infeld coupling coefficient b determines the microscopic interaction of the black hole.

8.2 Future Directions

We are intended to extend our research to the thermodynamics of black holes in the de-Sitter background. In the de-Sitter spacetime, we have to deal with two horizons: the black hole event horizon and the cosmological event horizon. These two horizons emit thermal radiations at different temperatures. Therefore the black hole does not possess thermal stability. However, the study of black hole thermodynamics in de-Sitter space is more appealing since the current phase of the universe is undergoing an accelerated expansion. The cosmological constant arises from the fluctuating vacuum energy regarded as the possible candidate for the accelerated expansion of the universe. For the de-Sitter black holes, separate thermodynamics laws are formulated for each horizon, and their thermodynamics is studied as if they were independent systems characterised by their own temperature ([Kubiznak and Simovic, 2016](#)).

Another possible extension of our work is in the direction of horizon thermodynamics. In this exciting domain of thermodynamics of spacetime, the dynamical equations of gravity often interpreted as thermodynamic equation state ([Jacobson, 1995](#)). In horizon thermodynamics, Einstein equations on the horizon of a spherically symmetric spacetime can be interpreted as a thermodynamic identity ([Padmanabhan, 2002](#)). There were attempts to compare the horizon thermodynamics with the extended phase space thermodynamics of asymptoti-

cally AdS black holes ([Hansen et al., 2017](#)). We seek more investigations in this regard.

We aim to meet the following objectives in future,

- To make a more detailed study on the connection between extended phase space thermodynamics and horizon thermodynamics.
- To study thermal energy extraction (black hole as heat engine ([Johnson, 2014](#))), the correlation between the photon orbit and phase transition, and the Joule Thomson expansion for de-Sitter black holes.
- To apply the Ruppeiner geometry methods to de-Sitter black holes and probe the nature of its microstructure interaction.
- To explore more about the connection between gravity and condensed matter system in a more general perspective.

Appendix

Gravity Coupled to Non-linear Electrodynamics

Nonlinear electrodynamics (NED) appeared in the famous work due to Born and Infeld to remove the central singularity of a point charge and the related energy divergence by generalising Maxwell's theory (Born and Infeld, 1934), including an arbitrary function of the electromagnetic field invariants. Such generalisation, when applied to the black hole solution, does not remove the very existence of central curvature singularity. For that, we need models of NED in modern studies, which to a large extent is motivated by the discovery that some kinds of NED appear as limiting cases of certain models of string theory (Seiberg and Witten, 1999; Tseytlin, 1999). For example, recently, it has been studied in (Nicolini et al., 2019) to show that some stringy corrections to black hole spacetimes may emerge directly from string T -duality, wherein the authors have exploited the relation between the T -duality and the path integral duality, and derive a consistent black hole metric for the spherically symmetric, electrically neutral case. It turns out that the new spacetime is regular and is formally equivalent to the Bardeen metric, apart from a different ultraviolet regulator.

It is also clear that the real electromagnetic field should lose its linearity at high energies due to interactions with other physical fields, and NED theories may be considered as a simplified phenomenological description of these interactions. On the other hand, NED as a possible material source of gravity is able to create various non-singular geometries of interest, in particular, regular black holes in the framework of general relativity (GR) and alternative theories. Such solutions are widely discussed in the literature. In (Bronnikov and Shikin, 2002), a no-go theorem was proved to show that if NED is specified by a Lagrangian function $\mathcal{L}(\mathcal{F})$ (where $\mathcal{F} = F_{\mu\nu}F^{\mu\nu}$ and $F_{\mu\nu}$ is the Maxwell tensor), then for a static, spherically symmetric solution of GR with an electric field has a regular centre, there exists no such function $\mathcal{L}(\mathcal{F})$ which has a Maxwell weak-field limit ($\mathcal{L} \sim \mathcal{F}$ as $\mathcal{F} \rightarrow 0$). For purely mag-

netic regular configurations, the black hole solutions are possible and are readily obtained under the condition $\mathcal{L}_{\mathcal{F}} \rightarrow \mathcal{L}_{\infty} < \infty$ as $\mathcal{F} \rightarrow \infty$. Electric models with the same regular metrics can be obtained from the magnetic ones using the so-called *FP* duality that connects solutions with the same metric corresponding to different NED theories. It should be stressed that *FP* duality connects solutions of different theories: given $\mathcal{L}(\mathcal{F})$, the functional dependence $\mathcal{H}(P) = 2\mathcal{F}\mathcal{L}_{\mathcal{F}} - \mathcal{L}(\mathcal{F})$ (with $\mathcal{L}_{\mathcal{F}} = \frac{\partial \mathcal{L}}{\partial \mathcal{F}}$ and $P = P_{\mu\nu}P^{\mu\nu}$, where $P_{\mu\nu} = \mathcal{L}_{\mathcal{F}}F_{\mu\nu}$) is in general quite different from $\mathcal{L}(\mathcal{F})$, an evident exception being the Maxwell theory, where $\mathcal{L} = \mathcal{F} = \mathcal{H} = P$, where the present duality turns into the conventional electric-magnetic duality. So *FP* duality has nothing to do with the electric-magnetic one studied in (Bronnikov et al., 1979; Bronnikov, 2001, 2000), where the field equations of a specific theory were required to be duality invariant, and this condition selected a narrow class of Lagrangians.

Construction of regular black holes solution

We present the regular black holes solutions in the background of anti-de Sitter spacetime. The solutions we are interested in, the Hayward and the Bardeen black holes, can be derived from Einstein gravity minimally coupled to nonlinear electrodynamics with negative cosmological constant Λ given by the action (Fan and Wang, 2016),

$$\mathcal{I} = \frac{1}{16\pi G} \int d^4x \sqrt{-\hat{g}} [R - \mathcal{L}(\mathcal{F}) + 2\Lambda] \quad (8.1)$$

where R and \hat{g} are the Ricci scalar and the determinant of the metric tensor, respectively. $\mathcal{L}(\mathcal{F})$ is the Lagrangian density of nonlinear electrodynamics which is a function of $\mathcal{F} = F_{\mu\nu}F^{\mu\nu}$ with $F_{\mu\nu} = 2\nabla_{[\mu}A_{\nu]}$, the strength tensor of nonlinear electrodynamics. Varying the action (Eq. 8.1), with respect to $g_{\mu\nu}$ and A_{μ} , we have the field equations of the form,

$$G_{\mu\nu} + \Lambda g_{\mu\nu} = T_{\mu\nu}, \quad (8.2)$$

$$\nabla_{\mu} \left(\frac{\partial \mathcal{L}(\mathcal{F})}{\partial F} F^{\nu\mu} \right) = 0, \quad \nabla_{\mu} (*F^{\nu\mu}) = 0, \quad (8.3)$$

where $T_{\mu\nu}$ is energy-momentum tensor, which can be written as

$$T_{\mu\nu} = 2 \left[\mathcal{L}_{\mathcal{F}} F_{\mu\alpha} F_{\nu}^{\alpha} - \frac{1}{4} g_{\mu\nu} \mathcal{L}(\mathcal{F}) \right], \quad (8.4)$$

where $\mathcal{L}_{\mathcal{F}} = \frac{\partial \mathcal{L}(\mathcal{F})}{\partial \mathcal{F}}$. In this chapter, we contemplate static spherically symmetric black holes with magnetic charges. To construct such black hole solutions, we follow the general procedure given as in Ref. (Fan and Wang, 2016). The regular Hayward black hole solution can be obtained from the Lagrangian density,

$$\mathcal{L}(\mathcal{F}) = \frac{12}{\alpha} \frac{(\alpha \mathcal{F})^{3/2}}{(1 + (\alpha \mathcal{F})^{3/4})^2}, \quad (8.5)$$

with $\alpha > 0$ which has the dimension of length squared. The four-dimensional spherically symmetric black hole is described by

$$ds^2 = - \left(1 - \frac{2m(r)}{r} \right) dt^2 + \frac{dr^2}{\left(1 - \frac{2m(r)}{r} \right)} + r^2 d\Omega_2^2, \quad (8.6)$$

where $m(r)$ is the mass function containing the mass within radius r and $d\Omega_2^2 = d\theta^2 + \sin^2 \theta d\varphi^2$, is a 2-dimensional unit sphere. For a spherically symmetric spacetime, $F_{\mu\nu}$ admits two non-vanishing components, F_{tr} and $F_{\theta\varphi}$. For a pure magnetic charge only $F_{\theta\varphi}$ survives. The ansatz for $F_{\mu\nu}$ for a purely magnetically charged black hole reads,

$$F_{\mu\nu} = 2 \delta_{[\mu}^{\theta} \delta_{\nu]}^{\varphi} \mathcal{X}(r, \theta). \quad (8.7)$$

Utilizing Eq. (8.7) in Eq. (8.3) and integrating it, we have,

$$F_{\mu\nu} = 2 \delta_{[\mu}^{\theta} \delta_{\nu]}^{\varphi} q(r) \sin \theta. \quad (8.8)$$

Eq. (8.3) implies $dF = 0$ which in turn reads $q'(r) dr \wedge d\theta \wedge d\varphi = 0$, leading to $q(r) = \text{constant} = Q_m$. The constant Q_m is identified with the magnetic monopole charge of the nonlinear electrodynamics. Then, the resulting Maxwell tensor reads with only component,

$$F_{\theta\varphi} = -F_{\varphi\theta} = -Q_m \sin \theta, \quad (8.9)$$

and hence the gauge potential and the Maxwell invariant for this field turn out to be,

$$A_\mu = Q_m \cos\theta \delta_\mu^\phi, \quad \mathcal{F} = \frac{2Q_m^2}{r^4}. \quad (8.10)$$

Using this result the Lagrangian (8.5) can be casted as,

$$\mathcal{L}(r) = \frac{12}{\alpha} \frac{(2\alpha Q_m^2)^{3/2}}{(r^3 + (2\alpha Q_m^2)^{3/4})^2}. \quad (8.11)$$

The two independent non-zero components of the Einstein field equations, using energy-momentum tensor (Eq. 8.4), can be obtained as

$$\frac{2m'(r)}{r^2} - \Lambda = \mathcal{L}(r), \quad (8.12)$$

$$\frac{m''(r)}{r} - \Lambda = \left(\mathcal{L}(r) - \mathcal{L}_{\mathcal{F}}(r) F^{\theta\phi} F_{\theta\phi} \right). \quad (8.13)$$

The solution of Eq.(8.12) is calculated to be,

$$m(r) = \frac{2Mr^2}{r^3 + g^3} + \frac{\Lambda r^3}{6}, \quad (8.14)$$

where M the mass of the black hole and g the free integration constant that is related to the magnetic charge Q_m , are identified as,

$$M = \alpha^{-1} g^3, \quad Q_m = \frac{g^2}{\sqrt{2\alpha}}. \quad (8.15)$$

Thus, from Eq. (8.6) the metric for a regular Hayward AdS black hole in four-dimensional spacetime reads,

$$ds^2 = -f(r)dt^2 + \frac{1}{f(r)}dr^2 + r^2 d\Omega_2^2, \quad (8.16)$$

with the metric function

$$f(r) = \left(1 - \frac{2Mr^2}{r^3 + g^3} - \frac{\Lambda r^2}{3} \right). \quad (8.17)$$

Similar procedures follow for the regular Bardeen AdS black hole with the following Lagrangian density,

$$\mathcal{L}(\mathcal{F}) = \frac{12}{\alpha} \frac{(\alpha\mathcal{F})^{5/4}}{(1 + (\alpha\mathcal{F})^{1/2})^{5/2}}. \quad (8.18)$$

The corresponding line element for a spherically symmetric spacetime has the same form as Eq. (8.16), with the metric function,

$$f(r) = \left(1 - \frac{2Mr^2}{(r^2 + g^2)^{3/2}} - \frac{\Lambda r^2}{3} \right). \quad (8.19)$$

Bibliography

- Naveena Kumara, A., Ahmed Rizwan, C. L., Hegde, K., Ajith, K. M., and Ali, M. S.** (2021a). Ruppeiner geometry, reentrant phase transition, and microstructure of Born-Infeld AdS black hole. *Phys. Rev. D*, 103:044025.
- Naveena Kumara, A., Ahmed Rizwan, C. L., Punacha, S., Ajith, K. M., and Ali, M. S.** (2020a). Photon orbits and thermodynamic phase transition of regular AdS black holes. *Phys. Rev. D*, 102(8):084059.
- Naveena Kumara, A., Rizwan, C. L. A., Hegde, K., and Ajith, K. M.** (2020b). Repulsive Interactions in the Microstructure of Regular Hayward Black Hole in Anti-de Sitter Spacetime. *Phys. Lett. B*, 807:135556.
- Naveena Kumara, A., Rizwan, C. L. A., Hegde, K., Ajith, K. M., and Ali, M. S.** (2021b). Microstructure and continuous phase transition of a regular Hayward black hole in anti-de Sitter spacetime. *PTEP*, 7:073.
- Naveena Kumara, A., Rizwan, C. L. A., Vaid, D., and Ajith, K. M.** (2019). Critical Behaviour and Microscopic Structure of Charged AdS Black Hole with a Global Monopole in Extended and Alternate Phase Spaces.
- Abbott, B. et al. (2016a). Observation of Gravitational Waves from a Binary Black Hole Merger. *Phys. Rev. Lett.*, 116(6):061102.
- Abbott, B. et al. (2016b). Tests of general relativity with GW150914. *Phys. Rev. Lett.*, 116(22):221101. [Erratum: *Phys.Rev.Lett.* 121, 129902 (2018)].
- Abbott, B. P. et al. (2016c). GW151226: Observation of Gravitational Waves from a 22-Solar-Mass Binary Black Hole Coalescence. *Phys. Rev. Lett.*, 116(24):241103.
- Abdujabbarov, A., Amir, M., Ahmedov, B., and Ghosh, S. G. (2016). Shadow of rotating regular black holes. *Phys. Rev. D*, 93(10):104004.
- Akiyama, K. et al. (2019a). First M87 Event Horizon Telescope Results. I. The Shadow of the Supermassive Black Hole. *Astrophys. J.*, 875(1):L1.
- Akiyama, K. et al. (2019b). First M87 Event Horizon Telescope Results. IV. Imaging the Central Supermassive Black Hole. *Astrophys. J. Lett.*, 875(1):L4.
- Akiyama, K. et al. (2019c). First M87 Event Horizon Telescope Results. V. Physical Origin of the Asymmetric Ring. *Astrophys. J. Lett.*, 875(1):L5.
- Ali, M. S. and Ghosh, S. G. (2018). Exact d -dimensional bardeen-de sitter black holes and thermodynamics. *Phys. Rev. D*, 98:084025.

- Altamirano, N., Kubiznak, D., and Mann, R. B. (2013). Reentrant phase transitions in rotating anti-de Sitter black holes. *Phys. Rev. D*, 88(10):101502.
- Altamirano, N., Kubiznak, D., Mann, R. B., and Sherkatghanad, Z. (2014a). Thermodynamics of rotating black holes and black rings: phase transitions and thermodynamic volume. *Galaxies*, 2:89–159.
- Altamirano, N., Kubiznak, D., Mann, R. B., and Sherkatghanad, Z. (2014b). Kerr-AdS analogue of triple point and solid/liquid/gas phase transition. *Class. Quant. Grav.*, 31:042001.
- Aman, J. E., Bengtsson, I., and Pidokrajt, N. (2003). Geometry of black hole thermodynamics. *Gen. Rel. Grav.*, 35:1733.
- Amir, M. and Ghosh, S. G. (2016). Shapes of rotating nonsingular black hole shadows. *Phys. Rev. D*, 94(2):024054.
- Aros, R. and Estrada, M. (2019). Regular black holes and its thermodynamics in Lovelock gravity. *Eur. Phys. J. C*, 79(3):259.
- Ashtekar, A. and Das, S. (2000). Asymptotically Anti-de Sitter space-times: Conserved quantities. *Class. Quant. Grav.*, 17:L17–L30.
- Ashtekar, A. and Magnon, A. (1984). Asymptotically anti-de Sitter space-times. *Class. Quant. Grav.*, 1:L39–L44.
- Ayon-Beato, E. and Garcia, A. (1998). Regular black hole in general relativity coupled to nonlinear electrodynamics. *Phys. Rev. Lett.*, 80:5056–5059.
- Ayon-Beato, E. and Garcia, A. (2000). The Bardeen model as a nonlinear magnetic monopole. *Phys. Lett.*, B493:149–152.
- Banerjee, R., Ghosh, S., and Roychowdhury, D. (2011a). New type of phase transition in Reissner Nordström–AdS black hole and its thermodynamic geometry. *Phys. Lett. B*, 696:156–162.
- Banerjee, R., Modak, S. K., and Samanta, S. (2011b). Second Order Phase Transition and Thermodynamic Geometry in Kerr-AdS Black Hole. *Phys. Rev. D*, 84:064024.
- Banerjee, R. and Roychowdhury, D. (2012). Critical phenomena in Born-Infeld AdS black holes. *Phys. Rev. D*, 85:044040.
- Bardeen, J. (1968). Non-singular general-relativistic gravitational collapse, in proceedings of the international conference gr5. *Tbilisi, USSR*.
- Bardeen, J. M., Carter, B., and Hawking, S. W. (1973). The Four laws of black hole mechanics. *Commun. Math. Phys.*, 31:161–170.
- Bekenstein, J. D. (1972). Black holes and the second law. *Lett. Nuovo Cim.*, 4:737–740.
- Bekenstein, J. D. (1973). Black holes and entropy. *Phys. Rev.*, D7:2333–2346.
- Bekenstein, J. D. (1974). Generalized second law of thermodynamics in black-hole physics. *Physical Review D*, 9(12):3292–3300.

- Born, M. and Infeld, L. (1934). Foundations of the new field theory. *Proc. Roy. Soc. Lond. A*, A144(852):425–451.
- Bozza, V. (2002). Gravitational lensing in the strong field limit. *Phys. Rev. D*, 66:103001.
- Bronnikov, K., Melnikov, V., Shikin, G., and Staniukovich, K. (1979). Scalar, electromagnetic, and gravitational fields interaction: Particlelike solutions. *Annals of Physics*, 118(1):84 – 107.
- Bronnikov, K. A. (2000). Comment on ‘Regular black hole in general relativity coupled to nonlinear electrodynamics’. *Phys. Rev. Lett.*, 85:4641.
- Bronnikov, K. A. (2001). Regular magnetic black holes and monopoles from nonlinear electrodynamics. *Phys. Rev. D*, 63:044005.
- Bronnikov, K. A. and Shikin, G. N. (2002). Spherically symmetric scalar vacuum: No go theorems, black holes and solitons. *Grav. Cosmol.*, 8:107–116.
- Cai, R.-G. and Cho, J.-H. (1999). Thermodynamic curvature of the BTZ black hole. *Phys. Rev. D*, 60:067502.
- Cai, R.-G., Pang, D.-W., and Wang, A. (2004). Born-Infeld black holes in (A)dS spaces. *Phys. Rev. D*, 70:124034.
- Caldarelli, M. M., Cognola, G., and Klemm, D. (2000). Thermodynamics of Kerr-Newman-AdS black holes and conformal field theories. *Class. Quant. Grav.*, 17:399–420.
- Cardoso, V., Miranda, A. S., Berti, E., Witek, H., and Zanchin, V. T. (2009). Geodesic stability, Lyapunov exponents and quasinormal modes. *Phys. Rev. D*, 79:064016.
- Chabab, M., El Mounni, H., Iraoui, S., and Masmarr, K. (2020). Probing correlation between photon orbits and phase structure of charged AdS black hole in massive gravity background. *Int. J. Mod. Phys. A*, 34(35):1950231.
- Chabab, M., El Mounni, H., Iraoui, S., Masmarr, K., and Zhizeh, S. (2018). More Insight into Microscopic Properties of RN-AdS Black Hole Surrounded by Quintessence via an Alternative Extended Phase Space. *Int. J. Geom. Meth. Mod. Phys.*, 15(10):1850171.
- Chamblin, A., Emparan, R., Johnson, C. V., and Myers, R. C. (1999a). Charged AdS black holes and catastrophic holography. *Physical Review D - Particles, Fields, Gravitation and Cosmology*, 60(6):1–17.
- Chamblin, A., Emparan, R., Johnson, C. V., and Myers, R. C. (1999b). Holography, thermodynamics and fluctuations of charged AdS black holes. *Phys. Rev.*, D60:104026.
- Chandrasekhar, B. and Mohapatra, S. (2019). A Note on Circular Geodesics and Phase Transitions of Black Holes. *Phys. Lett. B*, 791:367–374.
- Chaturvedi, P., Das, A., and Sengupta, G. (2017). Thermodynamic Geometry and Phase Transitions of Dyonic Charged AdS Black Holes. *Eur. Phys. J. C*, 77(2):110.
- Chaturvedi, P., Mondal, S., and Sengupta, G. (2018). Thermodynamic Geometry of Black Holes in the Canonical Ensemble. *Phys. Rev. D*, 98(8):086016.

- Chen, Y., Li, H., and Zhang, S.-J. (2019). Microscopic explanation for black hole phase transitions via Ruppeiner geometry: Two competing factors—the temperature and repulsive interaction among BH molecules. *Nucl. Phys.*, B948:114752.
- Cvetic, M., Gibbons, G. W., Kubiznak, D., and Pope, C. N. (2011). Black Hole Enthalpy and an Entropy Inequality for the Thermodynamic Volume. *Phys. Rev. D*, 84:024037.
- Dehyadegari, A. and Sheykhi, A. (2018). Reentrant phase transition of Born-Infeld-AdS black holes. *Phys. Rev. D*, 98(2):024011.
- Dehyadegari, A., Sheykhi, A., and Montakhab, A. (2017). Critical behavior and microscopic structure of charged AdS black holes via an alternative phase space. *Phys. Lett.*, B768:235–240.
- Dehyadegari, A., Sheykhi, A., and Wei, S.-W. (2020). Microstructure of charged AdS black hole via $P - V$ criticality. *Phys. Rev. D*, 102(10):104013.
- Deng, G.-M. and Huang, Y.-C. (2017). $Q - \Phi$ criticality and microstructure of charged AdS black holes in $f(R)$ gravity. *Int. J. Mod. Phys.*, A32(35):1750204.
- Dey, T. K. (2004). Born-Infeld black holes in the presence of a cosmological constant. *Phys. Lett. B*, 595:484–490.
- Dolan, B. P. (2011a). Pressure and volume in the first law of black hole thermodynamics. *Class. Quantum Grav.*, 28:235017–13.
- Dolan, B. P. (2011b). Pressure and volume in the first law of black hole thermodynamics. *Class. Quant. Grav.*, 28:235017.
- Dolan, B. P. (2015). Intrinsic curvature of thermodynamic potentials for black holes with critical points. *Phys. Rev. D*, 92(4):044013.
- Du, Y.-Z., Zhao, H.-H., and Zhang, L.-C. (2020). Microstructure and Continuous Phase Transition of the Einstein-Gauss-Bonnet AdS Black Hole. *Adv. High Energy Phys.*, 2020:6395747.
- Eiroa, E. F. and Sendra, C. M. (2011). Gravitational lensing by a regular black hole. *Class. Quant. Grav.*, 28:085008.
- Fan, Z.-Y. (2017). Critical phenomena of regular black holes in anti-de Sitter space-time. *Eur. Phys. J.*, C77(4):266.
- Fan, Z.-Y. and Wang, X. (2016). Construction of Regular Black Holes in General Relativity. *Phys. Rev.*, D94(12):124027.
- Fernando, S. and Krug, D. (2003). Charged black hole solutions in Einstein-Born-Infeld gravity with a cosmological constant. *Gen. Rel. Grav.*, 35:129–137.
- Flachi, A. and Lemos, J. P. S. (2013). Quasinormal modes of regular black holes. *Phys. Rev. D*, 87(2):024034.
- Frassino, A. M., Kubiznak, D., Mann, R. B., and Simovic, F. (2014). Multiple Reentrant Phase Transitions and Triple Points in Lovelock Thermodynamics. *JHEP*, 09:080.

- Ghosh, A. and Bhamidipati, C. (2020a). Thermodynamic geometry and interacting microstructures of BTZ black holes. *Phys. Rev. D*, 101(10):106007.
- Ghosh, A. and Bhamidipati, C. (2020b). Thermodynamic geometry for charged Gauss-Bonnet black holes in AdS spacetimes. *Phys. Rev.*, D101(4):046005.
- Gibbons, G. W. (2001). Aspects of Born-Infeld theory and string / M theory. *AIP Conf. Proc.*, 589(1):324–350.
- Gliner, E. B. (1966). Algebraic Properties of the Energy-momentum Tensor and Vacuum-like States of Matter. *Soviet Journal of Experimental and Theoretical Physics*, 22:378.
- Gunasekaran, S., Mann, R. B., and Kubiznak, D. (2012). Extended phase space thermodynamics for charged and rotating black holes and Born-Infeld vacuum polarization. *JHEP*, 11:110.
- Guo, X.-Y., Li, H.-F., Zhang, L.-C., and Zhao, R. (2019). Microstructure and continuous phase transition of a Reissner-Nordstrom-AdS black hole. *Phys. Rev.*, D100(6):064036.
- Han, S.-Z., Jiang, J., Zhang, M., and Liu, W.-B. (2018). Photon orbits and thermodynamic phase transition in Gauss-Bonnet AdS black holes. *arXiv:1812.11862 [gr-qc]*.
- Hansen, D., Kubiznak, D., and Mann, R. B. (2017). Universality of P-V Criticality in Horizon Thermodynamics. *JHEP*, 01:047.
- Hawking, S. W. (1975). Particle Creation by Black Holes. *Commun. Math. Phys.*, 43:199–220. [167(1975)].
- Hawking, S. W. and Ellis, G. F. R. (2011). *The Large Scale Structure of Space-Time*. Cambridge Monographs on Mathematical Physics. Cambridge University Press.
- Hawking, S. W. and Page, D. N. (1983). Thermodynamics of Black Holes in anti-De Sitter Space. *Commun. Math. Phys.*, 87:577.
- Hawking, S. W. and Penrose, R. (1970). The Singularities of gravitational collapse and cosmology. *Proc. Roy. Soc. Lond. A*, 314:529–548.
- Hayward, S. A. (2006). Formation and evaporation of regular black holes. *Phys. Rev. Lett.*, 96:031103.
- Hegde, K., **Naveena Kumara, A.**, Rizwan, C. L. A., Ali, M. S., and Ajith, K. M. (2020). Null Geodesics and Thermodynamic Phase Transition of Four-Dimensional Gauss-Bonnet AdS Black Hole.
- Hendi, S. H. and Naderi, R. (2015). Geometrothermodynamics of black holes in Lovelock gravity with a nonlinear electrodynamics. *Phys. Rev. D*, 91(2):024007.
- Henneaux, M. and Teitelboim, C. (1985). Asymptotically anti-De Sitter Spaces. *Commun. Math. Phys.*, 98:391–424.
- Hennigar, R. A. (2018). *Explorations in black hole chemistry and higher curvature gravity*. PhD thesis, Waterloo U.

- Hennigar, R. A., Brenna, W. G., and Mann, R. B. (2015). $P-v$ criticality in quasitopological gravity. *JHEP*, 07:077.
- Hennigar, R. A. and Mann, R. B. (2015). Reentrant phase transitions and van der Waals behaviour for hairy black holes. *Entropy*, 17(12):8056–8072.
- Hosseini Mansoori, S. A. and Mirza, B. (2019). Geometrothermodynamics as a singular conformal thermodynamic geometry. *Phys. Lett. B*, 799:135040.
- Hudson, C. S. (1904). Die gegenseitige löslichkeit von nikotin in wasser. *Zeitschrift für Physikalische Chemie*, 47(1):113–115.
- Jacobson, T. (1995). Thermodynamics of space-time: The Einstein equation of state. *Phys. Rev. Lett.*, 75:1260–1263.
- Janyszek, H. (1990). Riemannian geometry and stability of thermodynamical equilibrium systems. *Journal of Physics A Mathematical General*, 23(4):477–490.
- Janyszek, H. and Mrugala, R. (1989). Riemannian geometry and the thermodynamics of model magnetic systems. *Phys. Rev. A*, 39:6515–6523.
- Janyszek, H. and Mrugala, R. (1990). Riemannian geometry and stability of ideal quantum gases. *Journal of Physics A: Mathematical and General*, 23(4):467–476.
- Johnson, C. V. (2014). Holographic Heat Engines. *Class. Quant. Grav.*, 31:205002.
- Kastor, D. (2008). Komar Integrals in Higher (and Lower) Derivative Gravity. *Class. Quant. Grav.*, 25:175007.
- Kastor, D., Ray, S., and Traschen, J. (2009). Enthalpy and the Mechanics of AdS Black Holes. *Class. Quant. Grav.*, 26:195011.
- Kord Zangeneh, M., Dehyadegari, A., Sheykhi, A., and Mann, R. B. (2018). Microscopic Origin of Black Hole Reentrant Phase Transitions. *Phys. Rev.*, D97(8):084054.
- Kubiznak, D. and Mann, R. B. (2012a). P-V criticality of charged AdS black holes. *JHEP*, 07:033.
- Kubiznak, D. and Mann, R. B. (2012b). P-V criticality of charged AdS black holes. *JHEP*, 07:033.
- Kubiznak, D. and Mann, R. B. (2015). Black hole chemistry. *Can. J. Phys.*, 93(9):999–1002.
- Kubiznak, D., Mann, R. B., and Teo, M. (2017). Black hole chemistry: thermodynamics with Lambda. *Class. Quant. Grav.*, 34(6):063001.
- Kubiznak, D. and Simovic, F. (2016). Thermodynamics of horizons: de Sitter black holes and reentrant phase transitions. *Class. Quant. Grav.*, 33(24):245001.
- Kubizňák, D., Mann, R. B., and Teo, M. (2017). Black hole chemistry: thermodynamics with lambda. *Classical and Quantum Gravity*, 34(6):063001.
- Kumar, A., Veer Singh, D., and Ghosh, S. G. (2019). D -dimensional Bardeen-AdS black holes in Einstein-Gauss-Bonnet theory. *Eur. Phys. J. C*, 79(3):275.

- Landau, L. D. and Lifshitz, E. M. (1980). *Statistical Physics, Part I*, volume 5 of *Course of Theoretical Physics*. Butterworth-Heinemann, Oxford.
- Li, H., Chen, Y., and Zhang, S.-J. (2020). Photon orbits and phase transitions in Born-Infeld-dilaton black holes. *Nucl. Phys. B*, 954:114975.
- Liu, H., Lu, H., Luo, M., and Shao, K.-N. (2010). Thermodynamical Metrics and Black Hole Phase Transitions. *JHEP*, 12:054.
- Liu, Y., Zou, D.-C., and Wang, B. (2014). Signature of the Van der Waals like small-large charged AdS black hole phase transition in quasinormal modes. *JHEP*, 09:179.
- Ma, M.-S. and Zhao, R. (2014). Corrected form of the first law of thermodynamics for regular black holes. *Class. Quant. Grav.*, 31:245014.
- Maldacena, J. (1999). The Large-N Limit of Superconformal Field Theories and Supergravity. *International Journal of Theoretical Physics*, 38(4).
- Man, J. and Cheng, H. (2013). The description of phase transition of Bardeen black hole in the Ehrenfest scheme. *arXiv:1312.6566 [hep-th]*.
- Man, J. and Cheng, H. (2014). The calculation of the thermodynamic quantities of the Bardeen black hole. *Gen. Rel. Grav.*, 46:1660.
- Mann, R. B. (2015). *Black Holes: Thermodynamics, Information, and Firewalls*. Springer-Briefs in Physics. Springer.
- Mansoori, S. A. H. and Mirza, B. (2014). Correspondence of phase transition points and singularities of thermodynamic geometry of black holes. *Eur. Phys. J. C*, 74(99):2681.
- Mansoori, S. A. H., Mirza, B., and Fazel, M. (2015). Hessian matrix, specific heats, Nambu brackets, and thermodynamic geometry. *JHEP*, 04:115.
- Mansoori, S. A. H., Mirza, B., and Sharifian, E. (2016). Extrinsic and intrinsic curvatures in thermodynamic geometry. *Phys. Lett. B*, 759:298–305.
- May, H.-O., Mausbach, P., and Ruppeiner, G. (2013a). Thermodynamic curvature for attractive and repulsive intermolecular forces. *Phys. Rev. E*, 88:032123.
- May, H.-O., Mausbach, P., and Ruppeiner, G. (2013b). Thermodynamic curvature for attractive and repulsive intermolecular forces. *Phys. Rev. E*, 88:032123.
- Mbarek, S. (2019). *Explorations of Black Hole Thermodynamics in de Sitter Spacetime*. PhD thesis, Waterloo U.
- Miao, Y.-G. and Xu, Z.-M. (2018). On thermal molecular potential among micromolecules in charged AdS black holes. *Phys. Rev.*, D98:044001.
- Miao, Y.-G. and Xu, Z.-M. (2019). Microscopic structures and thermal stability of black holes conformally coupled to scalar fields in five dimensions. *Nucl. Phys.*, B942:205–220.
- Mirza, B. and Mohammadzadeh, H. (2008). Ruppeiner geometry of anyon gas. *Phys. Rev. E*, 78:021127.

- Mirza, B. and Zamani-Nasab, M. (2007). Ruppeiner Geometry of RN Black Holes: Flat or Curved? *JHEP*, 06:059.
- Mo, J.-X., Zeng, X.-X., Li, G.-Q., Jiang, X., and Liu, W.-B. (2013). A unified phase transition picture of the charged topological black hole in Horava-Lifshitz gravity. *JHEP*, 10:056.
- Myers, R. C. and Perry, M. J. (1986). Black Holes in Higher Dimensional Space-Times. *Annals Phys.*, 172:304.
- Nam, C. H. (2018). Non-linear charged AdS black hole in massive gravity. *Eur. Phys. J. C*, 78(12):1016.
- Narayanan, T. and Kumar, A. (1994). Reentrant phase transitions in multicomponent liquid mixtures. *physrep*, 249(3):135–218.
- Nicolini, P., Spallucci, E., and Wondrak, M. F. (2019). Quantum Corrected Black Holes from String T-Duality. *Phys. Lett. B*, 797:134888.
- Niu, C., Tian, Y., and Wu, X.-N. (2012). Critical Phenomena and Thermodynamic Geometry of RN-AdS Black Holes. *Phys. Rev. D*, 85:024017.
- Oshima, H., Obata, T., and Hara, H. (1999). Riemann scalar curvature of ideal quantum gases obeying gentile's statistics. *Journal of Physics A: Mathematical and General*, 32(36):6373–6383.
- Padmanabhan, T. (2002). Classical and quantum thermodynamics of horizons in spherically symmetric space-times. *Class. Quant. Grav.*, 19:5387–5408.
- Page, D. N. (2005). Hawking radiation and black hole thermodynamics. *New Journal of Physics*, 7(1):203.
- Panella, O. and Roy, P. (2016). Re-entrant phase transitions in non-commutative quantum mechanics. In *Journal of Physics Conference Series*, volume 670 of *Journal of Physics Conference Series*, page 012040.
- Poisson, E. (2009). *A Relativist's Toolkit: The Mathematics of Black-Hole Mechanics*. Cambridge University Press.
- Quevedo, H. (2007). Geometrothermodynamics. *J. Math. Phys.*, 48:013506.
- Ruppeiner, G. (1979). Thermodynamics: A riemannian geometric model. *Phys. Rev. A*, 20:1608–1613.
- Ruppeiner, G. (1981). Application of riemannian geometry to the thermodynamics of a simple fluctuating magnetic system. *Phys. Rev. A*, 24:488–492.
- Ruppeiner, G. (1995). Riemannian geometry in thermodynamic fluctuation theory. *Rev. Mod. Phys.*, 67:605–659. [Erratum: *Rev. Mod. Phys.* 68,313(1996)].
- Ruppeiner, G. (2008). Thermodynamic curvature and phase transitions in Kerr-Newman black holes. *Phys. Rev.*, D78:024016.

- Ruppeiner, G. (2014). Thermodynamic curvature and black holes. *Springer Proc. Phys.*, 153:179–203.
- Sahay, A., Sarkar, T., and Sengupta, G. (2010). Thermodynamic Geometry and Phase Transitions in Kerr-Newman-AdS Black Holes. *JHEP*, 04:118.
- Sakharov, A. D. (1966). The Initial Stage of an Expanding Universe and the Appearance of a Nonuniform Distribution of Matter. *Soviet Journal of Experimental and Theoretical Physics*, 22:241.
- Seiberg, N. and Witten, E. (1999). String theory and noncommutative geometry. *JHEP*, 09:032.
- Sherkatghanad, Z., Mirza, B., Mirzaiyan, Z., and Hosseini Mansoori, S. A. (2016). Critical behaviors and phase transitions of black holes in higher order gravities and extended phase spaces. *Int. J. Mod. Phys. D*, 26(03):1750017.
- Smarr, L. (1973). Mass formula for Kerr black holes. *Phys. Rev. Lett.*, 30:71–73. [Erratum: *Phys.Rev.Lett.* 30, 521–521 (1973)].
- Stefanov, I. Z., Yazadjiev, S. S., and Gyulchev, G. G. (2010). Connection between Black-Hole Quasinormal Modes and Lensing in the Strong Deflection Limit. *Phys. Rev. Lett.*, 104:251103.
- Tseytlin, A. A. (1999). Born-Infeld action, supersymmetry and string theory. pages 417–452.
- Tzikas, A. G. (2019). Bardeen black hole chemistry. *Phys. Lett. B*, 788:219–224.
- Wei, S.-W., Liang, B., and Liu, Y.-X. (2017). Critical phenomena and chemical potential of a charged AdS black hole. *Phys. Rev. D*, 96(12):124018.
- Wei, S.-W. and Liu, Y.-X. (2013). Critical phenomena and thermodynamic geometry of charged Gauss-Bonnet AdS black holes. *Phys. Rev. D*, 87(4):044014.
- Wei, S.-W. and Liu, Y.-X. (2014). Triple points and phase diagrams in the extended phase space of charged Gauss-Bonnet black holes in AdS space. *Phys. Rev. D*, 90(4):044057.
- Wei, S.-W. and Liu, Y.-X. (2015). Insight into the Microscopic Structure of an AdS Black Hole from a Thermodynamical Phase Transition. *Phys. Rev. Lett.*, 115(11):111302. [Erratum: *Phys. Rev. Lett.* 116, no. 16, 169903 (2016)].
- Wei, S.-W. and Liu, Y.-X. (2018). Photon orbits and thermodynamic phase transition of d -dimensional charged AdS black holes. *Phys. Rev. D*, 97(10):104027.
- Wei, S.-W. and Liu, Y.-X. (2019). Null Geodesics, Quasinormal Modes, and Thermodynamic Phase Transition for Charged Black Holes in Asymptotically Flat and dS Spacetimes. *arXiv:1909.11911 [gr-qc]*.
- Wei, S.-W. and Liu, Y.-X. (2020a). Extended thermodynamics and microstructures of four-dimensional charged Gauss-Bonnet black hole in AdS space. *Phys. Rev. D*, 101(10):104018.
- Wei, S.-W. and Liu, Y.-X. (2020b). Intriguing microstructures of five-dimensional neutral Gauss-Bonnet AdS black hole. *Phys. Lett.*, B803:135287.

- Wei, S.-W., Liu, Y.-X., and Mann, R. B. (2019a). Repulsive Interactions and Universal Properties of Charged Anti-de Sitter Black Hole Microstructures. *Phys. Rev. Lett.*, 123(7):071103.
- Wei, S.-W., Liu, Y.-X., and Mann, R. B. (2019b). Ruppeiner Geometry, Phase Transitions, and the Microstructure of Charged AdS Black Holes. *Phys. Rev.*, D100(12):124033.
- Wei, S.-W., Liu, Y.-X., and Wang, Y.-Q. (2019c). Probing the relationship between the null geodesics and thermodynamic phase transition for rotating Kerr-AdS black holes. *Phys. Rev. D*, 99(4):044013.
- Weinhold, F. (1975a). Metric geometry of equilibrium thermodynamics. *The Journal of Chemical Physics*, 63(6):2479–2483.
- Weinhold, F. (1975b). Metric geometry of equilibrium thermodynamics ii. *The Journal of Chemical Physics*, 63:2479–2483.
- Witten, E. (1998). Anti-de Sitter space, thermal phase transition, and confinement in gauge theories. *Adv. Theor. Math. Phys.*, 2:505–532. [89(1998)].
- Wu, B., Wang, C., Xu, Z.-M., and Yang, W.-L. (2020). Ruppeiner geometry and thermodynamic phase transition of the black hole in massive gravity.
- Xu, Y.-M., Wang, H.-M., Liu, Y.-X., and Wei, S.-W. (2019). Photon sphere and reentrant phase transition of charged Born-Infeld-AdS black holes. *Phys. Rev. D*, 100(10):104044.
- Xu, Z.-M., Wu, B., and Yang, W.-L. (2020a). Fine micro-thermal structures for Reissner-Nordström black hole. *Chin. Phys. C*, 44(9):095106.
- Xu, Z.-M., Wu, B., and Yang, W.-L. (2020b). Ruppeiner thermodynamic geometry for the Schwarzschild-AdS black hole. *Phys. Rev. D*, 101(2):024018.
- Yerra, P. K. and Bhamidipati, C. (2020). Ruppeiner Geometry, Phase Transitions and Microstructures of Black Holes in Massive Gravity. *Int. J. Mod. Phys. A*, 35(22):2050120.
- Zhang, M., Han, S.-Z., Jiang, J., and Liu, W.-B. (2019). Circular orbit of a test particle and phase transition of a black hole. *Phys. Rev. D*, 99(6):065016.
- Zhang, Y. and Gao, S. (2018). First law and Smarr formula of black hole mechanics in nonlinear gauge theories. *Class. Quant. Grav.*, 35(14):145007.
- Zou, D.-C., Zhang, S.-J., and Wang, B. (2014). Critical behavior of Born-Infeld AdS black holes in the extended phase space thermodynamics. *Phys. Rev. D*, 89(4):044002.

List of publications

Peer Reviewed International Journals

- **A. Naveena Kumara**, C. L. Ahmed Rizwan, Kartheek Hegde, Md Sabir Ali, Ajith K. M., “Ruppeiner Geometry, Reentrant Phase transition and Microstructure of Born-Infeld AdS Black Hole”, *Physical Review D* 103, 044025 (2021) [arXiv:2007.07861]
- **A. Naveena Kumara**, C. L. Ahmed Rizwan, Shreyas Punacha, Ajith K. M., Md Sabir Ali, “Photon Orbits and Thermodynamic Phase Transition of Regular AdS Black Holes”, *Physical Review D* 102, 084059 (2020), [arXiv:1912.11909]
- **A. Naveena Kumara**, C. L. Ahmed Rizwan, Kartheek Hegde, Ajith K. M., “Repulsive Interactions in the Microstructure of Regular Hayward Black Hole in Anti-de Sitter Spacetime”, *Physics Letters B*, 807, 135556 (2020), [arXiv:2003.10175]
- **A. Naveena Kumara**, C. L. Ahmed Rizwan, Kartheek Hegde, Ajith K. M., Md Sabir Ali, “Microstructure and continuous phase transition of a regular Hayward black hole in anti-de Sitter spacetime”, *Progress of Theoretical and Experimental Physics* 7, 073 (2021) [arXiv:2003.00889]
- C. L. Ahmed Rizwan, **A. Naveena Kumara**, Kartheek Hegde, Md Sabir Ali, Ajith K. M., “Rotating Black Hole with an Anisotropic Matter Field as a Particle Accelerator”, *Classical and Quantum Gravity* 38, 075030 (2021) [arXiv:2008.01426]
- Shreyas Punacha, **Naveena Kumara A.**, and T. K. Shajahan, ”Theory of unpinning of spiral waves using circularly polarized electric fields in mathematical models of excitable media”, *Physical Review E* 102, 032411 (2020)
- C. L. Ahmed Rizwan, **A. Naveena Kumara**, Kartheek Hegde, Deepak Vaid, “Coexistent Physics and Microstructure of the Regular Bardeen Black Hole in Anti-de Sitter Spacetime”, *Annals of Physics*, 422, 168320 (2020), [arXiv:2008.06472]
- K.V. Rajani, C. L. Ahmed Rizwan, **A. Naveena Kumara**, Deepak Vaid, K.M. Ajith, “Regular Bardeen AdS Black Hole as a Heat Engine”, *Nuclear Physics B*, 960, 115166 (2020), [arXiv:1904.06914]
- C. L. Ahmed Rizwan, **A. Naveena Kumara**, V. Deepak and K. M. Ajith, ”Joule Thomson expansion in AdS black hole with a global monopole”, *International Journal of Modern Physics A*, 33 (2018) 14, [arXiv:1805.11053]

- C.L. Ahmed Rizwan, **A. Naveena Kumara**, K.V. Rajani, Deepak Vaid., K.M. Ajith, "Effect of Dark Energy in Geometrothermodynamics and Phase Transitions of Regular AdS Black Hole", *General Relativity and Gravitation* 51, 161 (2019), [arXiv 1811.10838]
- Kartheek Hegde, **A. Naveena Kumara**, C. L. Ahmed Rizwan, Md Sabir Ali, Ajith K. M, "Null Geodesics and Thermodynamic Phase Transition of Four-Dimensional Gauss-Bonnet AdS Black Hole", *Annals of Physics* 429, 168461 (2021) [arXiv:2007.10259]
- K.V. Rajani, C. L. Ahmed Rizwan, **A. Naveena Kumara**, Deepak Vaid, Md. Sabir Ali, "Joule-Thomson Expansion of Regular Bardeen AdS Black Hole Surrounded by Static Anisotropic Matter Field", *Physics of the Dark Universe* 32, 100825 (2021) [arXiv:2002.03634]

arXiv Pre-prints

- **A. Naveena Kumara**, S. Punacha, K. Hegde, C. L. Ahmed Rizwan, Md Sabir Ali and K. M. Ajith, "Dynamics and kinetics of phase transition for regular AdS black holes in general relativity coupled to non-linear electrodynamics", [arXiv:2106.11095]
- **A. Naveena Kumara**, C. L. Ahmed Rizwan, Kartheek Hegde, Md Sabir Ali, Ajith K. M, "Microstructure of five-dimensional neutral Gauss-Bonnet black hole in anti-de Sitter spacetime via P-V criticality", [arXiv:2006.13907]
- **A. Naveena Kumara**, C. L. Ahmed Rizwan, Kartheek Hegde, Md Sabir Ali, Ajith K. M, "Rotating 4D Gauss-Bonnet black hole as particle accelerator", [arXiv:2004.04521]
- **A. Naveena Kumara**, C. L. Ahmed Rizwan, Deepak Vaid, K. M. Ajith, "Critical Behaviour and Microscopic Structure of Charged AdS Black Hole with a Global Monopole in Extended and Alternate Phase Spaces", [arXiv:1906.11550]
- Kartheek Hegde, **A. Naveena Kumara**, C. L. Ahmed Rizwan, Ajith K. M., Md Sabir Ali, "Thermodynamics, Phase Transition and Joule Thomson Expansion of novel 4-D Gauss Bonnet AdS Black Hole", [arXiv:2003.08778]
- Md Sabir Ali, **A. Naveena Kumara**, Kartheek Hegde, C. L. Ahmed Rizwan and K. M. Ajith, "Greybody factor for an electrically charged regular de-Sitter black holes in d-dimensions", [arXiv:2105.05730]
- Kartheek Hegde, **A. Naveena Kumara**, C. L. Ahmed Rizwan, Md Sabir Ali and K. M. Ajith, "Thermodynamics, photon sphere and thermodynamic geometry of Eloy Ayon Beato – Garcia Spacetime", [arXiv:2104.08091]

Peer Reviewed International Journal proceedings

- **A. Naveena Kumara**, C.L. Ahmed Rizwan, K.M. Ajith “Criticality of Charged AdS Black Hole with a Global Monopole”, Proceedings, Workshop on Frontiers in High Energy Physics 2019 (FHEP 2019), *Springer Proc.Phys. 248 (2020) 75-79*
- **A. Naveena Kumara**, C.L. Ahmed Rizwan, Deepak Vaid, Ajith K.M. “On The Throttling Process Of AdS Black Hole With A Global Monopole”, 23rd DAE High energy symposium, *to be appear as Springer Proceedings in Physics*
- C.L. Ahmed Rizwan, **A.Naveena Kumara**, K.S. Ananthram, “Effect of Global Monopole on the Microscopic Structure of RN-AdS Black Hole” Proceedings, Workshop on Frontiers in High Energy Physics 2019 (FHEP 2019), *Springer Proc.Phys. 248 (2020) 81-85*
- K.V. Rajani, C.L. Ahmed Rizwan, **A.Naveena Kumara**, “Phase transition and thermodynamic geometry of regular Bardeen black hole in higher dimensions”, Proceedings, 3rd International Conference on Condensed Matter & Applied Physics (ICC 2019), *AIP Conf.Proc. 2220 (2020) 1, 030003*
- C.L. Ahmed Rizwan, **A. Naveena Kumara**, Deepak Vaid, “Thermodynamic Geometry of Regular black hole surrounded by Quintessence”, 23rd DAE High energy symposium, *to be appear as Springer Proceedings in Physics*

International Conferences Presentations

- The 15th Kavli Asian Winter School on Strings, Particles and Cosmology, Beijing, China, (Digital School), 18th to 27th of January 2021. *Gong show: "Null Geodesics and Thermodynamic Phase Transition of Regular AdS Black Holes"*
- XXIII DAE-BRNS HIGH ENERGY PHYSICS SYMPOSIUM 2018, IIT Madras, Chennai, December 10-14, 2018. *Talk: "On The Throttling Process Of AdS Black Hole With A Global Monopole"*
- International Conference on Gravitation and Cosmology (ICGC), Indian Institute of Science Education and Research Mohali (IISERM), December 10-13, 2019. *Poster: "Microscopic Structure of RN-AdS Black Hole in an Alternate Approach"*
- International Workshop on frontiers in high energy physics (FHEP 2019), University of Hyderabad, 14 -17 October 2019. *Poster: "Criticality of Charged AdS Black Hole with a Global Monopole"*
- 30th meeting of the Indian Association for General Relativity and Gravitation(IAGRG), BITS Pilani , Hyderabad Campus, 3-5 January, 2019. *Poster: "Gravitational Waves in Chern Simons' Gravity"*
- National Conference on Cosmology and Particle Physics (NC-CAPP 2018), Women's Christian College, Chennai, 1- 2 October 2018. *Best Poster award for the poster: "Curvature Divergences and Phase transitions in Regular black hole"*

CURRICULUM VITAE



NAVEENA KUMARA A

Permanent Address :

Athithamoole House
P.O. Kuntar, Kasaragod Dist,
Kerala, India - 671543

Mobile:(+91)-9035207005

E-mail: naviphysics@gmail.com

Academic Qualifications :

Master of Science in Physics

S.D.M. College (Autonomous) Ujire
Mangalore University,
Mangalore, Karnataka, India

Bachelor of Science in Physics

Govt. College Kasaragod
Kannur University,
Kerala, India

Research Publications :

Articles in International Journals : 12
Articles in International Proceedings : 5
Papers presented in International Conferences : 6
Workshops and Schools attended : 20+